A Theoretical Study of the Effect of Molecular Absorption and Re-radiation on Millimeter Wave and Terahertz Wireless Networking

Author:
Hoseini, Sayed Amir

Publication Date:
2017

DOI:
https://doi.org/10.26190/unsworks/3323

A Theoretical Study of the Effect of Molecular Absorption and Re-radiation on Millimeter Wave and Terahertz Wireless Networking

THE UNIVERSITY OF NEW SOUTH WALES

SYDNEY · AUSTRALIA

Dissertation submitted in fulfilment
of the requirements for the degree of

Doctor of Philosophy

in

Computer Science and Engineering

Sayed Amir Hoseini

Supervisor: Professor Mahbub Hassan

Co-supervisor (CSIRO): Dr Ming Ding

Co-supervisor (UNSW): A.Professor Chun Tung Chou

November 2017

THE UNIVERSITY OF NEW SOUTH WALES
Thesis/Dissertation Sheet

Surname or Family name: Hoseini

First name: Sayed Amir Other name/s:

Abbreviation for degree as given in the University calendar: PHD

School: Computer Science and Engineering Faculty: Engineering

Title: Theoretical Study of the Effect of Molecular Absorption and Re-radiation on Millimeter Wave and Terahertz Wireless Networking

Abstract 350 words maximum:

The rapidly growing demand for higher networking capacity and data rates is forcing researchers to explore the unused spectrum in the higher frequency bands. Two such bands, the millimeter wave (mmWave), ranging from 30 GHz to 300 GHz, and the Terahertz (THz) band, ranging from 0.1 THz to 10 THz, are currently being investigated for possible use in future networks. Because many atmospheric molecules have their natural resonance frequencies in these bands, it is important to understand the effects of molecular absorption and re-radiation on the wireless networking performance in such high frequency bands. Building on the recently discovered molecular absorption models, this thesis conducts a theoretical study on the effect of molecular absorption and re-radiation on both single-antenna and multi-antenna wireless communications. For the single-antenna communication, the study focuses on quantifying the temporal and spatial variation of path loss and noise, which is caused by variation in the molecular composition in the air. In particular, it studies the extent of spatio-temporal variation of mmWave channels in three largest cities of Australia by investigating the hourly air quality and weather data over 12 months. The study finds that mmWave channels experience significant variation in both space and time domains, which causes undesirable network capacity fluctuation in various places and hours. For the multi-antenna communication, the study yields a new theoretical discovery that the MIMO capacity can be significantly influenced by atmosphere molecules. In more detail, some common atmosphere molecules, such as Oxygen and water, can absorb and re-radiate energy in their natural resonance frequencies, such as 60 GHz, 120GHz and 180 GHz, which belong to the mmWave spectrum. Such phenomenon can provide equivalent non-Lineof-Sight (NLoS) paths in an environment that is dominated by Line-of-Sight (LoS) transmissions, and thus greatly improve the spatial multiplexing and diversity of a MIMO mmWave system. Finally, the performance of two main MIMO techniques, beamforming and multiplexing, in the mmWave/THz band is studied. Our results reveal a surprising observation that the MIMO multiplexing could be a better choice than the MIMO beamforming under certain conditions in multiple bands.
We believe that our findings will open the door for a new direction of research and development toward the feasibility of communication in mmWave and THz spectrum.

Declaration relating to disposition of project thesis/dissertation

I hereby grant to the University of New South Wales or its agents the right to archive and to make available my thesis or dissertation in whole or in part in the University libraries in all forms of media, now or here after known, subject to the provisions of the Copyright Act 1968. I retain all property rights, such as patent rights. I also retain the right to use in future works (such as articles or books) all or part of this thesis or dissertation.

I also authorise University Microfilms to use the 350 word abstract of my thesis in Dissertation Abstracts International (this is applicable to doctoral theses only).

…… …… ……

Signature Witness Signature Date

The University recognises that there may be exceptional circumstances requiring restrictions on copying or conditions on use. Requests for restriction for a period of up to 2 years must be made in writing. Requests for a longer period of restriction may be considered in exceptional circumstances and require the approval of the Dean of Graduate Research.

FOR OFFICE USE ONLY Date of completion of requirements for Award:

ORIGINALITY STATEMENT

'I hereby declare that this submission is my own work and to the best of my knowledge it contains no materials previously published or written by another person, or substantial proportions of material which have been accepted for the award of any other degree or diploma at UNSW or any other educational institution, except where due acknowledgement is made in the thesis. Any contribution made to the research by others, with whom I have worked at UNSW or elsewhere, is explicitly acknowledged in the thesis. I also declare that the intellectual content of this thesis is the product of my own work, except to the extent that assistance from others in the project's design and conception or in style, presentation and linguistic expression is acknowledged.'

Signed ……..

Date ……..

Abstract

The rapidly growing demand for higher networking capacity and data rates is forcing researchers to explore the unused spectrum in the higher frequency bands. Two such bands, the millimeter wave (mmWave), ranging from 30 GHz to 300 GHz, and the Terahertz (THz) band, ranging from 0.1 THz to 10 THz, are currently being investigated for possible use in future networks. Because many atmospheric molecules have their natural resonant frequencies in these bands, it is important to understand the effects of molecular absorption and re-radiation on the wireless networking performance in such high frequency bands. Building on the recently discovered molecular absorption models, this thesis conducts a theoretical study on the effect of molecular absorption and re-radiation on both single-antenna and multi-antenna wireless communications. For the single-antenna communication, the study focuses on quantifying the temporal and spatial variation of path loss and noise, which is caused by variation in the molecular composition in the air. In particular, it studies the extent of spatio-temporal variation of mmWave channels in three largest cities of Australia by investigating the hourly air quality and weather data over 12 months. The study finds that mmWave channels experience significant variation in both space and time domains, which causes undesirable network capacity fluctuation in various places and hours. For the multi-antenna communication, the study yields a new theoretical discovery that the Multiple-Input and Multiple-Output (MIMO) capacity can be significantly influenced by atmosphere molecules. In more detail, some common atmosphere molecules, such as Oxygen and water, can absorb and re-radiate energy in their natural resonant frequencies, such as 60 GHz, 120GHz and 180 GHz, which belong to the mmWave spectrum. Such phenomenon can provide equivalent Non-Line-of-Sight (NLoS) paths in an environment that is dominated by Line-of-Sight (LoS) transmissions, and thus greatly improve the spatial multiplexing and diversity of a MIMO mmWave system. Finally, the performance of two main MIMO techniques, beamforming and multiplexing, in the terahertz band is studied.

Our results reveal a surprising observation that the MIMO multiplexing could be a better choice than the MIMO beamforming under certain conditions in multiple THz bands.

We believe that our findings will open the door for a new direction of research and development toward the feasibility of communication in mmWave and THz spectrum.

This thesis is dedicated to my beloved wife Akram

for her love, support and encouragement,

To my lovely little son Ali

and

To Ali's grandparents for their timeless love

Acknowledgements

Working at the School of Computer Science and Engineering at the University of New South Wales (UNSW) has been a great pleasure and a wonderful privilege. In the first place, I would like to express my sincere appreciation and deep gratitude to my supervisor, Professor Mahbub Hassan for his exceptional support, encouragement and guidance during all stages of this research. His truly valuable academic excellence, scientific intuition and beautiful mind have made him a constant oasis of ideas and passions in science. This has inspired and enriched my growth as a student. I also express my genuine thanks to Dr Ming Ding, as my co-supervisor, for his kind help, incredible support and valuable discussion contributing to my thesis. It was an honor for me to work closely with such a talented, polite and creative personality. In addition, I express my sincere appreciation to my university co-supervisor Associated Prof. Chun Tung Chu for great help and support and novel ideas. His deep understanding in math always opened the research obstacles for us.

I also appreciate the University of New South Wales (UNSW) and DATA61 research group in CSIRO for funding my research during three and half years.

Sayed Amir Hoseini
Sydney, Australia
November 2017

Contents

List of Figures

List of Tables

PUBLICATIONS

1. **S. A. Hoseini**, Ming Ding, and Mahbub Hassan. "A New Look at MIMO Capacity in the Millimeter Wave." *In IEEE Global Communications Conference (GLOBECOM)*, Singapore, December 4-8, 2017.

2. **S. A. Hoseini**, Ming Ding, and Mahbub Hassan. "Massive MIMO Performance Comparison of Beamforming and Multiplexing in the Terahertz Band." *IEEE Globecom Workshops (GC Wkshps)*, Singapore, December 4-8, 2017.

3. **S. A. Hoseini**, Eisa Zarepour, Mahbub Hassan, and Chun Tung Chou. "Analyzing diurnal variations of millimeter wave channels." *In Computer Communications Workshops (INFOCOM WKSHPS)*, 2016 IEEE Conference on, pp. 377-382. IEEE, 2016.

4. **S. A. Hoseini**, Azade Fotouhi, Mahbub Hassan, Chun Tung Chou, and Mostafa H. Ammar. "Efficient and Transparent Use of personal device storage in opportunistic data forwarding." *Computer Communications* 73 (2015): 47-55.

5. **S. A. Hoseini**, Azade Fotouhi, Mahbub Hassan, Chun Tung Chou, and Mostafa Ammar. "A message ferrying approach to low-cost backhaul in cellular networks." *In Proceedings of the 9th ACM MobiCom workshop on Challenged networks*, pp. 25-30. ACM, 2014.

6. **S. A. Hoseini**, and Ayub Bokani. "Video Ferrying: A Low Cost Video Streaming Approach for Cellular Networks." *In Proceedings of the ACM CoNEXT workshop on Video: VideoNEXT2014*. ACM, 2014.

7. Ayub Bokani, **S. A. Hoseini**, Mahbub Hassan, and Salil S. Kanhere. "Implementation and evaluation of adaptive video streaming based on Markov decision process." In Communications (ICC), 2016 IEEE International Conference on, pp. 1-6. IEEE, 2016.

8. Ayub Bokani, **S. A. Hoseini**, Mahbub Hassan, and Salil S. Kanhere. "Empirical evaluation of MDP-based DASH player." In International Telecommunication Networks and Applications Conference (ITNAC), 2015, pp. 332-337. IEEE, 2015.

Chapter 1

Introduction

The current rapid growth of data traffic presents great challenges for wireless network providers. According to a Cisco forecast [5], wireless devices will account for 67% of total Internet traffic by 2021, up from 49% in 2016. Furthermore, mobile data traffic will increase sevenfold between 2016 and 2021, requiring enormous capacity enhancements in wireless communication systems. For example, 5th Generation mobile networks (5G) aim to provide peak data rates of 10 Gbps per user [6]. In addition to cellular network users, short-range local wireless networks or point-to-point links between home devices are expected to support Tbps links [7] and more bandwidth-thirsty applications, such as wireless virtual reality (VR) devices, are on the horizon.

On the other hand, the major portion of wireless communication traffic currently uses frequencies below 6 GHz. This part of the spectrum is highly used and will soon become overloaded. In spite of the very efficient use of the spectrum in recent wireless standards such as Wireless Local Area Network (WLAN) and cellular mobile communication, using new parts of the spectrum to accommodate increasing traffic demand is becoming a necessity. A largely unused part of the spectrum in the range of 30-300 GHz, which is called millimeter wave (mmWave) is attracting attention for data transmission. Thanks its short wavelengths, mmWave can use a large array of antennas co-located on a small transmitter or receiver. This can boost data capacity to realize the dream of 1+ Tbps data rates. However, the spectral

efficiency of mmWave is also limited, and to achieve the extremely high bit rates of over 1 Tbps, a much larger bandwidth is required than the 1-10 GHz available in the mmWave band [7]. However, Many challenges still remain, especially regarding the very high propagation loss in THz band communication.

A key difference between existing lower frequency wireless communication systems and mmWave/THz is that some molecules in the air, such as water and oxygen, have their natural resonant frequencies within these bands and can absorb signal energy at very high rates if excited. This means that the mmWave/THz band is very sensitive to the amount of water in the air in the form of humidity, moisture, or rain.

In this thesis, we focus on this molecular absorption phenomenon and its negative and positive effects on wireless communication.

1.1 Motivation

Exploiting the unused spectrum in the mmWave and THz bands is considered as a feasible solution to the tremendous data traffic requirements of wireless communication in near future [8, 9]. However, the technologies and techniques of existing communication bands cannot simply be assumed to be applicable to the new spectrum. In spite of following the same electromagnetic laws, the propagation characteristics can be fundamentally different. The major difference comes from the very short wavelengths in the mmWave and THz frequency ranges, which results in new challenges such as blockage sensitivity, directivity, huge path loss and the natural resonance of atmospheric molecules.

Each species of molecule in the atmosphere not only absorbs signal energy (causing attenuation), but also re-radiates the absorbed energy. The re-radiated wave is usually referred to as "noise" in the literature, but interestingly, recent works show that it is highly correlated to the main signal [10] and can be considered as scattered signal components which arrive at the receiver later than the original wave [11, 12]. The main atmospheric molecules which cause significant molecular absorption in the

0.03-10 THz range are water (H_2O) and oxygen (O_2).

The intensity of molecular absorption is related to the mole ratio of each species of molecule in the air. Oxygen molecule absorption peaks are observed at around 60 and 120 GHz. While the oxygen content of the atmosphere is almost constant at around 20%, the amount of water varies spatially and temporally. Moreover, air temperature and pressure also affect absorption.

One of the key techniques in mmWave/THz communication is massive Multiple-Input and Multiple-Output (MIMO). The short wavelengths of frequencies above 30 GHz allows the co-location of a large number of antennas within a relatively small footprint, for example, 144 elements in 1 cm^2 at 60 GHz [2]. On the other hand, huge path loss reduce the multipath ray strength, and mmWave/THz is mostly considered as a Line-of-Sight (LoS) communication. In the absence of multi-path signal components, MIMO performance is downgraded, and instead of sending multiple data streams, one stream with a beam directed to the receiver is created by the MIMO system. This beamforming also significantly improves the Signal-to-Noise-Ratio (SNR). However, the resulted capacity is not as expected where spatial multiplexing exists in the channel.

Our findings show that, in spite of the challenges created by molecular absorption/re-radiation in a communication channel, there are potential capacity enhancements when multiple antennas are used.

1.2 Problem Statement

Given that temperature and humidity at any given location vary throughout the day, 5G communication services seeking to exploit the mmWave/THz band must expect some sort of diurnal variation in attenuation and noise, even in the absence of any movement. Furthermore, the atmospheric channel conditions may also vary according to location at any given time, leading to faster channel variation for high-speed mobile users. Although there have been extensive studies to characterize mmWave channels under different weather conditions, little study has been made on

spatio-temporal variations. We believe that detailed knowledge of spatio-temporal variation in mmWave/THz attenuation and noise is important for designing higher layer protocols, systems, and services for 5G.

On the other hand, for a given number of transmitter and receiver antennas, the common understanding is that the MIMO capacity is not frequency selective if the received signal strength is fixed to a certain level. Such a conclusion has been validated in the sub-6GHz spectrum, *but does this conclusion still hold when we march into the mmWave spectrum in 5G or short range Tbps communication in the THz band?*

As discussed, the very high path loss at higher frequencies leads to LoS-dominated communication where the lack of scatterer reduces the possibility of spatial multiplexing. Hence, the focus research has been on beamforming, which aims to boost the SNR in contrast with throughput. A recent study shows that light rain can improve the multiplexing gain of MIMO channels in mmWave [13]. Conversely, in [11,12], the authors estimated molecular re-radiation with a multi-scattering model. Therefore, molecular absorption may be able to improve the channel environment scattering richness and boost MIMO capacity in the mmWave/THz band.

1.3 Contributions

Using the recently discovered molecular absorption models, this thesis conducts a theoretical study on the effects of molecular absorption and re-radiation on both single-antenna and multi-antenna wireless communication systems. The main contributions towards our objective are summarized as:

- For single-antenna communication, the study focuses on quantifying the temporal and spatial variations in attenuation and noise that result from variations in the molecular composition of the air. In particular, it investigates the extent of spatio-temporal variation in mmWave channels in the three largest cities of Australia by analyzing hourly air quality and weather data over 12 months. The study found that mmWave channels experience significant variations in

both space and time, which causes undesirable network capacity fluctuations in various times and places. Furthermore, for high-speed users, spatial atmospheric variation causes extra temporal channel variation which leads to significant link quality fluctuation.

- For multi-antenna communication, our new theoretical discovery is that MIMO capacity can be significantly influenced by atmospheric molecules. Specifically, some common atmospheric molecules, such as oxygen and water, can absorb and re-radiate energy in their natural resonant frequencies, such as 60 GHz, 120 GHz, and 180 GHz, which belong to the mmWave spectrum. Such phenomenon can provide equivalent Non-Line-of-Sight (NLoS) paths in an environment that is dominated by LoS transmissions, and thus greatly improve the spatial multiplexing and diversity of MIMO mmWave systems. This study also shows that MIMO performance can be frequency-selective, which is contrary to the common understanding of MIMO systems in existing microwave band communication systems.

- Finally, the performance of two main MIMO techniques, *beamforming* and *multiplexing*, in the both the millimeter and terahertz bands, is studied. Our results reveal a surprising observation that MIMO multiplexing could be a better choice than MIMO beamforming under certain conditions in multiple THz bands. In this way, high spectral efficiency can be achieved by resulted spatial multiplexing by molecules while it is not necessary to transfer Channel State Information (CSI) to the transmitter for beamforming. This helps to reduce system complexity and signaling overhead.

1.4 Dissertation Organization

The remainder of this thesis is organized as follows. Chapter 2 presents a literature review on the mmWave/THz communication channel, molecular absorption and MIMO concepts. The diurnal and spatial variability of a single communication channel is presented in Chapter 3 where we assumed the molecular re-radiation to

be noise. In Chapter 4, we investigate how the re-radiation of molecules in some frequency windows can boost the MIMO capacity by increasing spatial multiplexing. The comparative performance of MIMO techniques in the presence of molecular re-radiation is investigated in Chapter 5. The thesis concludes in Chapter 6, and finishes with proposals for future research directions.

Chapter 2

Background and the State of the Art

The need to connect everything, everywhere, and everyone results in a huge volume of data traffic among connected wireless devices in near future. It is expected to have 21 Billion *things* connected to the network by 2020 [14] which is known as *Internet of Things (IoT)*. However, the existing wireless communication technologies that employ frequency between 100 MHz to 10 GHz are heavily congested and almost close to the upper capacity limit. The only solution to overcome this limitation and provide ultra high capacity wireless communication is therefore to exploit higher frequency bands. Millimeter wave (mmWave) and terahertz (THz) bands ranges from 0.3 to 10 GHz could be potential candidates to serve this purpose as it has been recently proposed to be used in 5th and future generation of mobile networks (5G and 5G$^+$) [9, 15] and Gigabit/s WiFi (also known as WiGig) [16]. In spite of the mmWave/THz spectrum follow same electromagnetic propagation theory, there are various of frequency dependent characteristic in compare with conventional sub-6GHz spectrum. The higher free space path loss because of frequency, blockage, and molecular absorption make the channel different than what has been deeply investigated in microwave band.

2.1 mmWave and THz communication challenges

The huge bandwidth of mmWave is the main motivation to be considered as a part of 5G mobile network. Hence, some mmWave sub-bands have been interested in by research, such as 28 GHz, 38 GHz, 60 GHz and the E-band (71-76,81-86 GHz). In 60 GHz many theoretical and experimental works have been done [17–24] and the IEEE802.11ad is published as Gbps wifi standard [25]. A series of experimental studies also have been done on 28 GHz and 73 GHz in New York city for LoS and NLoS scenarios [26–30]. To overcome the high path loss in mmWave/THz beamforming and directivity of electromagnetic power is needed. Thanks to very small wavelength, electronically steerable arrays can be used at either of transmitter or receiver or both which with current technology can be implemented as patterns of metal on circuit board [31] or plasmonic transceiver which can generate, modulate and propagate signal in THz band [32]. Thanks to the large number of arrays beam can be steered toward the receiver electronically with a gain up to 55 dB [2] while the gain on other directions is much lower. However, the performance of formed beam is highly related to the information that the transmitter has from the channel state. Measuring and communication channel state information between transmitter and receiver cost the channel th signaling overhead [33]. In addition, the procedure of beam training and precoding add more complexity to communication system.

The diffraction of electromagnetic wave in mmWave/THz is significant because of very small wavelength. The measurement study in [34] showed in a room with 5 people there will be around 1-2% blockage in 60 GHz. Hence, the sensitivity of mmWave/THz band to blockage can dramatical reduce the communication reliability.

Wireless communication over terahertz band has been recently investigated for both nanoscale networking (due to the very small size of the nanoradio) [35, 36] and macroscale high-capacity short range wireless communication [7, 37, 38]. Although terahertz band is currently not widely used and the required device and circuit technologies are not matured, many attempts have been conducted to design efficient terahertz transceivers [39–41] and characterize the wave propagation in this band

[42, 43]. In one of the recent cases, researchers have developed a small transmitter, known as *T-ray*, which is able to transfer information in distances less than 3 meters at 3 Gbps (Theoretically up to 100 Gbps) in the frequency range from 300 GHz to 3 THz [39].

2.2 Absorption and Re-radiation in mmWave and THz channel

Wireless communication over higher frequency band such as mmWave and terahertz band is strongly affected by the molecular absorption noise and attenuation [7, 43]. Indeed, radio communication in these bands is affected by the chemical compositions of the medium (i.e., the existing molecules in the communication channel) in two different ways. First, the radio signal is attenuated because molecules in the channel absorb energy in certain frequency bands. Second, this absorbed energy is re-radiated by the molecules which creates noise in the channel.

2.2.1 Channel Modeling

This section first explains the concept of *absorption coefficient* used to characterize the absorption capacity of a given molecule species, followed by the attenuation and noise models that build on this coefficient.

2.2.2 Molecular Absorption Coefficient

The effect of a given molecule, S_i on the radio signal is characterized by its molecular absorption coefficient at frequency f, $k_i(f)$ which varies with pressure and temperature of the environment as well. The molecular absorption coefficients of many chemical species for different pressure and temperature are available from the publicly available databases such as *HITRAN* [44] and *NIST Atomic Spectra* [45]. Nevertheless, the atmospheric air as the communication medium, is a mixture of different gases and as we will see in Chapter 3, the mixing ratio of its constituent

gases may change in hourly basis. The pressure and temperature of the air are also variable. We, therefore, need to take these variations into account. In order to model these variations, we assume the mmWave radio channel is a medium consisting of N chemical species $S_1, S_2, ..., S_N$ and $m_i(t)$ is the mole fraction per volume, i.e., mixing ratio of molecule S_i in the medium at time t. We further assume that the temperature and pressure of the medium at time t is $\mathcal{T}(t)$ and $\mathcal{P}(t)$. The *medium absorption coefficient*, $k(t, f)$, at time t and frequency f is therefore a weighted sum of the molecular absorption coefficients in the medium [35, 46]:

$$k(t, f) = \sum_{i=1}^{N} m_i(t) k_{i,t}(f) \tag{2.1}$$

where $k_{i,t}(f)$ is the molecular absorption coefficient of species S_i in the given temperature, $\mathcal{T}(t)$ and pressure $\mathcal{P}(t)$ that can be obtained from HITRAN [44] and NIST [45].

2.2.3 Attenuation

The attenuation of the radio signal over mmWave is due to spreading and molecular absorption [7, 35]. The total attenuation at time t , frequency f and a distance d from the radio source, $A(t, f, d)$ is:

$$A(t, f, d) = A_{\text{spread}}(f, d) \times A_{\text{abs}}(t, f, d) \tag{2.2}$$

where A_{spread} and $A_{\text{abs}}(f, d)$ are respectively, the attenuation due to spreading and attenuation due to molecular absorption at time t , frequency f and a distance d from the radio source. The spreading attenuation is given as [47]:

$$A_{\text{spread}}(f, d) = \left(\frac{4\pi f_0 d}{c}\right)^2 \tag{2.3}$$

where f_0 is the central frequency and c is the speed of light and f_0 is the central frequency. The attenuation due to molecular absorption is given as [7]:

$$A_{\text{abs}}(t, f, d) = e^{k(t,f)\times d} \tag{2.4}$$

where $k(t, f)$ is the absorption coefficient of the medium at time t and frequency f. Many linear approximations for equation 2.2 have been proposed in the literature for different frequencies (in dB or dB/Km) [48]. For some high frequencies over Milliliter band, the ITU Radio communication Sector (ITU-R) provides various procedures to estimate specific attenuation due to the dominant molecules in the air (O_2 and H_2O) [49] which both can be easily derived from equations 2.3 and 2.4.

2.2.4 Noise

The receivers usually encounter with few types of noises including the thermal noise (N_{Thermal}) generated by the thermal agitation of the charge carriers; electronic noise (Elec) from receiver input circuits and ambient noise from the environment. The ambient noise in the higher frequencies channel is mainly originated by the molecular absorption noise (N_{abs}) which is due to re-radiation of the absorbed energy by the molecules in the channel [7, 43]. The total noise power at the receiver therefore is:

$$N_{\text{mmWave}} = N_{abs} + N_{\text{Thermal}} + N_{\text{Elec}} + N_{\text{Others}} \tag{2.5}$$

where N_{Others} is the noise from other probable sources. N_{thermal} and N_{Elec} depend on the receiver's technology in use. However, there are some promising evidences that point to the future generation of antenna (such as Graphene-based transceivers) which has a very low thermal noise that means molecular noise is expected to be the dominant source of noise in future nanomaterial-based receiver systems [43].

The molecular absorption noise has been studied in the literature since 1986 when F. Box proposed a model for sky atmospheric noise for frequencies higher than 18GHz [50]. There are a number of works that have studied the atmospheric noise for higher frequencies (mainly Millimeter waves) such as [51] which experimentally measured the atmospheric noise variation in Mauna Kea in Hawaii over many night and days using a 143 GHz and 268 GHz transmitter. Recently the molecular noise

has been re-considered for mmWave and terahertz band [7,43]. Molecular absorption is not white and its Power Spectral Density (PSD) is not flat because of the difference in the resonant frequency of different molecules.

There are two main models for molecular absorption noise in the literature. The first noise model assumes that the magnitude of the noise is not influenced by the amplitude of the transmitted power, so the molecular noise PSD, $N_{\text{abs}}(t, f, d)$, is given by: [52, 53]:

$$S_{N_{abs}}(t, f, d) = k_B T_0 (1 - e^{-k(t,f)\times d}) \tag{2.6}$$

where T_0 is the reference temperature $296K$ and k_B is the Boltzmann constant. In the second noise model, recently proposed in [10, 50, 54], it is assumed that the intensity of the transmitted power affects the noise, therefore different transmitted powers create different levels of noise in a given condition. Based on this noise model, the PSD of the molecular absorption noise that affects the transmission of a signal X, $S_{N_{abs}}$, is contributed by the atmospheric noise, S_N^B and the self-induced noise, S_N^X as [50, 54]:

$$S_{N_{abs}}(t, f, d) = S_N^B(t, f, d) + S_N^X(t, f, d) \tag{2.7}$$

$$S_N^B(t, f, d) = lim_{d\to\infty}(k_B T_0 (1 - e^{-k(t,f)d}))\left(\frac{c}{\sqrt{4\pi} f_0}\right)^2 \tag{2.8}$$

$$S_N^X(t, f, d) = U(t, f)(1 - e^{-k(t,f)d})\left(\frac{c}{4\pi d f_0}\right)^2 \tag{2.9}$$

where $k(t, f)$ is the absorption coefficient of the medium at time t and frequency f; f_0 is the central frequency; T_0 is the reference temperature ($296K$); k_B is the Boltzmann constant; $U(t, f)$ is the PSD of the transmitted signal at time t and frequency f; and c is the speed of light.

In this study, we use the second noise model. However, using the first noise model will not affect the contributions and the overall results.

2.2.5 Channel Capacity

Let $U(t, f)$ be the power spectral density of the transmitted radio signal at time t and frequency f. The signal-to-noise ratio (SNR) at time t, frequency f and distance d is:

$$\mathrm{SNR}(t, f, d) = \frac{U(t, f)}{A(t, f, d) S_{N_{abs}}(t, f, d)} \tag{2.10}$$

Consider a radio channel consisting of two nodes separated by a distance d, then at time t, the Shannon capacity over a sub-channel from B_1 to B_2 Hz is:

$$\mathrm{Capacity}(t, d) = \int_{B_1}^{B_2} \log_2(1 + \mathrm{SNR(t, f, d)})\mathrm{df} \tag{2.11}$$

2.3 Atmospheric Effects on Wireless Communication Channel

several studies investigated atmospheric conditions effects on the channel [1, 13, 55, 56]. The real measurement of rainfall attenuation in Madrid, Spain has been done in [1] and showed the rain attenuation can dominate other atmospheric effects on the channel for frequency below 90 GHz. a 24 hours graph, Figure 2.1, of rain attenuation over a 840 m distance is shown in their work for two different days. The work in [55] focused on the effects of the atmosphere and weather on the channel and showed the radio waves above 10 GHz is significantly influenced by molecular resonance and precipitation. Millimeter-wave communication can experience high attenuations in the presence of heavy rainfall [57] which is modeled and evaluated in [13]. They found low rainfall can increase capacity because of positive effect on antenna performance. In more details, the raindrops can act as scatterers and improve the MIMO multiplexing gain. However, they also showed when the rain rate increases, the attenuation of water-drops dominate the scattering effects and capacity will be lower for heavy rain.

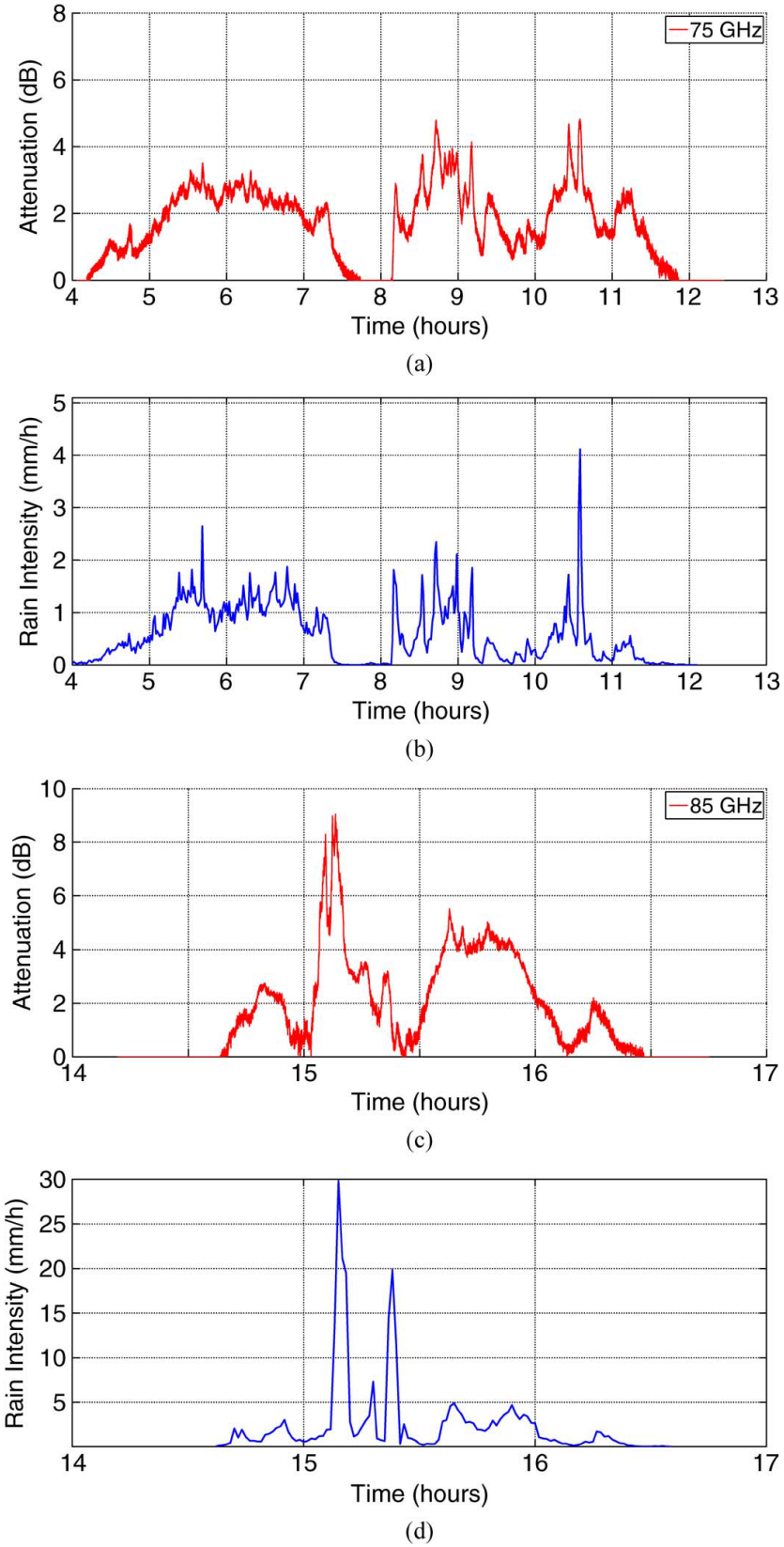

Figure 2.1: measured rain attenuation at 75 and 85 GHz in Madrid, Spain. a and b belongs to a low humidity day while c and d shows the data for a very humid day [1].

2.4 Channel Variation for High Speed Users

Today, many of people spending part of their daily time in intraurban traveling by cars, buses and high-speed trains. Australian government report shows 90% of Australians spend more than 90 minutes for commuting to work daily [58] and the demands for broadband Internet access is not negligible for such a users. Furthermore, the traffic demand is also growing every day where the around 75% of all devices connected to the mobile network will be *smart* in 2021 [5]. In this way, the application of smart devices is not limited to conventional voice and text communication or web browsing. The same forecast report shows the video will consume more than three-quarter of mobile data traffic in 2021. Applications such as video streaming, online video games, virtual reality (VR) might require a high-speed data link where the stability and availability is a key factor to satisfy users.

As vehicles are supposed to be an integrated part of the future generation of the wireless communication such as $5\,G^{+}$ [15], mmWave/THz vehicular communication can play an important role in the cellular network. For instance, vehicles can act as mobile base stations to eliminate the network coverage holes [15] or serve at the temporal occasions that require high capacity links (e.g., sports matches). In addition, it could be used for future road-vehicles [59] where high-resolution real-time data/images/videos need to be exchanged with the infrastructure and with other vehicles for different purposes such as safety, fuel efficiency, and traffic prediction. To this end, recent works have been done for mmWave/THz vehicular communication [9,60,61]. Besides, The mmWave/THz communication is also proposed for smart rail mobility where several management and surveillance information such as HD video in combination with broadband Internet for passenger should be communicated among infrastructure, wagons and trains [62].

The wireless communication faces with several difficulties which are coming from the nature of electromagnetic wave propagation. While several characteristics of the signal including amplitude, phase, and frequency are used to carry the information, each of them can be corrupted because of multi-path propagation, shadowing, blockage, weather and so on. The problem is more intensive when the receiver changes

its position constantly. In this case, Since the distance is changing the signal attenuation also will be variable. On the other hand, Doppler effect also is another challenge for mobile wireless communication. The higher speed of transmitter or receiver, there would be more challenges in the wireless channel. While such challenges are well studied for microwave transmission, there is a different channel model and characteristic for mmWave/THz band [9]. For example, to overcome very high path loss in this band, beamforming is proposed as a major solution, but it is sensitive to mobility and the direction of transmit power need to be steered regards to the receiver location.

Location-dependent channel characteristics, such as path loss and fading, affect the signal quality received by the receiver. Current communication technologies use adaptive power adaptation and coding scheme to keep the bit error rate (BER) acceptable. In this way, the reliability or alternately the received bit error rate (BER) can be guaranteed at the cost of losing bit rate. Thus, Any significant spatio-temporal channel variation for high mobility users results in fluctuation in available bit rate and affects the quality of service (QoS) experienced by users [63]. Along with network infrastructure planning to improve coverage [64], some techniques in a higher level such application layer is also proposed to have a bandwidth map [63, 65, 66]. Such spatio-temporal bandwidth map can be used by applications to exploit high bit rate locations and mitigate the data rate drops in the rest of area during a trip. For example for video streaming, it can provide better user experience in video playing by providing higher quality and less video "freezing" [67, 68].

2.5 Multiple Input Multiple Output (MIMO) in mmWave and Terahertz Communication

Multiple-input-multiple-output (MIMO) paradigm has been an important research topic in communication area for the last two decades. The main idea is to co-locate multiple antennas to send multiple copies of data or divide the data to multiple streams. The former one is known as diversity which results in reliability and the

later one is called multiplexing [69] which aims to increase the throughput. In spite of the simple idea of MIMO there are several challenges in MIMO communication which have been deeply investigated in the literature.

Boosting the capacity through multiplexing is efficient when independent multipath signal components deliver information to the receiver. In this way, the channel environment should be rich in term of scattering and it results in a random independent channel gain for each pair of antennas in the transmitter and receiver [70]. The channel randomness is reflected as the degrees-of-freedom which can be in the range of one to the minimum of antenna number on either of the transmitter or the receiver [71]. The Later channel is refered as full rank [69] where there can be equivalently a maximum possible parallel information sub-channels. In addition to the rank, the channel also should statistically well-conditioned [72].

The richness of scatterer can be characterized by the ratio received power from main signal source to the received power from scatterers which is called the Rician K-Factor [73]. The total strength of multipath rays can be very smaller than line-of-sight (LoS) signal, which is a LoS dominated channel and the received signal at receiver antenna are highly correlated. The degrees-of-freedom for such a channel is one and almost no multiplexing gain can be achieved. The LoS MIMO can have full rank channel matrix for some specific inter-element antenna spacing, angles, and distances [74]. However, for mobile communication, the channel distance and array angles are variable and therefore for LoS scenarios the multiplexing gain hardly can be achieved.

The channel is called Rician where both non-line-of-sight NLoS and LoS components are non-negligible. In such a case, there is a level of randomness in the channel which improves the channel multiplexing gain [75]. For a very large K-Factor channel is LoS dominated as we discussed above and in contrast, for very low K-factor close to zero, the channel is highly random which usually is referred as Rayleigh when the channel transfer function elements are independently and identically distributed complex values [76].

The other key factor in the efficiency of diversity or multiplexing gain is SNR. At low SNR, the multiplexing approach provides little benefit because the transmitter

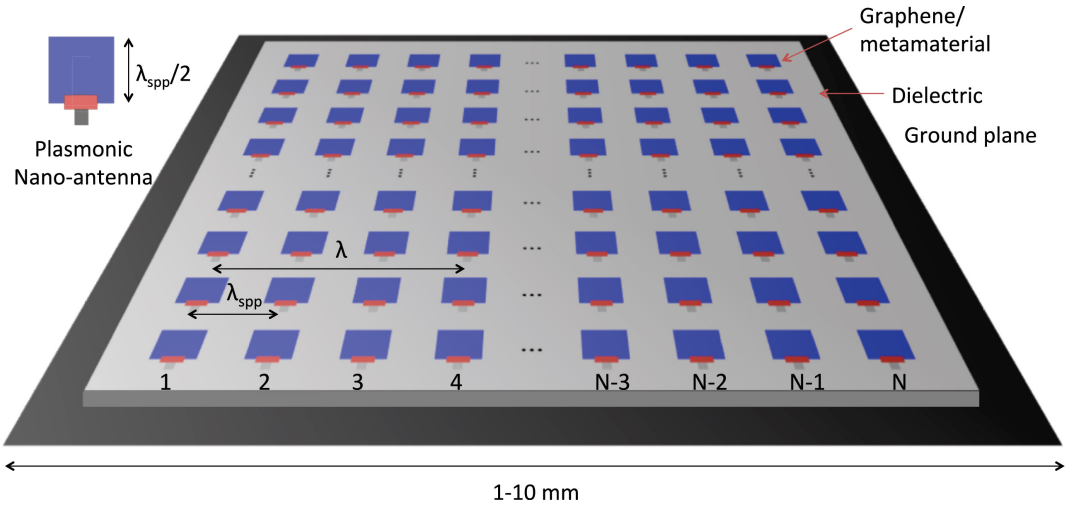

Figure 2.2: A square uniform plasmonic nano-antenna array. [2].

split the power to multiple streams. Alternately, the MIMO can be used as a beamformer. In this way, the spatial diversity helps to focus power toward the receiver to mitigate the path loss and reduce co-channel interference [77]. It also is more practical in lack of scatterer when the channel is rank-deficient and multiplexing gain is dramatically poor.

Along with emerging demands for communication in new spectrum such as mmWave and THz bands in recent years, MIMO is envisioned as one of the key players. mmWave/THz band suffer from very high propagation loss on the one hand and power limitation of transmitters on the other hand which results in much shorter communication distance than conventional sub-6GHz communication [7]. Hence, MIMO is a major candidate to enhance communication distance and capacity in the mmWave/THz bands. One of the benefits of the mmWave/THz band is a wide unused spectrum in comparison with very crowded microwave band. Hence, it is more power limited than bandwidth limited [77] and beamforming sounds to be more effective and most of the research is focused on beamforming rather than multiplexing [2, 78, 79].

The very small wavelength in higher frequency is a key advantage to place a large number of antennas in a relatively small footprint. The recently developed metamaterial can support the propagation of Surface Plasmon Polariton (SPP) waves where since the electromagnetic speed is much lower than free space the wave length is

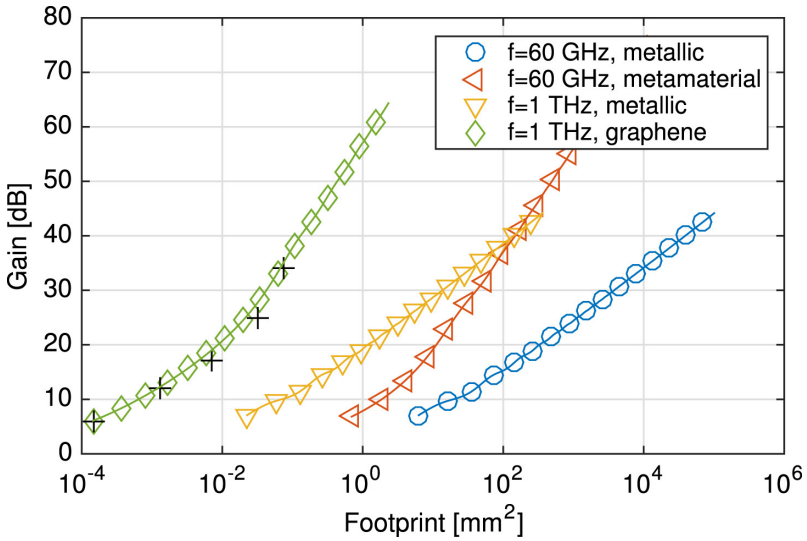

Figure 2.3: Gain of metallic and plasmonic nano-antenna arrays at different frequencies as a function of their footprint [2].

much smaller than same frequency free-space wavelength [80]. Thanks to the very small wavelength, hundreds of plasmonic antennas can be placed in a few square centimeters, 2.2, for example, 144 elements in 1 cm^2 at 60 GHz [2]. In this way, a huge beamforming gain up to 55 dB can be achieved with ultra-massive MIMO as shown in Figure 2.3

2.6 Summary

In recent years, research trends in employing mmWave and THz band is drastically increased to respond to the huge bandwidth demand in the wireless networks. Currently, the focus is on using the mmWave band for 5G, IoT and wireless LAN, where various frequency windows are being investigated to characterize the propagation model and to design the required protocols in the upper layers. The standardization of 60 GHz wifi (IEEE 802.11ad) is finalized and some commercial products are available in the market. However, the measurement equipment sets are still expensive and a small portion of studies are based on the realistic measurement. For the spectrum above 100 GHz, experimental studies are even far fewer than 30-100 GHz due to hardware cost and measurement difficulties. Extended applications of mmWave/THz such as IoT, wearable sensors, localization, and vehicular communi-

cation also have been proposed but, there is still a long way of standardization and implementation. Among the wide area of the higher frequency spectrum challenges, the molecular absorption is also one of the interesting topics since it was negligible in conventional sub 6 GHz communication. Most of the related works have studied the effect of atmospheric conditions like fog and rain on mmWave communication and older research mostly are about long-distance propagation such as radars and satellite. In spite of well-known theoretical model on molecular re-radiation, this phenomenon is not investigated in literature sufficiently, especially by experimental studies. To our knowledge, no existing research has studied the effect of re-radiation of molecules on MIMO systems. Therefore, in Chapters 4 and 5, we show how the molecules can play scatterer role and influence MIMO performance. Moreover, the molecular absorption is characterized by the absorption coefficient of the channel which is related to temperature, pressure and mole fraction of various gas molecules in the air. Since these parameters are variable during the day and across cities, the communication channel will also fluctuate. To the best of our knowledge, the spatial-temporal variation of mmWave/THz channel has not been studied. For this purpose, we investigate the diurnal and spatial channel variation of a single channel in Chapter 3. Finally, we acknowledge that the theoretical study is necessary but not sufficient to verify our discovery. The experimental study is the subject of future works.

Chapter 3

Spatio-temporal Channel variation in the mmWave and THz band

The mmWave/THz spectrum suffers from two main problems. First, the path loss in this band is significantly high due to high spreading loss and molecular absorption attenuation. This makes the long-range communication almost impossible which necessitates to deploy many small base stations in the back-haul. The remedy to this high path loss problem could be the use of high-power sources, efficient detectors and high gain antenna systems [81]. Second, this band coincides with the natural resonant frequency of many existing molecules in the air which can be potentially a new source of degradation in the channel. This happens when excited molecules absorb a fraction of the radiated energy (a new source of path loss in the channel) and start to re-radiate the absorbed energy (a new source of noise). This phenomenon that is called 'molecular absorption' is frequency sensitive and influenced by the composition, pressure and temperature of the medium.

It is well-known that the atmospheric conditions (air composition, pressure and temperature) in the urban areas could have some temporal and locational variations due to mainly climate change, the production of pollution, the modification of physical and chemical properties of the atmosphere, and the covering of the soil surfaces [82]. For example, due to forming *urban heat islands*[1] (Figure 3.1) the temperature

[1]Urban heat islands are defined as the "warm island" (due to rise in temperature of any man-made area) among the "cool sea" represented by the lower temperature natural landscape [82]

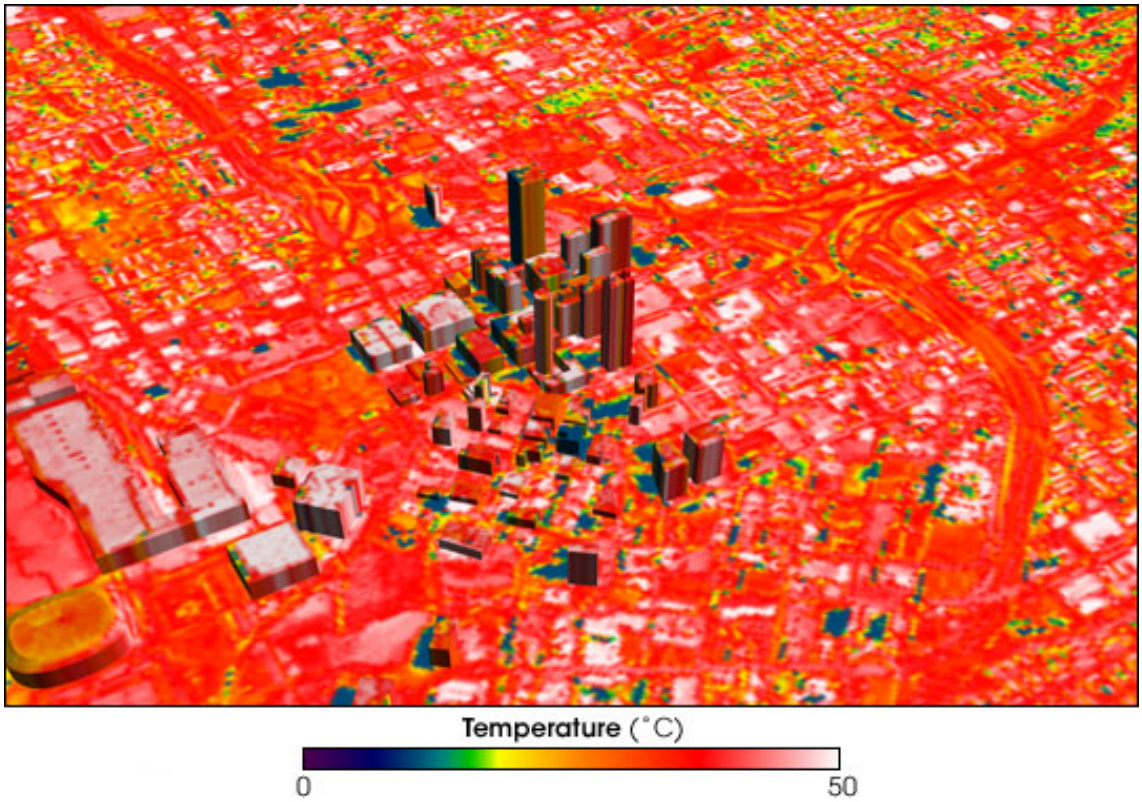

Figure 3.1: Urban heat islands in Atlanta on May 11-12 1997, was captured by NASA While the city's temperature was reported as 26.7 degrees Celsius, some of its surface temperatures soared to 47.8 degrees Celsius [3].

can potentially varies in different location at the same time. Wireless communication systems seeking to exploit mmWave and higher bands therefore may experience some sort of temporal and spatial variations in molecular attenuation and noise. As a result of this temporal and locational variation, the quality of communication link is expected to be variable specially for high speed mobile users across the urban area.

In this chapter, we study the spatio-temporal channel variation of mmWave and THz communication in three largest cities of Australia. The aim of this chapter is to explore the extent of channel variations that could be expected for channels during clear days in typical cities around the world. To achieve this, we apply well-known molecular absorption models to the air quality and weather data over 12 months in 2015/16 collected in three largest cities in Australia. First, We find that even if there is no rain, there can be significant temporal variation in both attenuation and noise

between two communicating devices. The attenuation and noise generally drop in the middle of the day when temperature rises and humidity falls, but remains high during the night. The diurnal variation is found to be more significant in summer compared to winter. Secondly, considering weather data of 273 stations across the city of Sydney, we find a significant difference in channel state among suburbs. We simulated several urban travels and the results show the spatial channel variation causes a notable fluctuation in channel capacity which will affect the high speed mobile user experience.

The rest of the chapter is structured as follows. The details of the air quality data are described in Section 3.1. Section 3.2 analyzes temporal and locational channel variations by applying the channel model to the air quality data. We simulate and discuss how the spatio-temporal variation effect high speed mobile users before we summarize chapter in Section 3.4.

3.1 Air Composition and Atmospheric Data

In Section 2.2.1, we have shown how the mmWave/THz channel is affected by the molecular composition of the communication medium. In the vehicular communication, the channel consists of normal air. In order to characterize the communication channel, the composition of the atmospheric air therefore needs to be investigated. The aim of this section is to study the composition of the atmospheric air in urban areas, mainly three big cities in Australia (Sydney, Melbourne and Brisbane). Note that the rainfall effect on the channel is out of scope of this work, so we do not present rainfall information as well as fog and snow. Therefore, in this thesis we only investigate clear days.

3.1.1 Air Composition Characterization

The major elements of the atmospheric air are nitrogen (78%), oxygen (about 21%) and other gases such as argon, helium, neon and carbon dioxide (totally less than 1%) [83]. Water in the form of moisture also exists in the air which is highly variable,

more commonly ranging from 0.2-3%. Ambient air composition is also affected by the air pollutants mainly ozone (O_3), nitrogen dioxide (NO_2), sulfur dioxide (SO_2), CO and Particulate Matter (PM), a general term that used for a mixture of solid particles and liquid droplets suspended in the air [84]. PM is characterized according to size, $PM_{2.5}$ and PM_{10} stand particles that are less than or equal to 2.5 and 10 microns in diameter, respectively.

Figure 3.2 and 3.3 show the absorption coefficient of the main constituent species of the normal air over 30 to 300 GHz and 0.3 to 10 THz[2]. The average absorption coefficient over 30 to 300 GHz for each molecule has been mentioned in its title. While the absorption of the nitrogen is almost zero, vapor, PM and SO_2 have the highest absorptions, respectively with 3.77, 1.28, 0.18 cm^{-1}. The molecular absorption of few constituent gases over mmWave frequencies are almost zero that includes argon, helium, neon and carbon dioxide [45].

Figure 3.4 shows the overall absorption coefficient of the Sydney Rozelle air over frequency range of 30 GHz to 300 GHz at 1am (11 Dec 2015) which has been calculated from equation 2.1 using the mole fractions of time equal to 1am, extracted from Figure 3.6(b). We also show the contribution of each individual constituent gas in the total absorption of the medium ($m_i \times K_i(f)$). As it can be seen, the water vapor and oxygen are the main effective molecules. Particulate matters, O_3 and SO_2 are the next contributors and the N_2 has the lowest contribution. Based on Figure 3.4, it seems that by only using the mole fraction of the water vapor the absorption of the channel can be estimated which is because the contribution of other species are relatively very low. In order to investigate this, for a given temperature and pressure of 20°C and 1 atm, we calculate the absorption coefficient of the air only using vapor (1%) and compare it with its counterpart when we included all constituent molecules in the air (Figure3.4).

We plot similar graph for THz band in Figure 3.5. As can be seen, water molecules are main absorption source in normal air over THz band.

[2] There is no absorption coefficient for PMs in HITRAN and NIST. Instead, as PM in Sydney are mainly composed of organic matters (46%), sea salt (20%), inorganic aerosol (15%), dust (9%) and elemental carbon (10%) [84], we use the absorption coefficient of available inorganic matters (HNO_3, NH_3), organic matter (CH_4) and chloride species (NCL, HOCL, CH_3CL) to approximate the absorption coefficient of PM in Sydney.

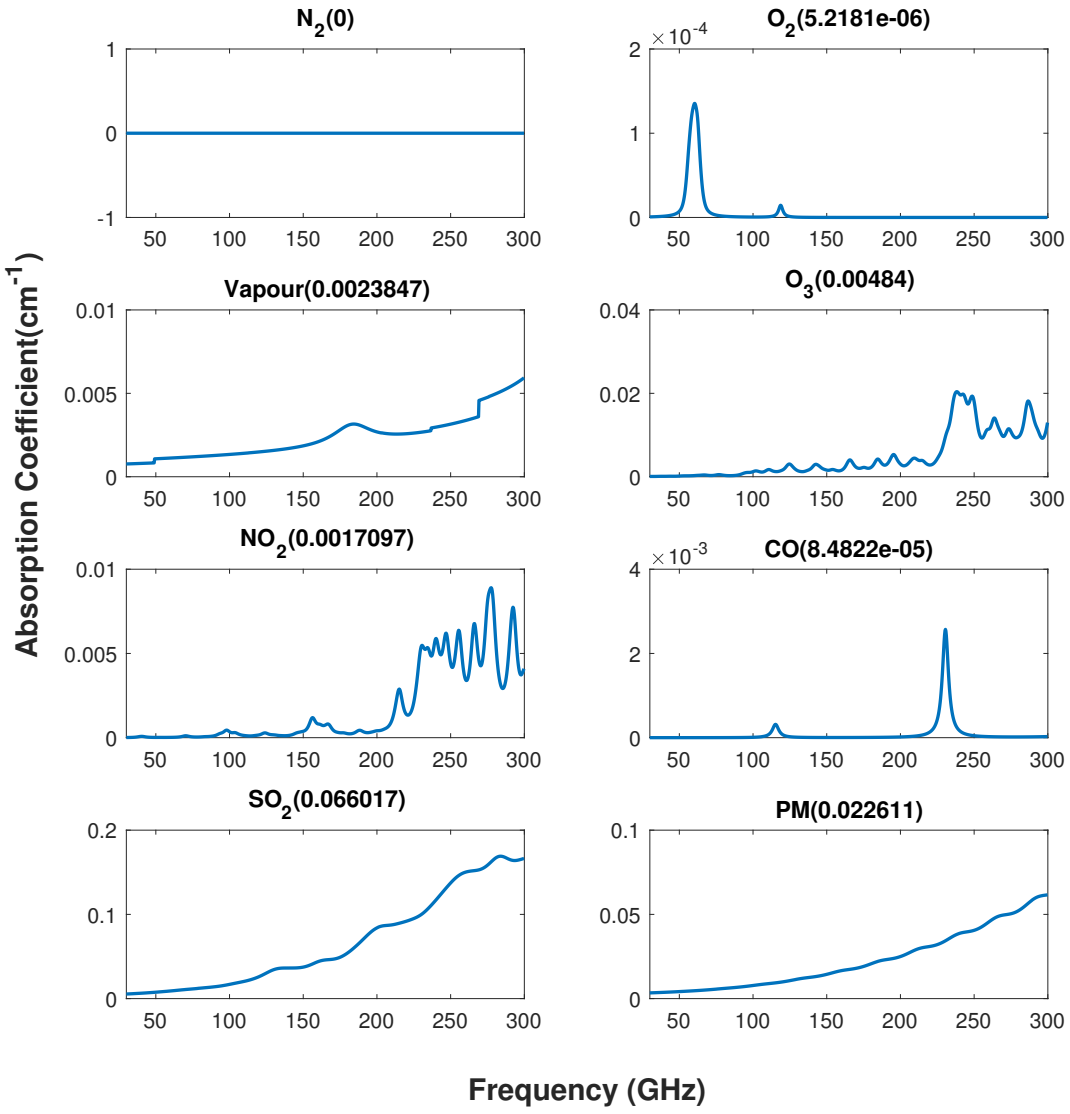

Figure 3.2: Absorption coefficient of the main constituent element of the normal air over mmWave ranging from 30 to 300 GHz.

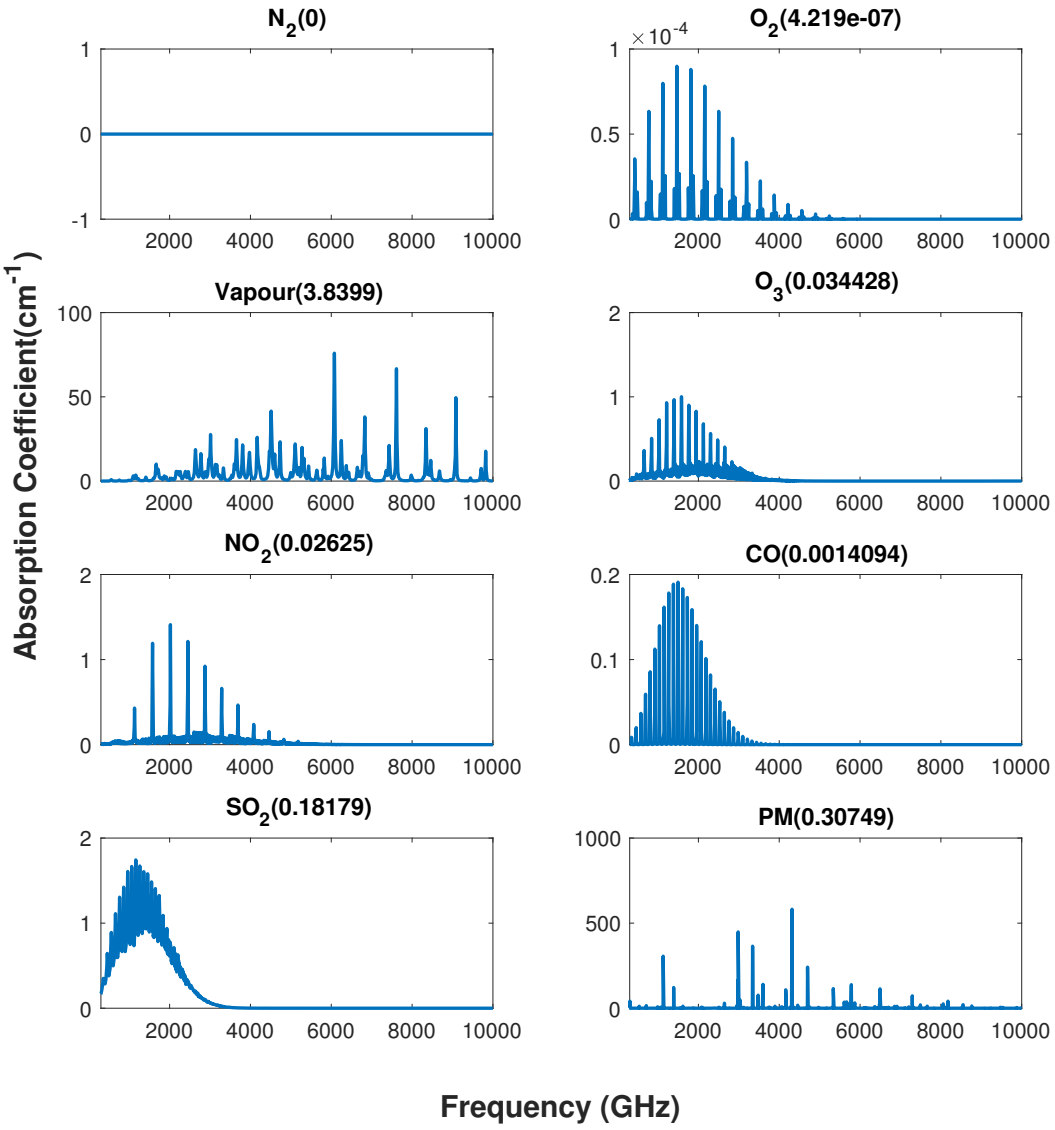

Figure 3.3: Absorption coefficient of the main constituent element of the normal air over 0.3-10 THz.

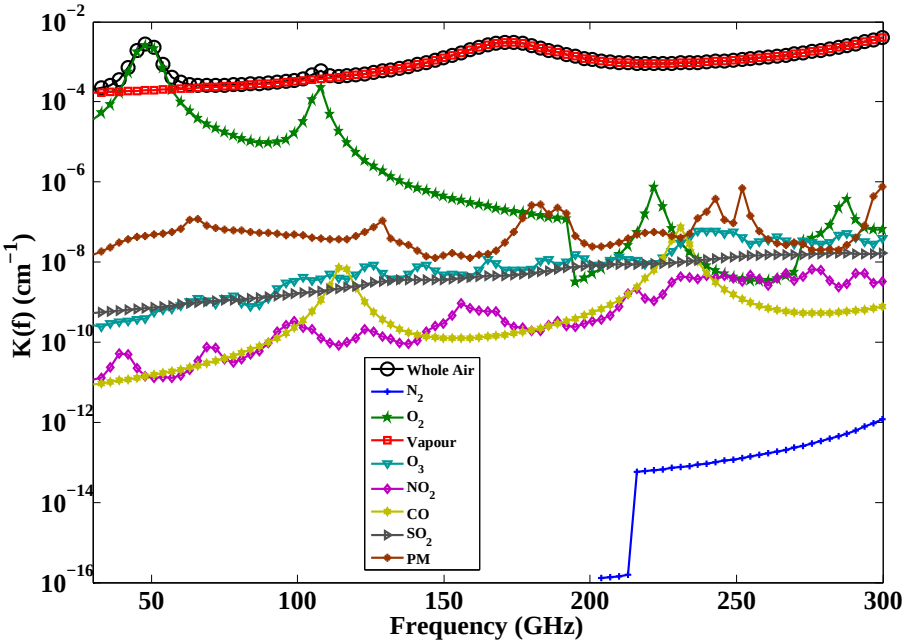

Figure 3.4: Absorption spectrum of the normal air (black curve marked by circles) over mmWave and the contribution of its constituent elements in atmospheric temperature/pressure of 21°C/1.009 atm.

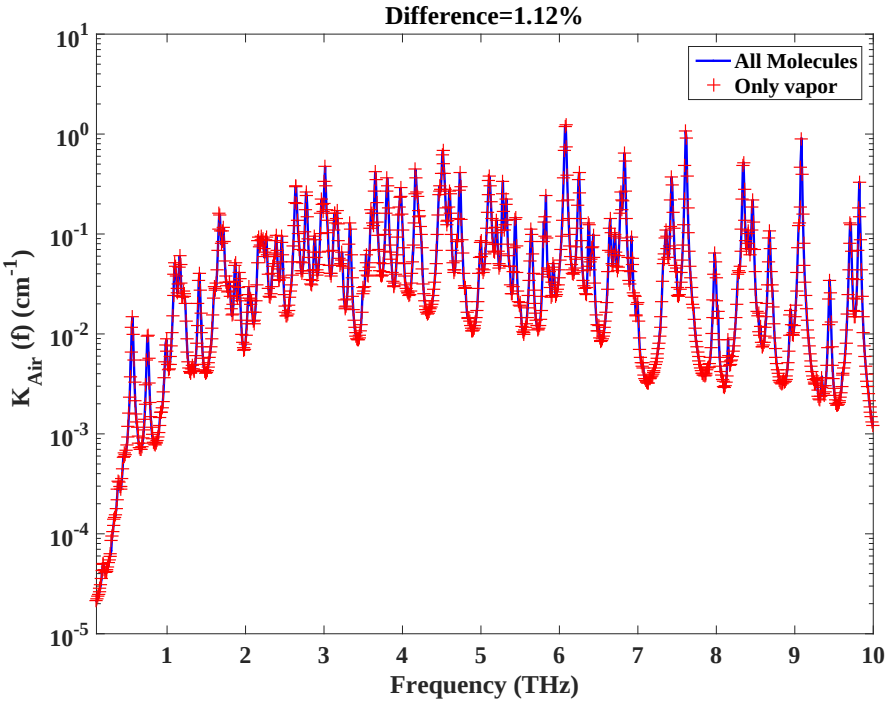

Figure 3.5: Absorption coefficient of the normal air considering all types of constituent molecules and approximated by only vapor. The difference is around only 1%.

3.1.2 Variation in the Air Composition and Condition

While the concentration of the main air components (nitrogen and oxygen) are almost constant, the concentration of some components such as water vapor and air pollutants are variable and depends on the location, time and atmospheric conditions, i.e., temperature and pressure. The air quality station in the cities (such as the one for Sydney [85]) provides hourly air quality data including the concentration of: Ozone O_3 in pphm[3], nitrogen dioxide NO_2 in pphm, carbon monoxide CO in ppm[4], sulfur dioxide SO_2 in pphm and particles PM_{10} and $PM_{2.5}$ in $\mu g/m^3$. Since in equation 2.1 the molar fractions (relative amounts) of these gases in the air are used to calculate the absorption, all the values need to be converted to the relative amount. ppm and pphm are in the ratio form where $1ppm = 0.0001\%$ of mole ratio [86]. To calculate the equivalent molar fraction of $\mu g/m^3$, the ideal gas law, $P_p = \frac{nRT}{V}$, is used where P_p is partial pressure of selected gas, $\frac{n}{V}$ is absolute gas concentration in *mole per volume*, T is temperature in *kelvin* and R is the ideal gas constant [5]. By using the Dalton's law [87], mole fraction will be partial pressure to the total pressure ratio.

In order to analyze the channel, the variation of water vapor mole fraction and atmospheric conditions including temperature and pressure are also required. The last two not only are required to convert gas concentration to mole fraction but are also used to extract absorption coefficients from available databases. This supplementary data have been provided through online available weather databases such as [88, 89]. The amount of vapor in the ambient atmosphere in these databases are presented in form of relative humidity. Relative humidity is the ratio of the partial pressure of water vapor to saturation vapor pressure at the same temperature. The saturation vapor pressure (P_s) in pascal can be achieved by $P_s = 610.78 \times \exp\left(t/(t+238.3) \times 17.2694\right)$ [90] where t is temperature in $^\circ C$. Our data also include the oxygen mole fraction which is almost constant in dry air (20.946%) but we recalculated it for the moist air from Dalton's law based on the moisture mole fraction [86].

[3] parts per hundred million
[4] parts per million
[5] $8.314 J/mol$

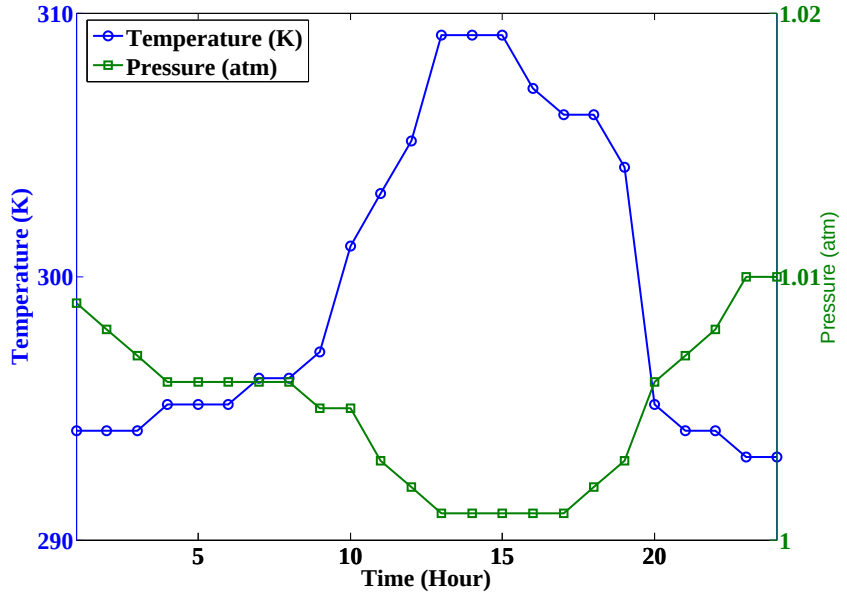

(a) Temperature/pressure

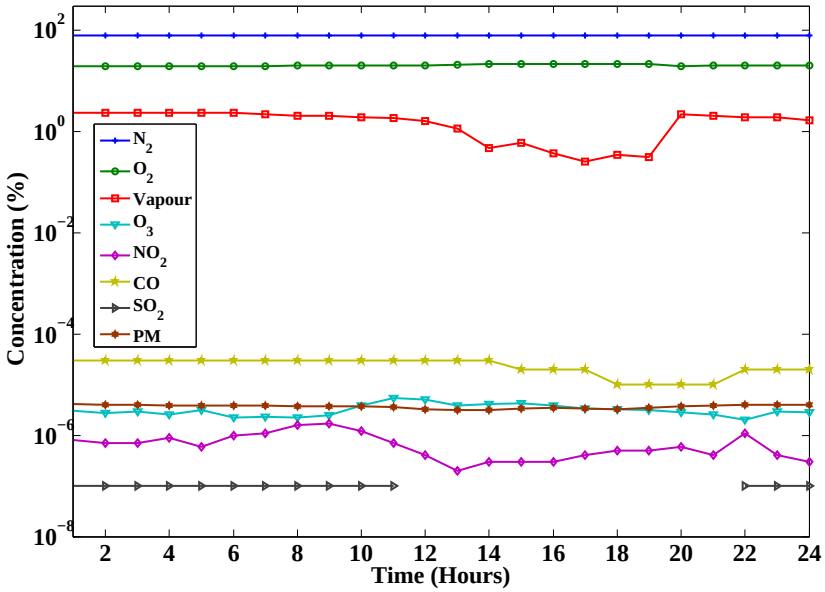

(b) Mole fraction variation

Figure 3.6: Atmospheric variation (air composition, pressure and temperature) in Sydney/Rozelle weather station on 11 of Dec 2015.

Figure 3.6(b) presents our collected data for one station in a particular date (Sydney, Rozelle on 11 Dec 2015) which includes the mole fraction of the main constituent components of the air. While mole fraction of oxygen is almost steady, water vapor as the other important component varies significantly. The corresponding temperature-pressure is also presented in Figure 3.6(a) for the same day and location which shows the temperature and pressure vary respectively by 16°C and 10 hPa (0.0001 atm) during 24 hours.

We also investigate the spatial variation in atmospheric conditions and vapor mole fraction. In this case, we obtain weather data from 273 stations across the Sydney available via an online database [89]. Our data shows about 8°C maximum temperature difference across Sydney at 1:30 pm, 28 January, 2016. We also extract the mole fraction of the water vapor from these 273 stations for the same date/time and as it can be seen from Figure 3.7, the vapor mole fraction varies between 0.018 and 0.03 that is more than 65% variation.

In the next section, we show how the temporal fluctuation and the spacial variation of the atmospheric conditions and vapor mole fraction can cause variation in communication channel.

3.2 Channel Variation Evaluation

As we have seen in Section 3.1, the air composition and atmospheric condition (temperature/pressure) have temporal(diurnal) and spatial(locational) variations. The communication channel, therefore, is expected to experience both temporal and spatial variations which not only affect the probable cellular communication but also significantly affects the high speed mobile users communication in this band. This section aims to study these channel variations using hourly air quality and atmospheric data from different stations in several cities .

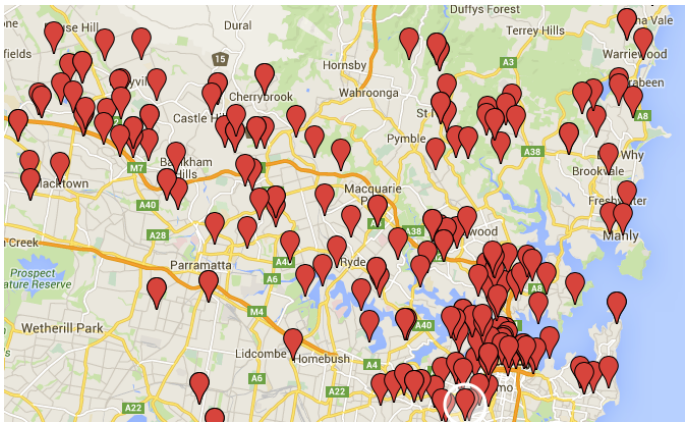

(a) Stations location, Map of Sydney

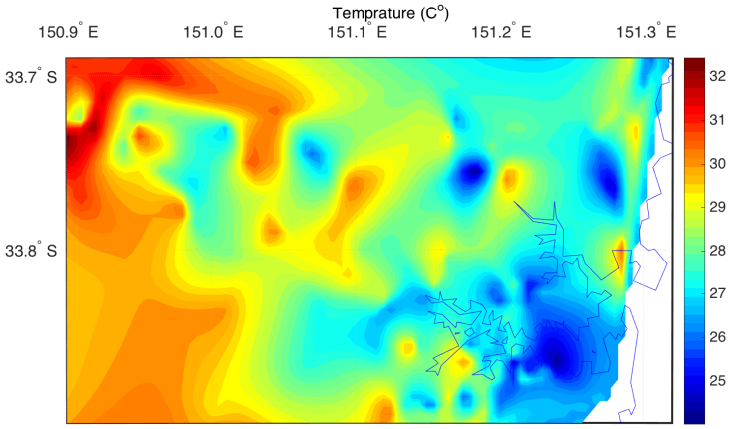

(b) Temperature (C)

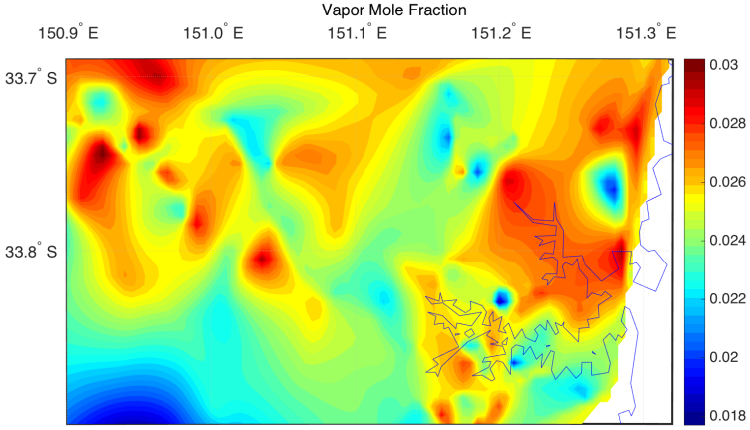

(c) Vapor mole fraction

Figure 3.7: The spatial variation of the temperature and the mole fraction of vapor in Sydney on 28th January (1:30 pm).

3.2.1 Methodology

We consider the three largest Australian cities, Sydney (Rozelle and airport), Melbourne (airport) and Brisbane (airport). We study each location over all months in 2015. For each location/day, we follow the procedure of Section 3.1 to extract hourly data for temperature, pressure and air composition from the publicly available air quality and weather stations located around. For each particular location/-date/hour, we then extract the absorption coefficient of the constituent molecules for the given pressure and temperature of that hour from online available HITRAN database. Finally, we plug in the absorption coefficient of each gas and the gas mole ratio to the the channel model explained in Section 2.2.1, we calculate the total absorption coefficient, attenuation, molecular noise and link capacity for the five frequency windows, 38, 60, 73, 150 and 250 GHz each with 1 GHz wide. These bands have been highlighted in the literature as the most promising sub-bands over mmWave and THz due to their lower absorption[7]. In summary, we used real measured atmospheric data and the experimental absorption coefficient of each molecule from public sources and calculate channel characteristic using the theoretical model [7, 10–12, 35, 46, 80]. Note that we consider an open space communication channel. The effect of possible existing objects in communication environment such as buildings is not in our scope.

3.2.2 Temporal Variation

First, we present the results for one city, Sydney (Rozelle station on 11 Dec 2015) for a fixed distance of 100m assumed between transmitter and receiver to gain insight to diurnal variations of weather and its impact on the channel performance. Figure 3.8(a) shows that the moisture varies between 0.2% and 2.3% and the temperature varies between 20° C and 36° C throughout the day. Figures 3.8(b), 3.8(c) and 3.8(d) show the impact of temperature and humidity variation on the channel quality over the five low absorption sub-bands.

It can be observed the channel quality varies noticeably during the day over all selected sub-bands, as the molecular absorption (Figure 3.8(b)) changes by a factor

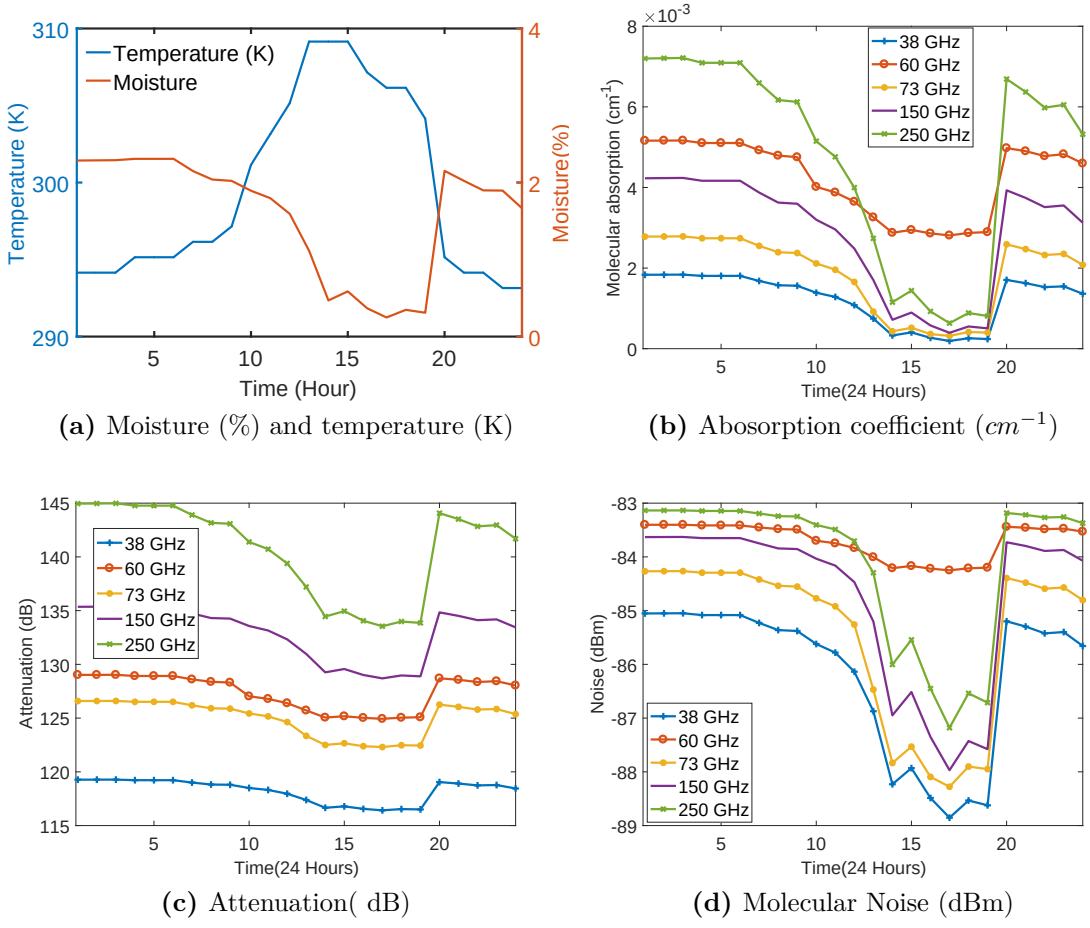

(a) Moisture (%) and temperature (K)

(b) Abosorption coefficient (cm^{-1})

(c) Attenuation(dB)

(d) Molecular Noise (dBm)

Figure 3.8: Diurnal channel status in Sydney (Rozelle) on 11 Dec 2015.

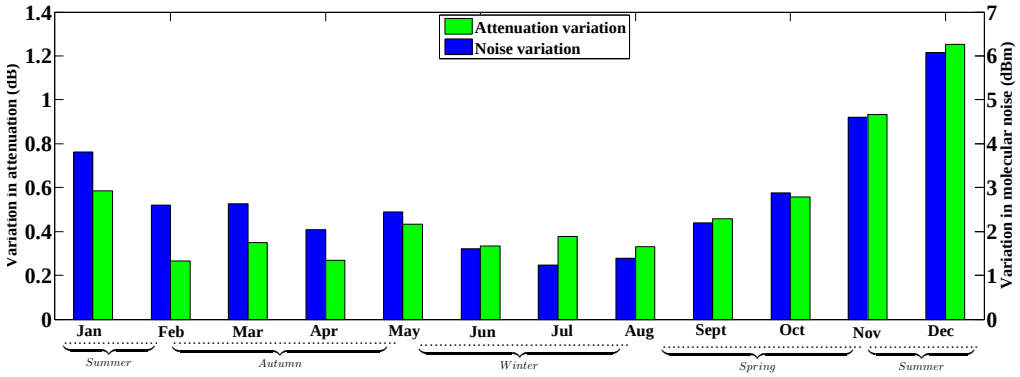

Figure 3.9: Annual channel variation of 250 GHz in Sydney, 2015.

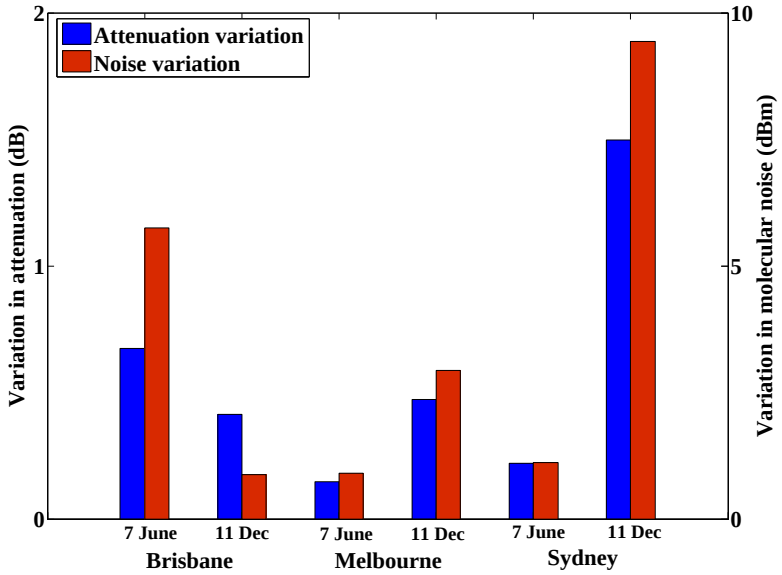

Figure 3.10: Maximum molecular noise and attenuation variation of two selected days for different cities of Australia, 2015

of 6 on average over these sub-bands. This variation in molecular absorption leads to an attenuation variation of 2 dB at 38 GHz and 10 dB at 250 GHz. Molecular noise also drops 4 dBm at the noon at 38 GHz sub-band while the maximum variation is only 1 dBm at 60 GHz(Figure 3.8(d)) where absorption at this frequency is mostly influenced by Oxygen and is less sensitive to vapor variation.

In order to investigate the diurnal variations over different seasons, Figure 3.9 plots the maximum daily variation of the attenuation and noise over all 12 months in 2015 in distance equal to 400m over the operating frequency of 150GHz, where we extract three non-rainy (clear) days for each month and average their results for that month. It is clear that the variations are noticeable in all seasons, but larger variations are expected in summer than in winter for Sydney. Also, the maximum daily variation is shown in Figure 3.10 for three largest cities of Australia in two example days in winter and summer. It can be seen the story in Brisbane is different than other two cities which can be the result of different climate. Note that unlike Melbourne and Sydney, which are located in the south of the continent, Brisbane is located in the more tropical region.

So far we have studied diurnal variation for a fixed distance of 400 meters between

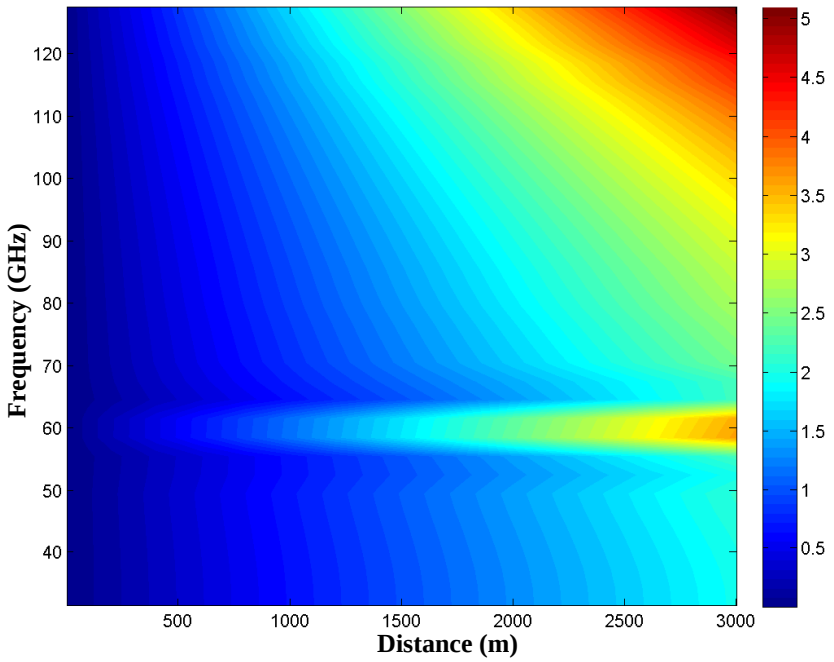

(a) Frequencies up to 130 GHz

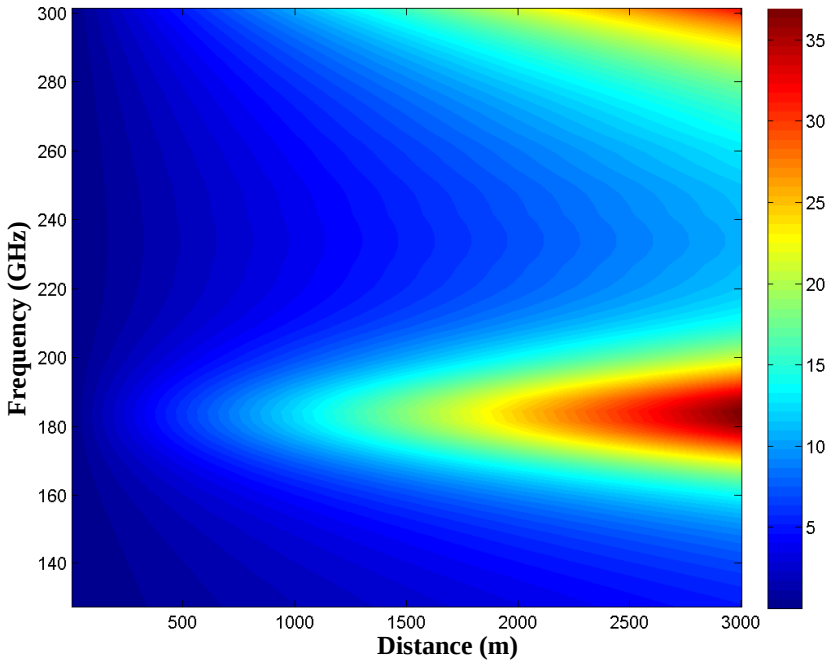

(b) Frequencies higher than 130GHz

Figure 3.11: Attenuation variation in dB as a function of distance and frequency.

two devices. Next, we study diurnal variation as a function of distance. This time we consider many different frequency bands within mmWave. Variations in attenuation and noise are shown as heat maps in Figures 3.11 and Figure 3.12, respectively, for

Sydney (Rozelle station on 11 Dec 2015). We observe that attenuation variation is more significant at longer distances, while it is the opposite for noise variation. This is because the molecular noise is dependent on the received signal power, which fades away with the distance. Therefore at long distances, molecular noise becomes negligible. In contrast, the signal attenuation is negligible at short distances, but becomes very significant with increasing distance.

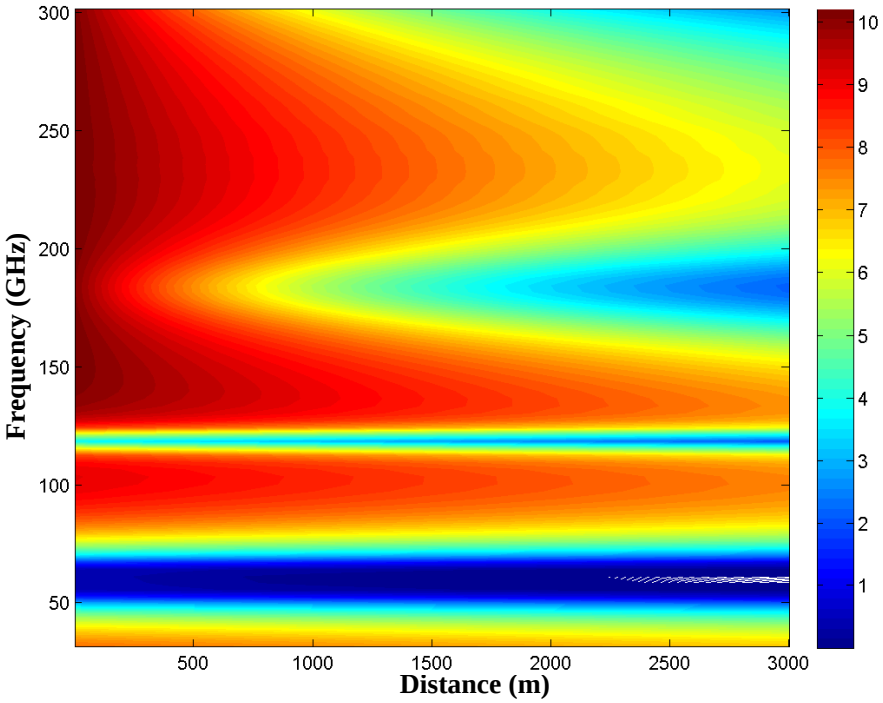

Figure 3.12: Noise variation in dBm as a function of distance and frequency.

3.2.3 Spatial variation

In our data collection, we found a significant difference in temperature and moisture across the city of Sydney which might cause channel variation for high-speed mobile users. In order to investigate the effect of this variation on the channel quality, we collect weather data of 273 stations available in [89] for various Sydney suburbs. The evaluation methodology is same as section 3.2.1 and we assume uniform air composition along the path between the transmitter and the receiver.

In the first step, we use all the station's geographical coordinations to plot the map graph of Sydney. The data has been captured at 1:30 pm, January 28, 2016,

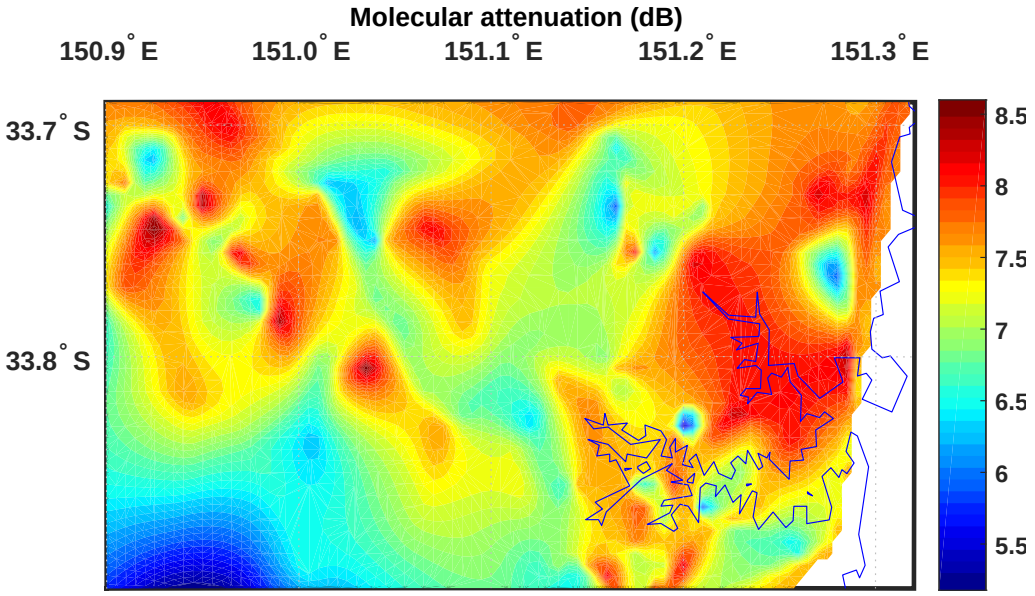

Figure 3.13: The spatial variation of molecular attenuation on map of Sydney

at several points across the city (Figure 3.7(a)). We use MATLAB interpolation to estimate the values for all the map points. We crop part of the map which has more observation point density. We also show the coastal line in the graphs which can be matched with Figure 3.7(a).

In section 3.1, Figure 3.7(a) shows the map and observation stations as red marks. Figure 3.7(b) illustrate the temperature graph of corresponding area in Celsius. There is a maximum 8°C difference in the map and temperature is generally lower in the areas near the ocean. In addition, Figure 3.7(c) presents the vapor mole fraction at the same time which is varying between 0.018 and 0.030 and its variation's pattern is different from temperature in Figure 3.7(b). Finally, we calculate the molecular attenuation for 400 m communication distance at 150 GHz which is shown in Figure 3.13. About 3.5 dB attenuation variation can be found across the city which in some areas it happens in a small neighborhood. Also, if we compare Figure 3.7 and 3.13, it can be seen a visible similarity between vapor mole fraction graph and the attenuation. It means the moisture plays the most important role in molecular absorption in mmWave/THz wireless channel although the temperature is also important.

In order to show spatial channel variation in different sub-bands, we select 11 observation points in several Sydney's suburbs. Figure 3.14 shows the evaluation results for this group of stations. The data are observed at 4:30 pm, January 21, 2016.

As shown in the Figure 3.14, there is about 8°C difference between the highest and lowest observed temperatures at Earlwood (35°C) and Palm beach (27°C). Also, the amount of vapor varies between 1.9 to 3.3 % across the selected locations. The difference in air composition results in different channel characteristics in each area. The noise and attenuation are calculated for 400m communication distance. It can be seen attenuation at Glebe differs 6 dB compared with Marrickville at 250 GHz while this variation reduces to only 1 dB at 38 GHz channel. The molecular noise also has been shown in the same figure where the results show that while maximum variation in attenuation happens in higher frequencies, the noise varies more in lower sub-bands where it is around 1 dBm and can be neglected.

3.3 Impact of High Mobility

In this section, we show how the spatial variation in atmospheric conditions effects on high speed mobile users such that spatial variation will turn to temporal variation for this kind of users because of changing location fast. For this purpose, four arbitrary routes in Sydney are considered on the map which have been shown in Figure 3.15. The route length for P1 to P4 are about 42, 34, 43 and 32.8 km respectively. We exploit the same data which was used in section 3.2.3 (Figure 3.13). The routes are exported by Google map in kml files. We simulate a trip on each route when the vehicle speed varies between 45 to 60 km/h randomly and trips long 40-50 minutes. Also, we ignore the diurnal variation in this section.

First, Figure 3.16 shows the signal attenuation which has been resulted by molecular absorption while the free-space path loss attenuation is not included in this Figure. As it can be seen, the signal attenuation varies about 6 dB/km in few minutes. For example, in route 3 the attenuation drops about 4 dB/km around 2000th second. It is much faster than diurnal variation that we discussed in 3.2.2 which

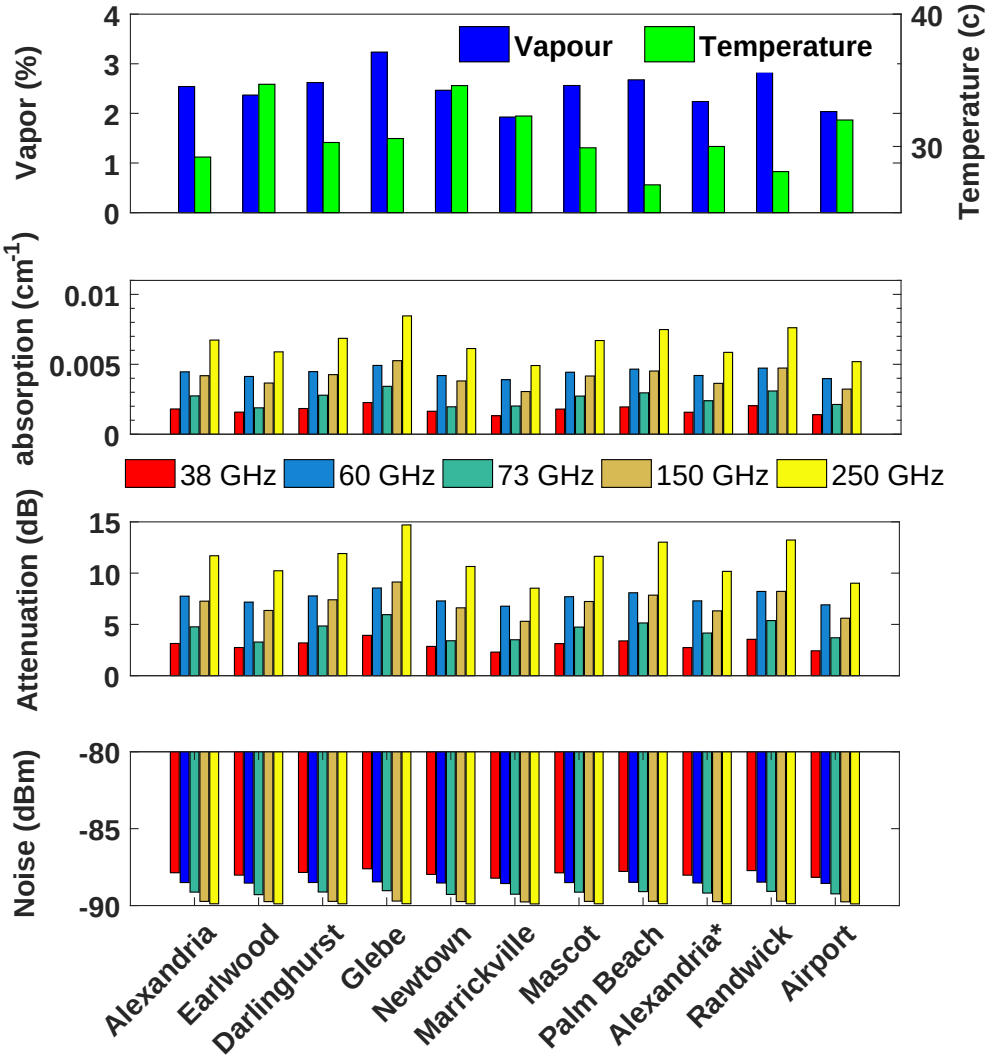

Figure 3.14: Channel spatial variation for five sub-bands.

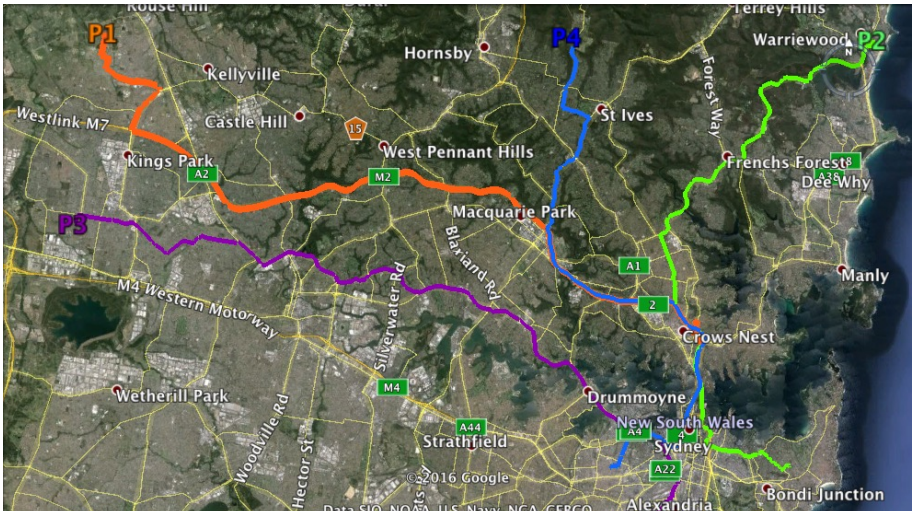

Figure 3.15: Four selected routes in Sydney

is a new source of channel variation for high speed users where to the best of our knowledge it was not considered before.

Such a signal variation can affect the link quality and user may experience significant fluctuation in the available data rate. To show how the absorption will affect the link quality, we calculate channel capacity theoretically by Shannon's theory while we assume a single link. We also assume a fixed communication distance of 400m, which can be vehicle to vehicle or vehicle to infrastructure, transmit power of 40 mW and total 15 dB antenna gain. Realistically, the communication distance also varies rapidly and changes the channel state but in this work we assume a constant distance for simplicity to only highlight the molecular absorption effect. Note that we consider both molecular and thermal noise to calculate the capacity. Figure 3.17 shows how the variation in attenuation results in fluctuation in available data rate for a channel with 1 GHz bandwidth at 150 GHz.

There are some effective link adaptation schemes in current wireless communication systems which measure channel quality periodically and aim to overcome slow and fast channel variations in order to keep the wireless link connected and reliable [91, 92]. These methods of capturing variations in the channel could also be used to capture channel variations due to molecular absorption. However, when the channel quality i.e SNR decreases, they mostly rely on downgrading modulation scheme

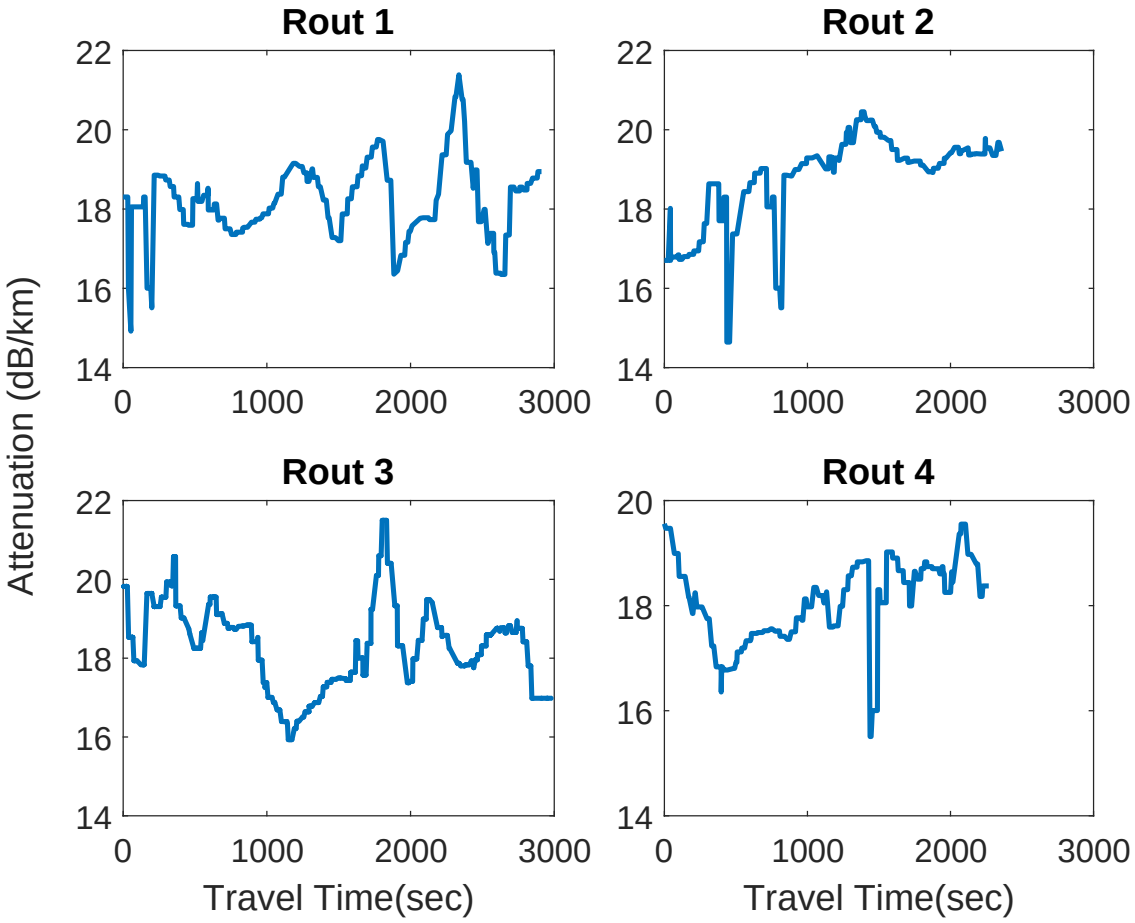

Figure 3.16: Molecular attenuation during the travel time at 150 GHz

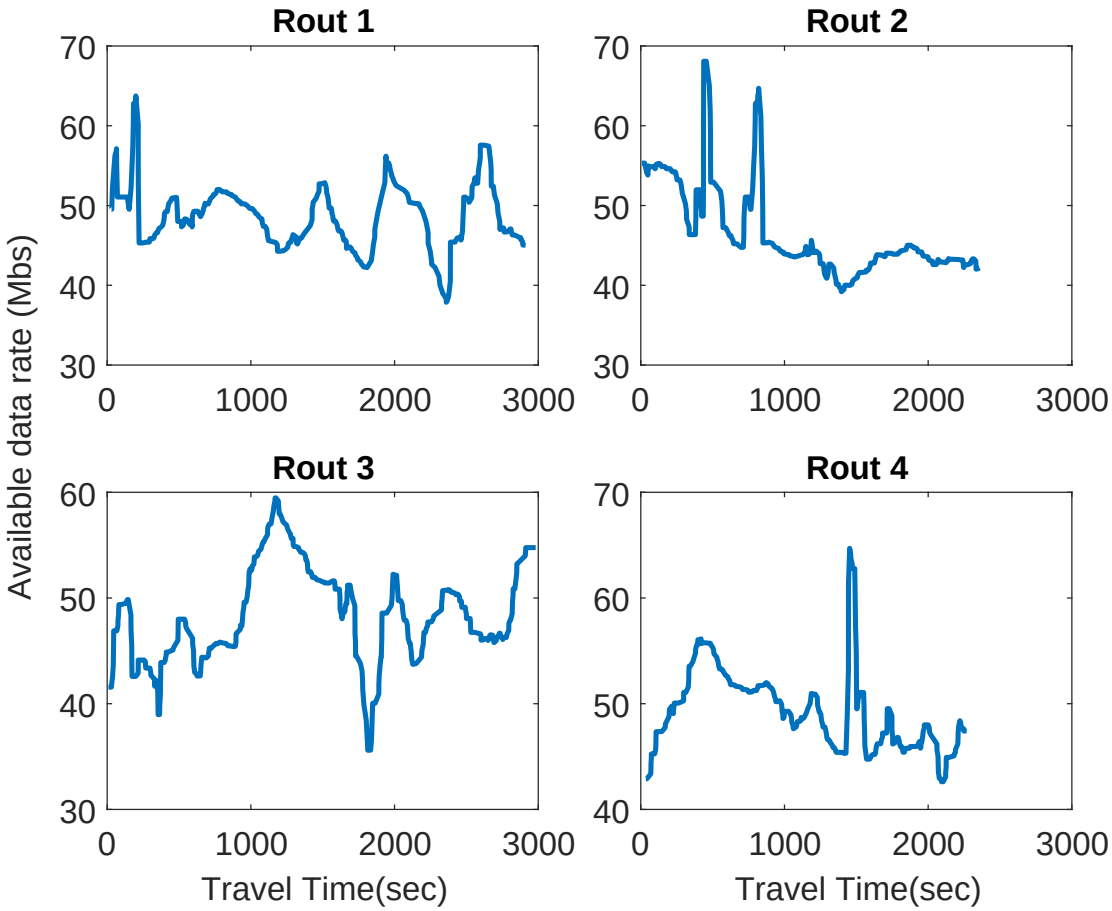

Figure 3.17: Possible data rate over selected routes in Sydney for 1 GHz channel at 150 GHz.

or decreasing the coding rate which leads lower bit rate [93]. The other possible option is power control which adjusts the transmission power to achieve a desirable performance [94]. But, dynamic power control affects the cellular network design because it will change signal to interference ratio on the cell edge. On the other hand, as shown in (2.9), the molecular noise will be amplified when the transmit power increases. Thus, further research should be done on how the atmospheric channel variations should be mitigated in mmWave/THz communication.

3.4 Summary

In this chapter, we studied the effect of atmospheric conditions on the communication over mmWave/THz channel as one of the emerging technologies for high speed

wireless communication. Using mmWave channel modeling and real air quality/condition data, we investigated the quality of wireless communication in three largest cities in Australia including Sydney, Melbourne and Brisbane. We found that the channel quality metrics such as noise, attenuation and capacity can vary temporally and spatially across the cities, mainly due to variation in air temperature and existing moisture in the air. We simulated few traveling routes in Sydney and showed that a high-speed mobile user will experience a significant variation (around 60%) in bit rate which is not appropriate for real-time services such as video streaming. In spite of the fact that attenuation and noise of molecular absorption reduce the channel quality based on common understanding, however the molecular re-radiation is correlated to signal power and thus can carry information in the channel. Thus in next chapter, will have a new look on molecular re-radiation in mmWave/THz band where interestingly, multi-input multi-output communication can exploit the re-radiation to improve the capacity.

Chapter 4

Effect of Molecular Re-radiation on mmWave and THz MIMO

In the near future, wireless communication such as the 5th-generation (5G) system is expected to deliver a massive increase in channel capacity and data rates. To achieve this, two key technologies have attracted lots of attention recently. The first one is the use of very high frequency spectrum in the range of higher than 30 GHz to 1 THz [8, 9]. The second one is the massive multiple-input multiple-output (MIMO) technology, which advocates the use of a large number of antennas in wireless communications. The above two technologies are compatible with each other. In more detail, a short wavelength in mmWave/THz helps to minimize the inter-element spacing of a MIMO system. As a result, a great number of antennas can be equipped on mobile devices, which is not practical for the current wireless systems that usually work in the sub-6GHz spectrum.

Note that the communication in mmWave/THz poses its own challenges, such as high free-space path loss, high Doppler shift and blockage [7, 9, 95]. Other than the above factors and according to more fundamental physics theories, another key difference between the existing wireless communication in sub-6GHz frequencies and the future one in mmWave/THz is the reaction of atmosphere molecules, which can absorb signal energy if excited in their natural resonant frequencies. For example, if we consider normal atmosphere, Oxygen and/or water molecules will play a major

role in the molecular absorption, and their natural resonant frequencies are around 60GHz, 120GHz and 180GHz. Interestingly, resonating Oxygen and water molecules not only absorb signal energy causing attenuation, they also re-radiate some of the absorbed energy. As we discussed in 2, this type of molecule-induced re-radiation is often referred to as *molecular noise* [7,50], but it is actually highly correlated to the signal waveform due to its re-radiation nature [10], and hence it can be considered as a distorted copy of the signal from a virtual non-line-of-sight (NLoS) path.

The aim of this chapter is to show how this molecular re-radiation can change the MIMO capacity performance as it is very similar to scattering, which is known as a very important factor to provide spatial diversity for a MIMO channel. Since the molecule absorption intensity is related to the natural resonant frequencies of the existing molecules in the realistic atmosphere on earth, (i.e., mainly the large amount of Oxygen and water molecules), the energy absorption and re-radiation are not flat especially in the mmWave spectrum. Thus, we propose a conjecture that the MIMO capacity should vary with frequency due to the impact of such molecular absorption and re-radiation. Then, **we verify our conjecture via theoretical studies and computer simulations, and find that the MIMO capacity increases dramatically in some high absorption bands around 60 GHz, 180 GHz and 550 GHz, thanks to the ubiquitous existence of Oxygen and water molecules.**

The intuition of our theoretical discovery is that the molecular re-radiation adds a random phase onto the distorted copy of the signal, which equivalently creates a richer scattering environment that can improve the line-of-sight (LoS) MIMO capacity commonly evaluated in the mmWave spectrum. The impact of our new discovery is significant, which fundamentally changes our understanding on the relationship between the MIMO capacity and the frequency spectrum. In particular, **our results predict that several mmWave bands can serve as valuable spectrum windows for high-efficiency MIMO communications, which in turn may shift the paradigm of research, standardization, and implementation in the field of mmWave communications.**

4.1 Molecular Re-radiation as Non-Line-of-Sight Signal Component

The existing molecules in communication medium will be excited by electromagnetic waves at specific frequencies. The excitement is temporary and the vibrational-rotational energy level of molecules will come back to a steady state and the absorbed energy will be re-radiated in the same frequency. These re-radiated waves are usually considered as noise in the literature. Recently, the molecular noise has been re-considered for higher frequencies such as THz band ranging from 0.1-10 THz [7, 11, 12]. First, We rewrite the molecular noise equations in Section 2.2.1 as a time invariant power spectral density:

$$S_{N_{\text{abs}}}(f,d) = S_N^B(f,d) + S_N^X(f,d), \tag{4.1}$$

$$S_N^B(f,d) = lim_{d\to\infty}(k_B T_0(1-e^{-k(f)d}))\Big(\frac{c}{\sqrt{4\pi}f}\Big)^2, \tag{4.2}$$

$$S_N^X(f,d) = P_t(f)(1-e^{-k(f)d})\Big(\frac{c}{4\pi f d}\Big)^2, \tag{4.3}$$

where $k(f)$ is the absorption coefficient of the medium at frequency f, T_0 is the reference temperature ($296K$), k_B is the Boltzmann constant, $P_t(f)$ is the power spectral density of the transmitted signal and c is the speed of light. The first term in (4.1), which is called sky noise and defined in (4.2) is independent of the signal wave. However, the self-induced noise in (4.3) is highly correlated with the signal wave [10], and can be considered as a distorted copy of the signal wave [11]. Thus, the received power of the re-radiated signal by molecules at the receiver can be expressed by

$$P_{\text{r,a}}(f,d) = P_t(f)(1-e^{-k(f)d})\Big(\frac{c}{4\pi f d}\Big)^2. \tag{4.4}$$

Since the phase of the re-radiated wave depends on the phase of molecular vibration, which varies from molecules to molecules [96], the received power in this case is affected by a large number of phase-independent re-radiated photons. Thus, we assume a uniformly distributed *random* phase for the received signal, with its power given by (4.4).

4.2 Integration of Molecular Re-radiation into MIMO Channel Model

4.2.1 Channel Transfer Function

The channel transfer function for a single LoS channel is given by

$$\begin{aligned}\tilde{h}_{\mathrm{LoS}}(f,d) &= \sqrt{\left(\frac{c}{4\pi f d}\right)^2 e^{-k(f)\times d}} \times e^{j2\pi\frac{d}{\lambda}} \\ &= \left(\frac{c}{4\pi f d}\right) e^{-k(f)\times\frac{d}{2}} \times e^{j2\pi\frac{d}{\lambda}}.\end{aligned} \tag{4.5}$$

Then, the partial channel transfer function resulted from the molecular absorption and excluding the LoS component can be represented by

$$\begin{aligned}\tilde{h}_{\mathrm{a}}(f,d) &= \sqrt{(1-e^{-k(f)d})\left(\frac{c}{4\pi f d}\right)^2} \times e^{j2\pi\beta_{\mathrm{random}}} \\ &= (1-e^{-k(f)d})^{\frac{1}{2}}\left(\frac{c}{4\pi f d}\right) \times e^{j2\pi\beta_{\mathrm{random}}}.\end{aligned} \tag{4.6}$$

Hence, the total channel transfer function is the superposition of the partial channel transfer functions, which is written as

$$\tilde{h}(f,d) = \tilde{h}_{\mathrm{LoS}}(f,d) + \tilde{h}_{\mathrm{a}}(f,d), \tag{4.7}$$

$$\begin{aligned}\tilde{h}(f,d) = &\left(\frac{c}{4\pi f d}\right) e^{-k(f)\times\frac{d}{2}} \times e^{j2\pi\frac{d}{\lambda}} \\ &+(1-e^{-k(f)d})^{\frac{1}{2}}\left(\frac{c}{4\pi f d}\right) \times e^{j2\pi\beta_{\mathrm{random}}}.\end{aligned} \tag{4.8}$$

4.2.2 MIMO Capacity

In this chapter, we consider a MIMO system that is consisted of n_t transmitting antennas and n_r receiving ones. The received signal vector y at n_r receiving antennas

can be formulated as [97]

$$y = \tilde{H}x + n, \tag{4.9}$$

where x is the transmitted signal vector form n_t transmitting antennas, and n is an $n_r \times 1$ vector with zero-mean independent noises with variance σ^2. The channel matrix $\tilde{H}$ is defined by

$$\tilde{H} \triangleq \begin{bmatrix} \tilde{h}_{11} & \tilde{h}_{12} & \dots & \tilde{h}_{1n_t} \\ \tilde{h}_{21} & \tilde{h}_{22} & \dots & \tilde{h}_{2n_t} \\ \vdots & \vdots & \ddots & \vdots \\ \tilde{h}_{n_r1} & \tilde{h}_{n_r2} & \dots & \tilde{h}_{n_rn_t}, \end{bmatrix} \tag{4.10}$$

where $\tilde{h}_{ij}$ is a complex value denoting the transfer coefficient associated with the jth transmitter antenna and the ith receiver antenna. Note that $\tilde{h}_{ij}$ can be obtained from (4.8) for frequency f and distance d_{ij}. A 3×3 MIMO system with a channel matrix is illustrated in Figure 4.1.

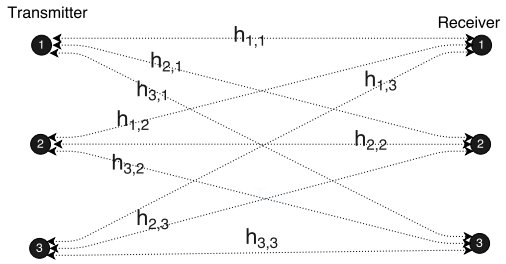

Figure 4.1: A 3x3 MIMO system, the channel gain of array pairs between transmitter and receivers

If we assume that the transmitter has no channel state information (CSI), and the transmitting power is equally distributed among transmitting antennas. Consequently, the capacity of MIMO channel can be written as

$$C = \log_2 \det(I_{n_r} + \frac{P}{n_t\sigma^2}\tilde{\mathbf{H}}\tilde{\mathbf{H}}^\dagger), \tag{4.11}$$

where P is total transmitting power, and I is the identity matrix [97]. Since the determinant of $(I_{n_r} + \frac{P}{n_t\sigma^2}\tilde{\mathbf{H}}\tilde{\mathbf{H}}^\dagger)$ can be computed by the product of the eigenvalues of the matrix $\tilde{\mathbf{H}}\tilde{\mathbf{H}}^\dagger$, the MIMO capacity can thus be written in the form of a product

of non-zero eigenvalues as [98]

$$C = \sum_{i=1}^{m} \log_2(1 + \frac{P\lambda_i^2}{m\sigma^2}), \tag{4.12}$$

where λ_i denotes singular values of the matrix $\tilde{\mathbf{H}}$, and hence the squared singular values λ_i^2 denotes the eigenvalues of the matrix $\tilde{\mathbf{H}}\tilde{\mathbf{H}}^{\dagger}$. Note that m denotes the number of non-zero λ_i^2, which is also called the rank of $\tilde{\mathbf{H}}$ with $m \leq \min(n_r, n_t)$ [98]. Each of the λ_i^2 characterize an equivalent information channel where $\frac{P\lambda_i^2}{m\sigma^2}$ is the corresponding signal-to-noise ratio (SNR) of the channel at the receiver. Note that (4.12) is valid for uniform power allocation at the transmitter. Furthermore, the equivalent channel SNR, $\frac{P\lambda_i^2}{m\sigma^2}$, should meet a minimum receiver threshold to be reliably detectable by the receiver. We assumed 0 dB as the SNR threshold and uniform power allocation at the transmitter. On other hand, if transmitter have the channel state information, the power can be allocated to each transmitter some how maximize the capacity. In this way, the equivalent channel with stronger again will receive more power while the total transmit power is limited to P. Thus, equation (4.12) should be revised as

$$C = \sum_{i=1}^{m} \log_2(1 + \frac{P_i\lambda_i^2}{\sigma^2}), \tag{4.13}$$

where $P_i, ..., P_m$ are the water-filling power allocations:

$$P_i = \left(\mu - \frac{\sigma^2}{\lambda_i^2}\right), \tag{4.14}$$

with μ has been chosen to satisfy the total power constraint $\sum P_i = P$.

The main difference between beamforming and multiplexing techniques is how to tune or exploit the eigenvalue distribution. In more details, beamforming technique aims to maximize λ_1 to improve the channel SNR for a single data stream while in the multiplexing technique, a uniform eigenvalue distribution is preferable. In this way, multiplexing technique can utilize parallel data streams through MIMO and maximize the data rate. The complexity of beamforming comes from eigenvalues tuning because it means the channel state information (CSI) should be measured

and sent back to the transmitter periodically for optimum precoding. This also results in a protocol overhead in the channel. On the other hand, multiplexing gain can take advantage of eigenvalue value distribution even with a blind preceding. This is more beneficial when there is a rich scattering environment. In next section, we will discuss how the re-radiation can provide a rich scattering environment.

4.3 Capacity Bounds for MIMO Capacity Under Molecular Re-radiation

To analyze the MIMO channel capacity and characterize the scattering richness of channel quantitatively, lets decompose and normalize channel transfer function $\tilde{H}$ regarding (4.7) as

$$H(f,d) = \sqrt{\frac{K}{K+1}} H_{\mathrm{LoS}}(f,d) + \sqrt{\frac{1}{K+1}} H_{\mathrm{a}}(f,d), \tag{4.15}$$

where H, H_{LoS} and H_{a} are normalized with corresponding channel gain. Because of uniformly distributed random phase of received re-radiated signal, elements of H_{a} are independent and identically distributed (i.i.d) complex Gaussian random variables with zero mean and unit magnitude variance. K is the ratio of powers of the LoS signal and the re-radiated components and if we assume the channel distance is much longer than antenna space, it can be obtained by

$$K = \frac{P_{\mathrm{r,LoS}}(f,d)}{P_{\mathrm{r,a}}(f,d)} = \frac{e^{-k(f)d}}{1-e^{-k(f)d}}. \tag{4.16}$$

This is same as the well-known Rician channel model where the K is called *Rician K-factor*. Equivalently, K-factor shows how much channel is rich in term of scattering and multipath rays. Equation (4.16) shows K is a function of absorption coefficient of channel medium $k(f)$ and the distance between the transmitter and receiver d so that a longer distance and higher absorption result in smaller K. Figure 4.2(a) illustrates how K-factor change for the practical range of absorption coefficient in the atmosphere for a distance of 1-100m. The capacity of MIMO

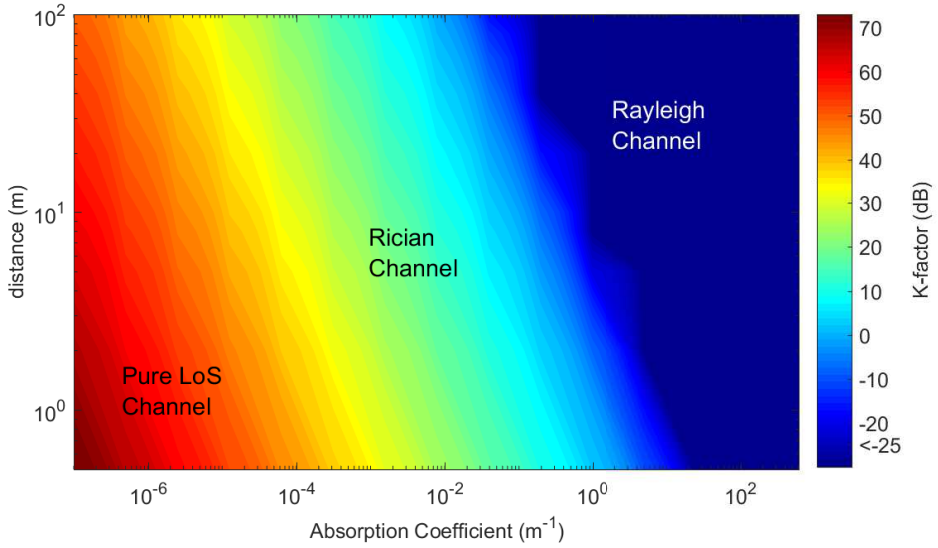

(a)

Figure 4.2: K-factor is an increasing function of distance and absorption coefficient.

channel considering Rician K-fator is studied in several works [75], [99] and [100]. Authors in [100] showed the lower bound of expected capacity of the Rician channel when the transmitter does not have CSI and the total transmit power P is allocated equally to all transmitter antennas is the capacity resulted by NLoS component.

$$E(C(H),\rho) \geq E(C(H_a), \sqrt{\frac{1}{K+1}}\rho), \tag{4.17}$$

$$\implies E(C(H),\rho) \geq E(C(H_a), \sqrt{1-e^{-k(f)d}}), \tag{4.18}$$

where $E(.)$ denotes the expectation, ρ is received SNR for equivalent single channel and $E(C(H),\rho)$ is the average capacity of a channel with normalized channel transfer matrix H and a reception SNR equal to ρ.

It is clear that the lower band is a increasing function of absorption coefficient, $\forall f_1, f_2$ such that $k(f_2) \geq k(f_1)$, $E_{min}(C(f_2)) \geq E_{min}(C(f_1))$. On the other hand, capacity upper band for a Rician MIMO channel with perfect CSI at receiver and transmitter where the power is optimally distributed among antennas with *water-filling* algorithm is also presented in [75] which is shown in (4.19) where K is

Racian K-factor and $[x]^+ = \max(x, 0)$.

$$E(C(H)) \leq \log_2\left(1 + \frac{n_r(1+n_tK)}{K+1}\Big(\min\left\{\frac{\rho}{n_t}, \frac{K(1+K)}{n_r(1+n_tK)}\right\}n_t + \left[\frac{\rho}{n_t} - \frac{K(1+K)}{n_r(1+n_tK)}\right]^+\Big)\right) + (n_t-1)\log_2\left(1 + \frac{n_r}{1+K}\left[\frac{\rho}{n_t} - \frac{K(1+K)}{n_r(1+n_tK)}\right]^+\right) \tag{4.19}$$

Let assume $n_r = n_t = n$ and put (4.16) in (4.19). The resulted equation is

$$E(C(H)) \leq \log_2\left(1 + (1+(n-1)e^{-k(f)d})\Big(\min\left\{\rho, \frac{\frac{e^{-k(f)d}}{1-e^{-k(f)d}}}{(1+(n-1)e^{-k(f)d})}\right\}n + \left[\rho - \frac{\frac{e^{-k(f)d}}{1-e^{-k(f)d}}}{(1+(n-1)e^{-k(f)d})}\right]^+\Big)\right) + (n-1)\log_2\left(1 + (1-e^{-k(f)d})\left[\rho, \frac{\frac{e^{-k(f)d}}{1-e^{-k(f)d}}}{(1+(n-1)e^{-k(f)d})}\right]^+\right) \tag{4.20}$$

, which we can see for two extreme cases very low absorption $k(f) = 0$ and vary high absorption $k(f) = \infty$ the capacity of a Rician channel for MIMO will limit to

$$\lim_{k(f)\to\infty} = n\log(1+\rho), \tag{4.21}$$

$$\lim_{k(f)\to 0} = \log(1+\mathrm{n}^2\rho), \tag{4.22}$$

Note that from (4.16), $k(f) = \infty$ means extremely high absorption re-radiation channel which provide a pure Rayleigh channel and $k(f) = 0$ presents no absorption or pure LoS channel.

It is well known that the maximum achievable capacity of a MIMO channel is proportional to the minimum number of antenna elements at the receiver and the transmitter. However, in an environment that is lack of spatial diversity, such capacity would be degraded due to the deficiency of parallel information paths, i.e., the rank of the MIMO channel, between the receiver and the transmitter [71]. More specifically, in a rich scattering environment, scatterers provide sufficient NLoS signal components, leading to a better diversity and capacity. But in the case of

a LoS scenario, the LoS signal component will dominate the received signal, and thus decrease the channel rank due to the linear dependence of the LoS antenna array phases [74]. Thus, in a LoS scenario that is assumed for most mmWave/THz communications, the maximum MIMO capacity is achievable only with some specific array configuration [74], where the LoS rays are perfectly orthogonal, resulting in an opportunistically full-rank MIMO channel. However, this is not practical for mobile communications, since such kind of optimal antenna setting requires a user steadily holding a device toward a specific direction.

Generally, the MIMO capacity becomes higher if the channel transfer matrix $\mathbf{H}$ is *full rank* and *well-conditioned*. In more detail, the rank of $\mathbf{H}$ determines how many data streams can be multiplexed over the channel, and $\mathbf{H}$ is well-conditioned if the condition number, which is defined as $\frac{\lambda max}{\lambda min}$, is small and close to one. In other words, the maximum MIMO capacity can be attained when all λ_is are equal.

In the next section, simulation results for with realistic absorption coefficients will be presented in comparison with analytical capacity bounds.

4.4 Simulation

4.4.1 Simulation set-up

To evaluate the MIMO capacity in mmWave/THz band and show the performance impact of the molecular absorption, we consider a simple $n \times n$ MIMO system with a square uniform Arrays , where at both transmitter and receiver, the inter-element spacing s is equal to half of the wavelength and the channel distance is d. The considered MIMO system is illustrated in Figure 4.3. Moreover,

In order to investigate the MIMO performance, we evaluate the theoretical MIMO capacity with several configurations using MATLAB. More specifically, the channel transfer matrix in (4.10) is obtained from (4.8), while the distance between each pair of transmitter-receiver antenna element is calculated by channel geometry. Finally, we compute the MIMO capacity using (4.13) or (4.12). Note that in this chapter, the term capacity is based on the spectral density which shows how

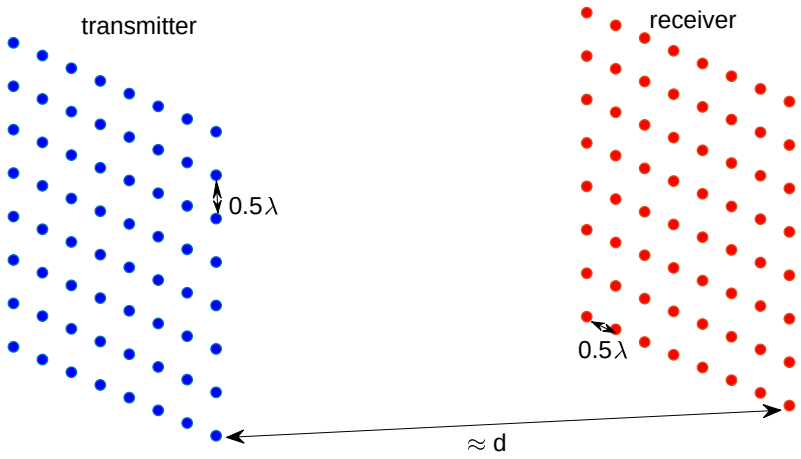

Figure 4.3: A 64x64 MIMO system with uniform square arrays

many bits can be communicated per second for a 1 Hz channel bandwidth. It can be multiplied by the actual channel bandwidth to calculate the final capacity which is not presented in this work. Since we apply random phases on NLoS components created by molecular re-radiation, we conduct the evaluation of the MIMO capacity with molecular re-radiation for 5000 times and show the average result.

We use the online browsing and plotting tools[1], which is based on HITRAN databases [4] to generate absorption coefficients for different single gas or some predefined standard gas mixture of atmosphere at sea level, as shown in Table 4.1. Since the Oxygen and water molecules play main roles in a normal air environment at mmWave/THz bands [101] and the Oxygen ratio is invariant, we use the highest and lowest water ratio in Table 4.1, i.e., the *"USA model, high latitude, winter"* and *"USA model, tropics"*. The corresponding absorption coefficients have been shown in Figure 4.6 and 4.11 for mmWave and THz band respectively. They are calculated for an ambient temperature of 273K and a sea level pressure of 1atm. It can be seen that there are three major absorption spikes in the mmWave spectrum as follows,

- A pair of them appear at around 60 GHz and 120 GHz, which are attributed to Oxygen molecules. Note that the absorption coefficients are the same for both

[1]http://hitran.iao.ru/gasmixture/simlaunch

Table 4.1: Atmosphere standard gas mixture ratio in percentage for different climates [4]

USA model, mean latitude, summer, H=0	H2O: 1.860000 CO2: 0.033000 O3: 0.000003 N2O: 0.000032 CO: 0.000015 CH4: 0.000170 O2: 20.900001 N2: 77.206000
USA model, mean latitude, winter, H=0	H2O: 0.432000 CO2: 0.033000 O3: 0.000003 N2O: 0.000032 CO: 0.000015 CH4: 0.000170 O2: 20.900001 N2: 78.634779
USA model, high latitude, summer, H=0	H2O: 1.190000 CO2: 0.033000 O3: 0.000002 N2O: 0.000031 CO: 0.000015 CH4: 0.000170 O2: 20.900001 N2: 77.876781
USA model, high latitude, winter, H=0	H2O: 0.141000 CO2: 0.033000 O3: 0.000002 N2O: 0.000032 CO: 0.000015 CH4: 0.000170 O2: 20.900001 N2: 78.925780
USA model, tropics, H=0	H2O: 2.590000 CO2: 0.033000 O3: 0.000003 N2O: 0.000032 CO: 0.000015 CH4: 0.000170 O2: 20.900001 N2: 76.476779

atmosphere cases, i.e., *"USA model, high latitude, winter"* and *"USA model, tropics"*. This is because the percentage of Oxygen is comparable for those two cases.

- The third one at 180 GHz is created by water (H_2O) molecules in the air. For a tropic atmosphere, the water ratio is higher than that of the winter atmosphere, and thus we can see a significant increase in terms of the absorption coefficient among these two atmosphere cases.

In THz band, the dominant absorption source in the air is water molecules. We can see in Figure 4.11 for the tropic atmosphere all absorption peaks are higher than the winter atmosphere which the main difference is the mole ratio of water molecules in the air.

4.4.2 MIMO performance as a Function of Absorption Coefficient

We discussed the analytical bound of MIMO capacity in 4.3 based on Rician K-factor and absorption coefficient. In the first step, we simulate the capacity of a 64x64 MIMO channel at 60 GHz for a realistic range of absorption coefficient between 10^{-5}∼10^{+3} which may be experienced for different climates over 0.3-10 THz. It should be noted that the actual value of absorption coefficient at 60 GHz is around 2.7×10^{-2}. The results are presented in Figure 4.4 for two different distances and reception SNRs. Simulation results are presented for two uniform and waterfilling power allocations which are labelled as *rx - CSI* and *tx/rx CSI* respectively. It can be observed the capacity of MIMO lies between the bounds for any absorption

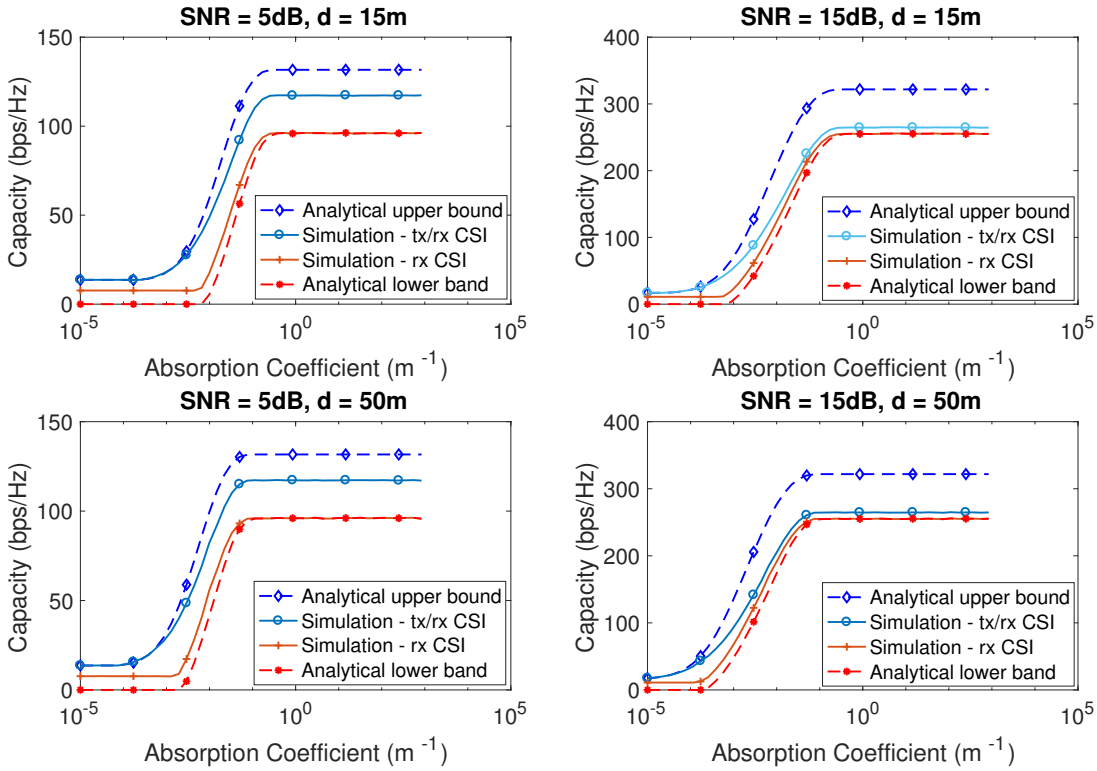

Figure 4.4: Analytical bounds and simulation results of 64x64 MIMO capacity versus absorption coefficient for different SNR and distance.

coefficient. When the capacity of MIMO system at 5 dB reception SNR for very low re-radiation, pure LoS channel, is only about 9.5 bps/Hz, it is shown that vary high re-radiation leads to a Rayleigh channel where capacity significantly increases to about 100 bps/Hz for uniform and 130 bps/Hz for waterfilling power allocation. Two different distances are used in Figure 4.4 and we can see for same SNR and at a longer distance, the maximum capacity can be achieved in lower absorption coefficient. This is because in a longer distance more molecules exist and act as scatterers. This is also observed in Figure 4.2 where the longer distance results in smaller Rician K-factor or equivalently richer scattering. However, for same transmit power longer distance suffering from more spreading loss. We will investigate capacity versus distance in section 4.4.3.

From another aspect, the re-radiation changes the channel transfer matrix from a deterministic matrix for very low absorption to a completely random matrix with zero mean and identically distributed arrays. The first one has a *degrees-of-freedom*

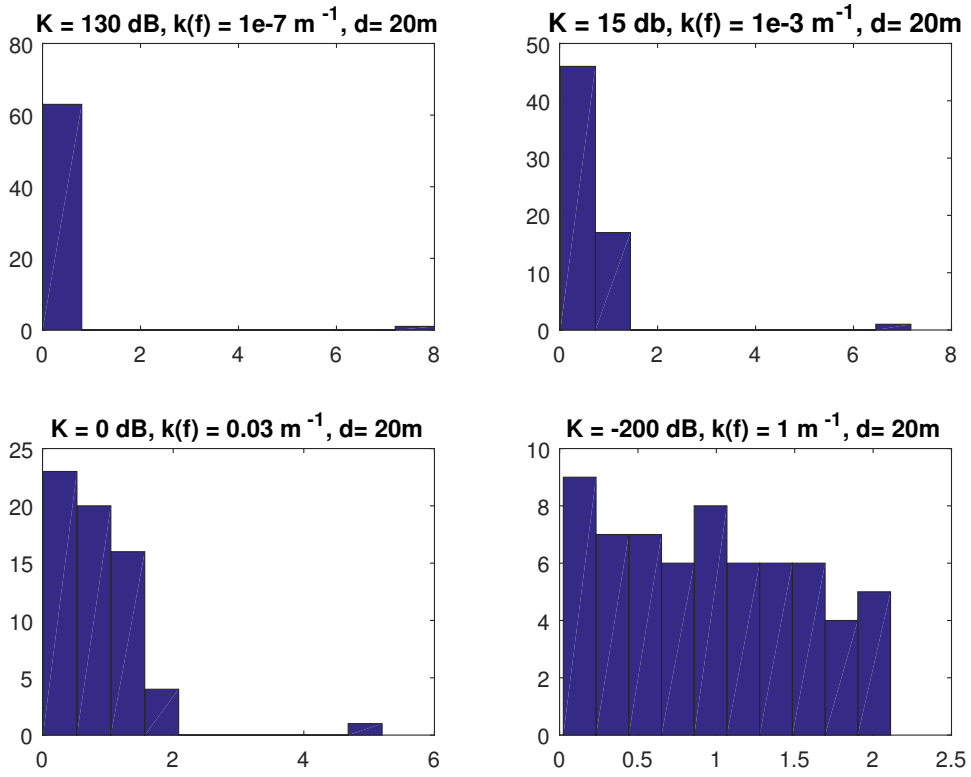

Figure 4.5: Empirical distribution of singular value of matrix $\frac{H}{\sqrt{k}}$ for different K-factor. For $K \to -\infty$ dB, it converges to the quarter circle law.

equal to one while the first singular value is very large and the rest are almost zero. Increasing the molecular re-radiation will change increase the degrees-of-freedom and singular value distribution. We show the empirical distribution of singular value for different absorption coefficient in Figure 4.5 and it can be seen the distribution is converge to the well-know quarter circle law, [69], for very large absorption coefficient.

4.4.3 mmWave MIMO Performance

In this section we aim to investigate MIMO performance considering the molecular re-radiation in mmWave as one of the 5G candidates for future spectrum. We first assume a uniform power allocation and constant reception SNR over the entire frequency spectrum, and display the MIMO capacity in bps/Hz for mmWave bands for a 16x16 MIMO in Figure 4.7. In this figure, the MIMO capacity with absorp-

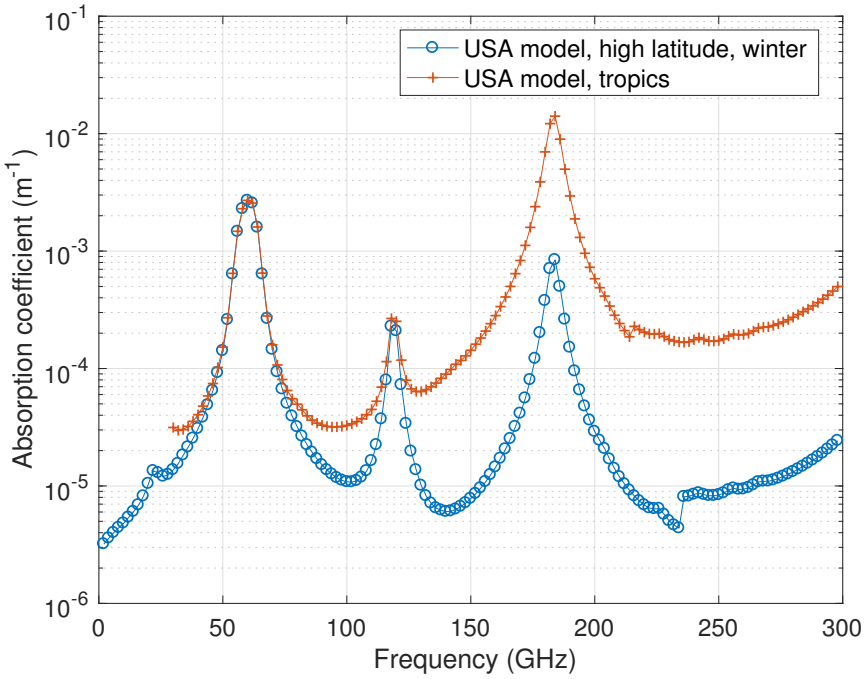

Figure 4.6: the absorption coefficient in two different atmosphere, temprature= 273 K, pressure= 1 atm.

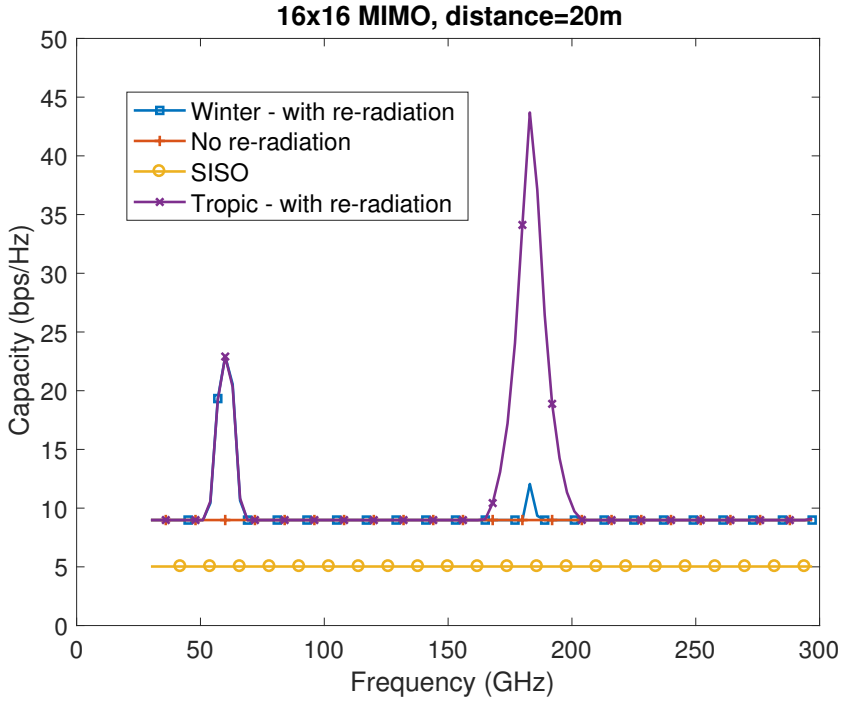

Figure 4.7: Capacity of MIMO versus frequency in mmWave band. SNR = 15 dB

tion is compared with that without absorption. As one can observe, the capacity of the latter case is flat over the entire band and is not frequency selective, which corroborates the common understanding up to now. However, when the absorption kicks in, a significant increase shows up in certain frequency bands with high absorption. For example, the capacity is boosted by around 150,% at 60 GHz for both atmosphere cases. Furthermore, since the tropic atmosphere contains more water molecules, it leads to a considerable capacity increase at 180 GHz in tropic atmosphere in comparison with those of the winter atmosphere and the case ignoring re-radiation.

Numerically speaking, we can calculate the capacity of a Single-Input and Single-Output (SISO) channel, which turns out to be 5 bps/Hz. According to the existing MIMO theory, for a full-rank 16x16 MIMO channel with enough spatial diversity, the theoretical capacity will be increased to $16 \times 5 \simeq 80$ bps/Hz. As discussed before, the LoS MIMO channel suffers from poor spatial diversity and can achieve the maximum capacity only with some specific geometry configuration [74], which is not feasible for mobile communications. Thus, it can be seen the MIMO capacity without absorption is close to that of a SISO channel. However, if the molecular re-radiation is taken into account, it can equivalently create a rich scattering environment, and in turn, increase the spatial diversity and the MIMO capacity, as shown in Figure 4.7. This is can be quantified by channel rank and condition number as was described in 4.3.

We know the physical MIMO channel can be modelled with m equivalent parallel channels with gains given by the singular values λ_i. Where $N = \min(n_r, n_t)$ and i= 1, 2, ...,m. The channel rank can practically be defined by a number of equivalent channels can provide SNR greater than a threshold. We assumed the receiver sensitivity 0 dB. The results are presented on Figure 4.8. We can see in high absorption frequency the channel rank is increased. However, the absorption is not high enough in the mmWave band to lead a full rank channel. Besides, the channel condition number which quantifies the equality of equivalent channels in MIMO is presented in Figure 4.8(b). It can be observed the molecular re-radiation improve the eigenvalues distribution at 60 GHz and 180 GHz.

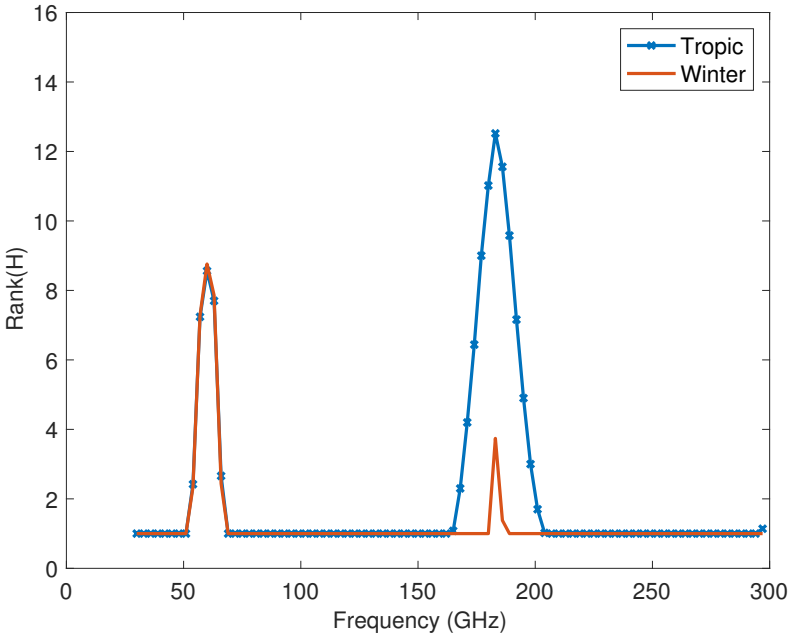

(a) Channel rank

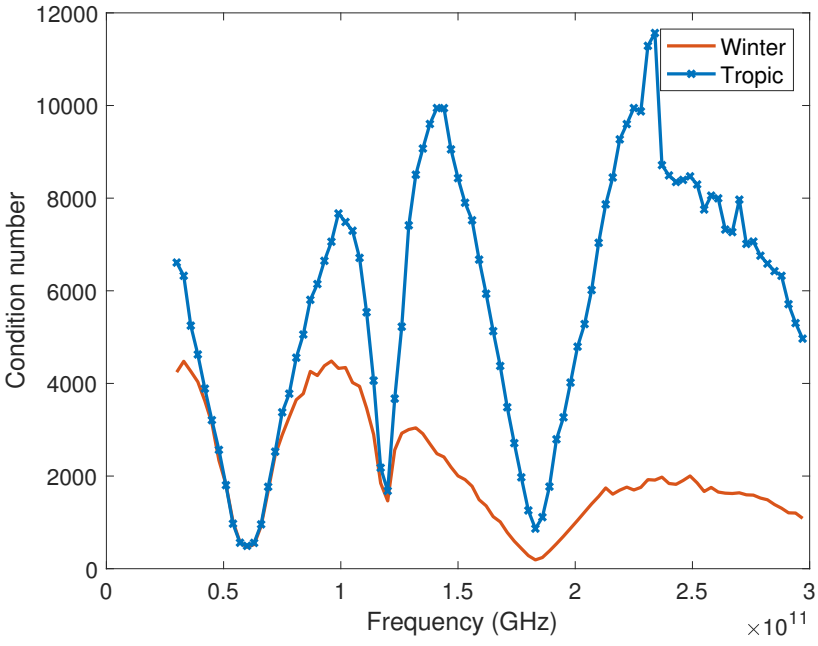

(b) Condition number

Figure 4.8: Channel rank and condition number of 16x16 MIMO channel over mmWave band.

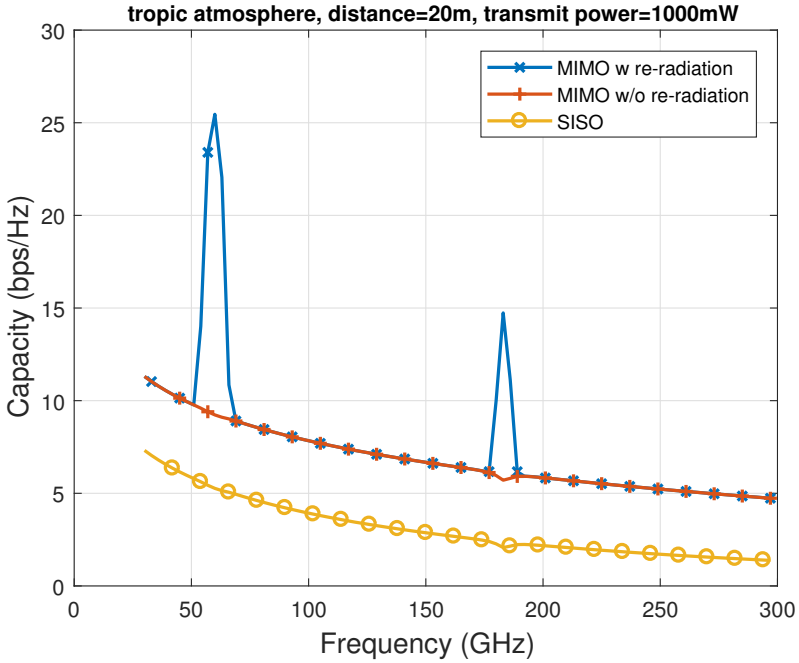

Figure 4.9: 16x16 MIMO capacity vs frequency, the transmit power is constant over the entire frequency spectrum.

Note that in Figure 4.7, we assume a constant reception SNR. However, the actual attenuation varies with the frequency because (i) the free-space path loss increases with frequency, and (ii) the molecular absorption also attenuates the signal. Hence, it is interesting to investigate whether the absorption attenuation will mitigate the MIMO performance improvement in high absorption frequency bands. For this purpose, a constant transmit power of 1 W and a constant noise power of -80 dBm are chosen in our next simulation. Note that such parameter setting provides an SNR value similar to that was used in the previous step. The results are exhibited in Figure 4.9, where the other parameter values are the same as those in Figure 4.7. As one can observe, the absorption attenuation has a marginal impact on the MIMO capacity improvement discussed before. To show this, we also simulate a SISO channel and plot its capacity in Figure 4.9, where we can see that the capacity slightly degrades at high absorption frequency bands at around 60 GHz and 180 GHz. In other words, the mmWave MIMO system can take advantage of the molecular absorption and re-radiation to generate more capacity, which prevails the absorption attenuation.

In Figure 4.2(a), the Rician K-factor has shown as a function of the absorption

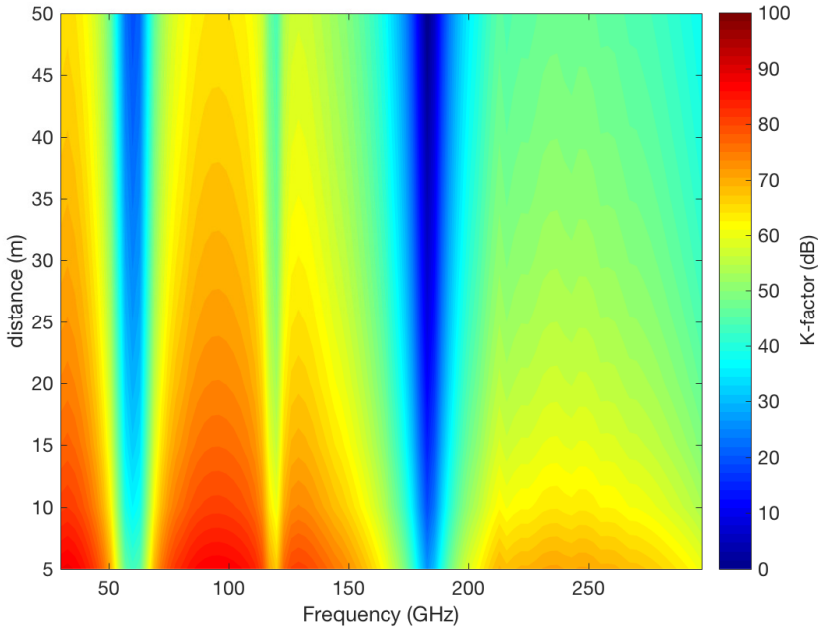

(a) Tropic atmosphere

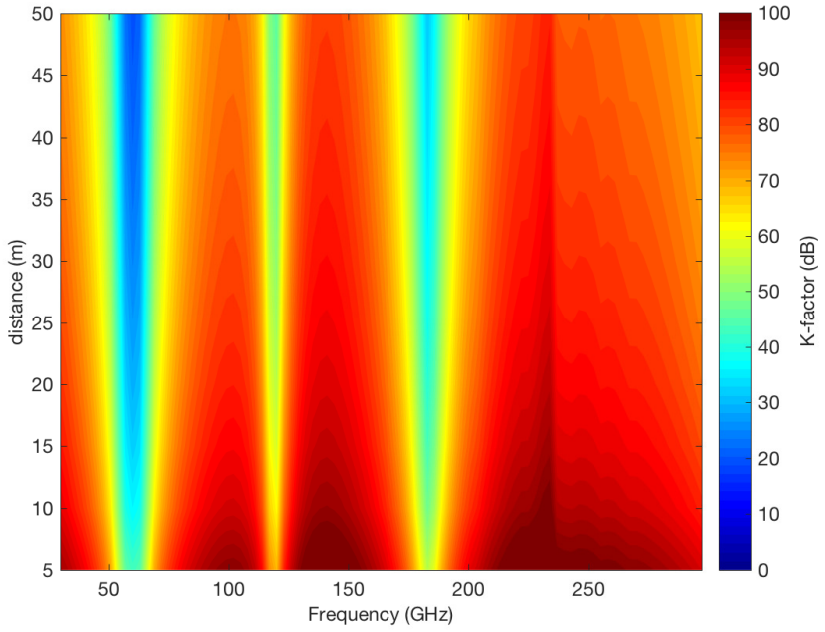

(b) Winter atmosphere

Figure 4.10: The Rician K-Factor of mmWave channel versus distance and frequency.

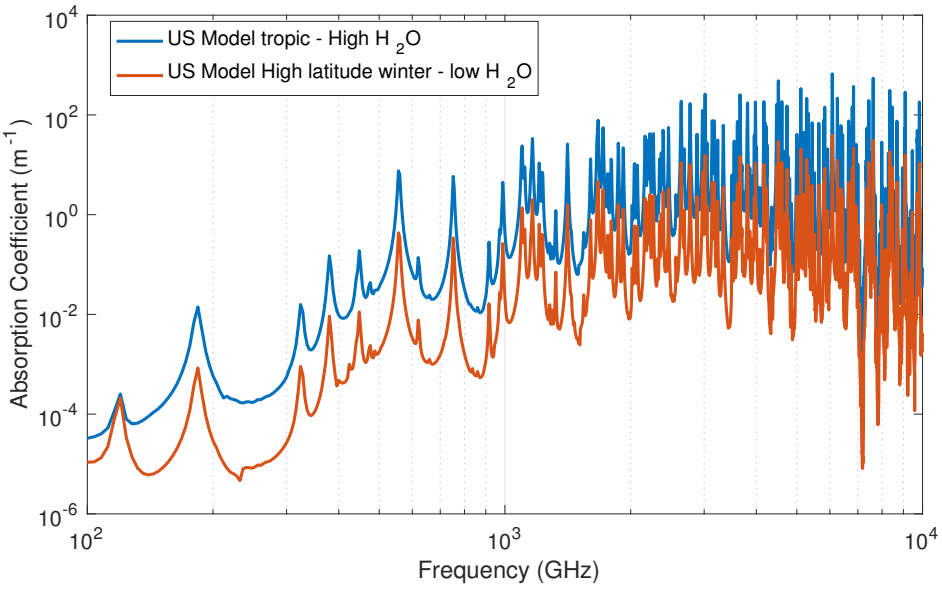

Figure 4.11: Absorption coefficient in THz band, temprature= 273 K, pressure= 1 atm.

coefficient and distance. Here, we plot the heat map of K-Factor versus frequency and distance. Figure 4.10 shows the K-Factor for two different atmospheres. This map shows in which frequency and distance, the NLoS re-radiation power becomes significant. Hence, when the SNR is high enough, the spatial multiplexing is applicable. Note that the dark red in Figure 4.10 illustrates the pure LoS channel.

4.4.4 THz MIMO Performance

In this section, we extend our investigation to the THz band. The channel is simulated for two different atmosphere gas mixture. Our assumption on the transmit power is based on current technology [7] and a previous work on THz massive MIMO [2]. We assume a 10 mW transmit power and 1 m distance as a short range communication. The absorption coefficient is shown in Figure 4.11 for a low humidity atmosphere (US model high latitude) and a high humidity atmosphere (US model tropic) over entire THz band (0.1-10THz). However, since the communication is more feasible in lower THz sub-bands, we show our results over 0.3-3 THz where the below 300 GHz is also cut because of overlap with mmWave. Furthermore, because of very short wave length in THz band, it is more practical to use a very large

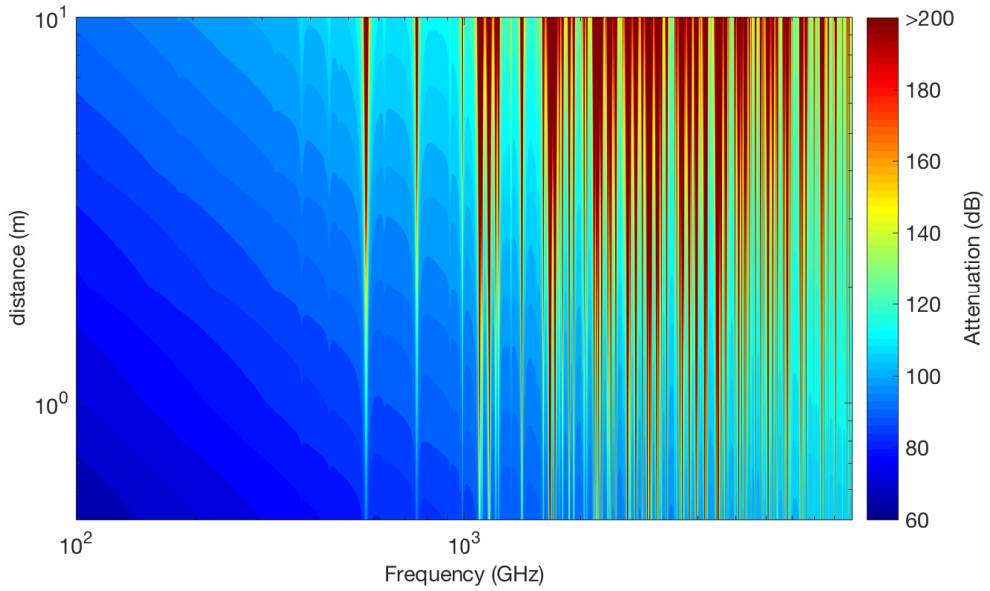

Figure 4.12: Signal Attenuation over THz band for tropic atmosphere.

number of antennas. hence, we use 225 antennas on each side in a uniform square formation such as Figure 4.3.

In addition to absorption coefficient graph, we provide the signal attenuation for a distance range 10cm-10m illustrated in 4.12. The signal attenuation includes molecular attenuation in (2.4) and spreading attenuation in equation (2.3). While the spreading attenuation is increasing linearly in dB with distance and frequency, the molecular attenuation is also increasing with distance but it is frequency selective. For example, while the total loss at 10m is 107 dB for 500 GHz, the total attenuation at 557 GHz is 86 dB at 1 m and it grows to 220 dB at 10 m which is mostly because of very high absorption of water molecules in the channel medium at this frequency. Note that the channel atmosphere for this case is from tropic data where the ratio of water molecules in the air is more than 0.02, as shown in Table 4.1.

The simulation results for 0.3-3 THz is presented in Figure 4.13. Similar to mmWave results, at high absorption frequencies the MIMO capacity is much higher when the re-radiation is taken to account. Furthermore, for low humidity atmosphere, the impact of re-radiation is disappeared in most frequencies which is because of the dominant absorption source in this frequency range is water molecules.

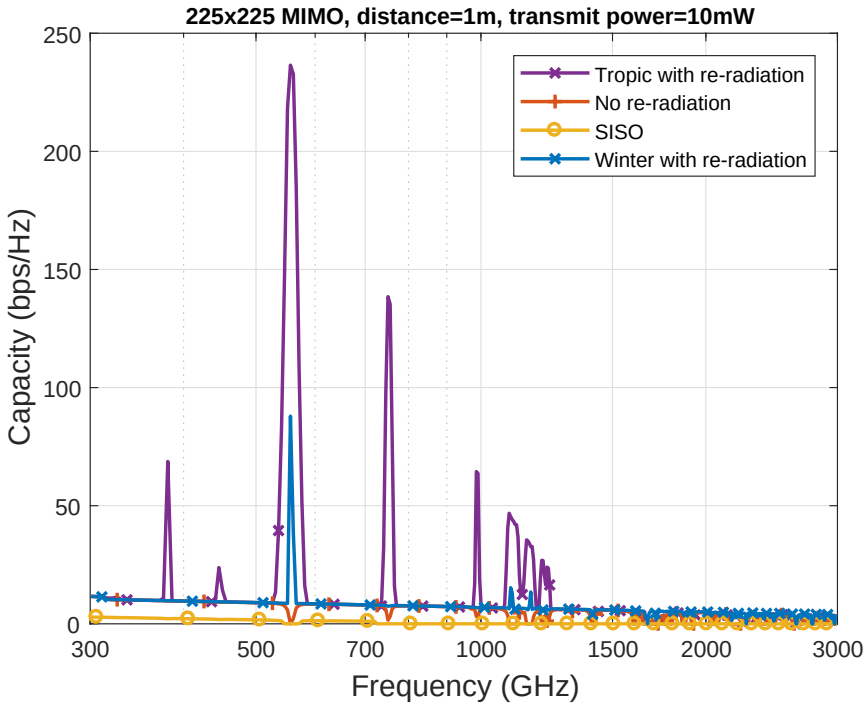

Figure 4.13: 225x225 MIMO capacity vs. frequency in Thz band.

On the other hand, for the second half of the simulated spectrum, we can see the MIMO capacity is almost same for with and without re-radiation graphs. The reason is SNR which is decreasing for the higher frequency where the spreading attenuation is higher.

In summary, the advantage of re-radiation cannot be obtained in low SNR. If we consider 557 GHz as a very high absorption frequency where SNR still is moderate, the MIMO capacity is about 235 and 90 bps/Hz for tropic and winter atmosphere while it drops to 1.4 bps/Hz for no re-radiation and SISO channels. This is because in former simulation molecular absorption only increase attenuation to the extent that the received signal cannot be extracted from noise. However, in presence of very intensive re-radiation when the SNR is very low the capacity drops same as no re-radiation case. Which is because we do not consider the equivalent sub-channel with very low eigenvalues in capacity calculation. We set a 0 dB threshold for $\frac{P\lambda_i^2}{m\sigma^2}$.

For both tropic and winter atmosphere, one of the capacity peaks is observed at 557 GHz. In more details, the capacity enhancement is achieved in a bandwidth of 10 GHz for winter atmosphere while the frequency window for tropic atmosphere is

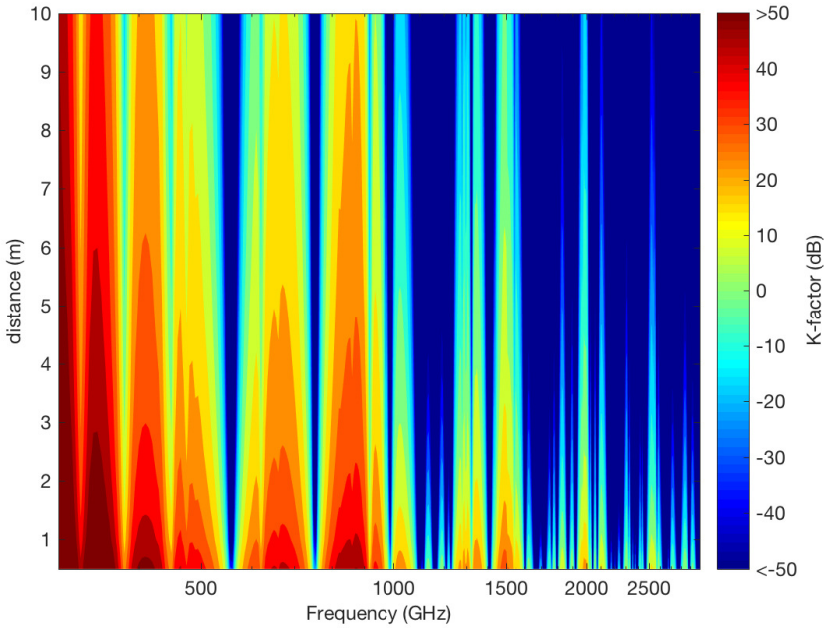

(a) Tropic atmosphere

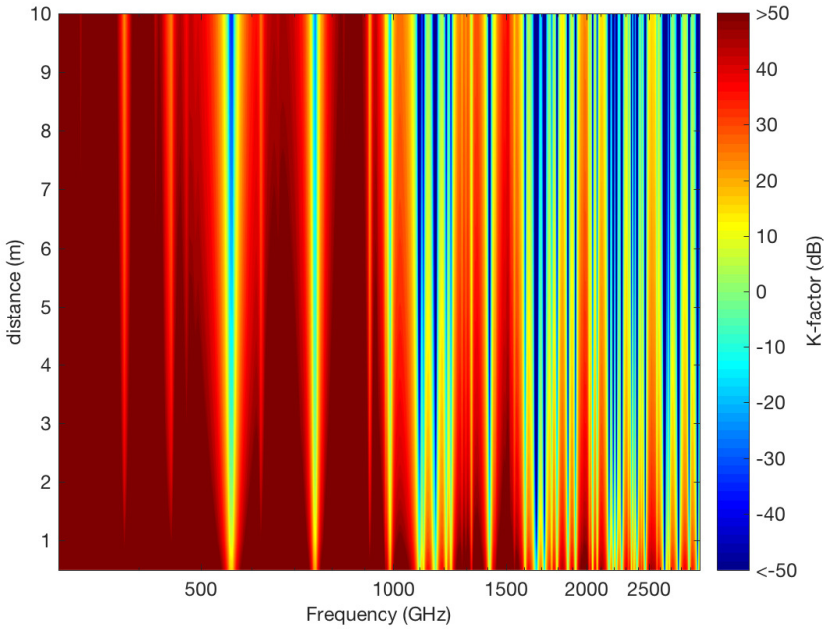

(b) Winter atmosphere

Figure 4.14: The Rician K-Factor of THz channel versus distance and frequency.

wider and about 50 GHz. From Figure 4.11, it can be seen there is a similar high absorption window around 750 GHz but in spite of same absorption coefficient, simulation results show a narrower capacity improvement at that frequency for tropic and almost no capacity rise for winter which is because of lower SNR. Therefore, the capacity enhancement frequency windows width is dependent on SNR and absorption coefficient. Hence, a dynamic bandwidth allocation based on SNR and absorption coefficient can be designed to exploit the high absorption frequency windows efficiently.

To characterize the scattering richness of channel independent of transmitting power, the Rician K-factor of 0.3-3 THz channel versus a distance range of 0.5-10 m is shown in Figure 4.14. The dark red illustrates the pure LoS channel and the dark blue shows a rich scattering Rayleigh channel. The lower humidity of winter atmosphere results in less scattering. Nevertheless, it still provides a sufficiently random channel in particular frequencies and distances which leads a significantly high spatial multiplexing gain.

4.5 Summary

In this chapter, we investigated the MIMO capacity for mmWave/THz, where the gas molecules in our atmosphere like Oxygen and water not only can increase the path loss, but also can re-radiate a copy of signal wave and equivalently create multipath channels. Our results showed that in certain frequency bands, where the absorption coefficient is significantly high, the MIMO channel can achieve a capacity that is close to the theoretical limit, thanks to the great improvement in spatial diversity. Our new discovery fundamentally changes our understanding on the relationship between the MIMO capacity and the frequency spectrum, especially for mmWave/THz communications with massive MIMO. While the re-radiation improve the scattering richness of channel, the scattering is not always beneficial for MIMO. In contrast with multiplexing technique which aim to maximize spectral capacity, the beamforming technique as a major solution in mmWave/THz band is used against very high path loss to maximize the SNR. The latter technique, not only does not take

advantage of multipath rays but also in intensive scattering loose the efficiency. We will discuss and compare this two MIMO approach in the next chapter.

Chapter 5

Beamforming and Multiplexing in the Presence of Re-radiation

The high propagation loss is the main issue of using mmWave/THz spectrum where part of the radio signal attenuation is due to molecular absorption. In more details, water molecules can intensify the total loss to more than 200 dB for some THz frequencies at 10-meters distance. Therefore, the potential applications the THz link are limited to short range communications such as nanosensors [102], wireless on-chip communications and wireless personal area networks [7].

To overcome the very high path loss, the transmit power could be largely increased. Unfortunately, this is not feasible with the current technology and it is limited to a few of mW [7]. Alternately, channel gain can be significantly improved by means of the multi-antenna *beamforming* technique. Indeed, due to the very small footprint of a large number of antennas at the THz band, beamforming using very large scale Multiple Input Multiple Output (MIMO) systems has been considered in the field as a practical solution which can provide up to 55 dB channel gain at 1 THz [2].

However, beamforming comes at the cost of system complexity and signaling overhead where the transmitter should receive the channel state information continuously and align the beam to the receiver. On the other hand, to achieve a significant MIMO beamforming gain in high frequency spectrum the beam would

become very narrow which is sometimes described as a *pencil beam*. This makes beamforming vulnerable to any transmitter/receiver mobility because it is difficult to perform beam re-alignment in a very short time interval.

Another approach to take advantage of MIMO is the MIMO multiplexing technique. While the beamforming technique strives to focus the transmission energy and achieve a large channel gain in a specific direction, the multiplexing technique builds it strength on creating parallel information channels. However, the multiplexing gain is significant only when there are enough non-negligible multipath signal components in a rich scattering environment. Because of the huge path loss, THz communication is usually assumed to be applied in as a Line-of-Sight (LoS) dominant channel and thus, the research focus has been on beamforming rather than multiplexing.

In chapter 4, we showed that in the channel medium, molecules absorb and re-radiate the electromagnetic energy in mmWave/THz band, which transforms the LoS channel into a rich-scattering environment. The re-radiation is usually considered as noise but the theoretical model(described in section 2.2) shows it is highly correlated to main signal [10]. In this chapter, we will theoretically investigate the mmWave/THz channel capacity for both cases of beamforming and multiplexing in a MIMO set-up. We find that the multiplexing technique can provide a considerable capacity gain in comparison with the beamforming technique on certain conditions. Also, in some other conditions where the beamforming yields a higher capacity, the multiplexing technique is still preferable choice due to its easier implementation. While multiplexing technique can use a blind precoding scheme without channel state information (CSI) to reduce the signaling overhead and transmitter complexity, in contrast, the beamforming technique always requires accurate CSI to smartly direct its energy in the spatial domain. Finally, we also find that in very low reception signal-to-noise (SNR) when CSI at transmitter is unavoidable, the multiplexing technique supplied with optimal power allocation is more efficient than beamforming.

5.1 System Description

5.1.1 Channel Decomposition

In this section, a general description of the beam forming and multiplexing is presented and the methodology of this chapter is formalized. The MIMO capacity formula is presented in chapter 4 where the channel is decomposed to equivalent independent parallel sub-channels. The channel transfer matrix H has a *singular value decomposition* (SVD):

$$\mathbf{H} = \mathbf{U}\mathbf{\Sigma}\mathbf{V}^* \tag{5.1}$$

Where $\mathbf{U}$ and $\mathbf{V}$ are $n_r \times n_r$ and $n_t \times n_t$ unitary matrices respectively, $\mathbf{\Sigma}$ is a rectangular diagonal $n_r \times n_t$ matrix and $\mathbf{V}^*$ is the conjugate transpose of $\mathbf{V}$. The non-negative real diagonal elements of $\mathbf{\Sigma}$, $\lambda_1 \geq \lambda_2 \geq ... \geq \lambda_n$, are the ordered singular values of matrix $\mathbf{H}$. If we assume:

$$\tilde{\mathbf{x}} = \mathbf{V}^*\mathbf{x}, \tag{5.2}$$

$$\tilde{\mathbf{y}} = \mathbf{U}^*\mathbf{y}, \tag{5.3}$$

$$\tilde{\mathbf{n}} = \mathbf{U}^*\mathbf{n}, \tag{5.4}$$

Then the channel equation (4.9) can be rewritten as

$$\tilde{\mathbf{y}} = \mathbf{\Sigma}\tilde{\mathbf{x}} + \tilde{\mathbf{n}}, \tag{5.5}$$

where the $\tilde{\mathbf{n}}$ has same distribution as $\mathbf{n}$ with the same variance σ^2 [98]. The equivalent parallel channels is shown in Figure 5.1 where i_{th} channel is a virtual SISO channel where gain is *eigenvalue* λ_i^2 and the power P_i can be allocated dedicatedly to. The capacity of MIMO is then calculated from (4.13).

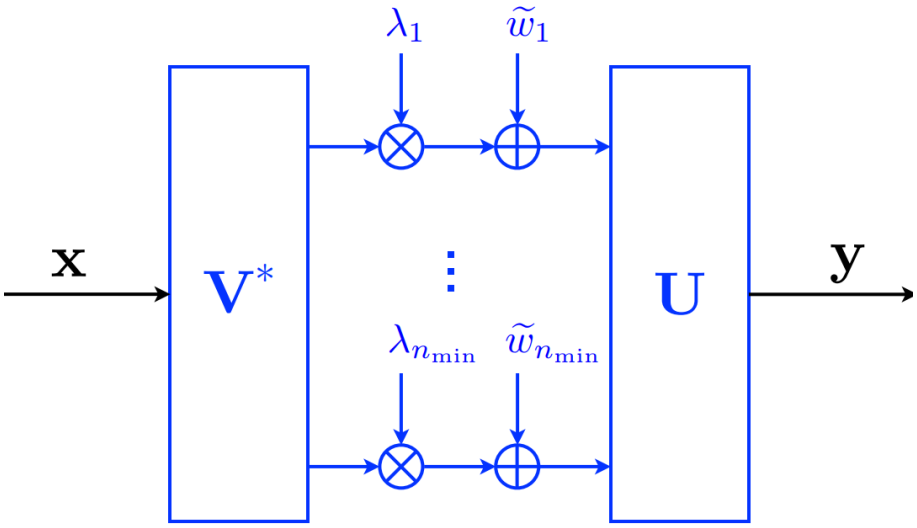

Figure 5.1: The equivalent independent parallel channels of MIMO channel through SVD.

5.1.2 Precoding Structure

The precoding is a technique to assign one or multiple information streams with a different weight to transmitter antennas. The aim of precoding is to maximize the bit rate or reliability. The first one results spatial multiplexing gain and second one diversity gain [103]. In the precoding, the channel state information (CSI) can be exploit to optimize the gain and precoding without channel state information is called blind precoding. We assume transmitter have z independent data streams to send simultaneously as a z-dimension symbol vector $\mathbf{s} = [s_1, ..., s_z]^T$ where $z \leq \min(n_r, n_t)$. In a linear precoding procedure, an $n_t \times z$ precoding matrix $\mathbf{W}$ is multiplied to symbol vector and generates the precoded signal vector $\mathbf{x}$.

$$\mathbf{x} = \mathbf{W}\mathbf{s} \tag{5.6}$$

In our work, we assume the precoder matrix is orthonormal such as $\mathbf{W}^\dagger\mathbf{W} = \mathbf{I}_z$.

SVD-Based Precoding

The optimum linear precoder in term of capacity can be obtained by choosing $\mathbf{W} = \mathbf{V}_z$ where the $\mathbf{V}_z\mathbf{Q}$ is an $n_t \times z$ matrix constructed from the first z columns of $\mathbf{V}$ derived from (5.1) and $\mathbf{Q}$ is $z \times z$ diagonal matrix for power allocation. The

optimum power allocation scheme is water-filling approach which is present in (4.14). Considering the total power constraint P

$$\mathbf{Q} = diag\{\sqrt{P_i}, ..., \sqrt{P_z}\} \quad \text{where} \quad \left(\sum_{i=1}^{z} P_i\right) \leq P. \tag{5.7}$$

Optimal Beamforming

To achieve the maximum SNR, beamforming is used to focus energy on one direction which leads to a large channel gain. In this approach, same copy of data is sent to all transmitter antennas to exploit the high single channel gain. Therefore, $z = 1$ and the optimal precoder vector is

$$\mathbf{W} = \sqrt{P}\mathbf{V}_1 \tag{5.8}$$

Where $\mathbf{V}_1$ is the first column of $\mathbf{V}$. What the transmitter requires from channel state is to receive only $\mathbf{V}_1$ from receiver to use as the precoder. However, it also results the complexity and signaling overhead .

In this chapter, to avoid confusion, we consider only SVD based transmit precoding and receive combining methods. Other beamforming methods are not in our scope since the upper bound of other beam-formers performance is SNR improvement of the SVD beam-former [104]. For further information, authors in [104] present comprehensive survey of beamforming-methods in the high-frequency band.

Multiplexing

As mentioned above, the multiplexing aims to exploit spatial multiplexing to increase the channel throughput. Hence, it is optimum when exploit all of parallel subchannels in Figure 5.1 to maximize the channel capacity. But the number of parallel channel depends on the channel rank which is equal to non-zero singular values in matrix $\mathbf{\Sigma}$. The channel rank is also called *degrees-of-freedom* and the maximum can be achieved if the channel matrix $\mathbf{H}$ is sufficiently random. In presence of CSI at transmitter the optimum multiplexing is to send an independent data stream on

each sub-channel. In other word, if we consider a full rank channel, $z = \min(n_r, n_t)$ and

$$\mathbf{W} = \mathbf{VQ} \tag{5.9}$$

Where the optimum $\mathbf{Q}$ is obtain by water-filling. For precoding, transmitter need to know the entire elements of matrix $\mathbf{V}$ and to run the water-filling, matrix $\mathbf{\Sigma}$. This results complexity and signaling overhead. To make the multiplexing simpler and avoid the waste of bandwidth, the multiplexing can implement with blind precoding. For this purpose, an arbitrary unitary matrix can be chosen and a uniform power allocation is considered $\mathbf{Q} = \sqrt{P}\mathbf{I}_{n_t}$. Hence, no CSI is needed in transmitter but this solution is not optimum especially when the channel is rank-deficient. In this case, part of power is allocated to sub-channel with zero gain. However, when the element of channel matrix $\mathbf{H}$ are i.i.d with zero mean (Rayleigh Channel) the channel is full rank and well conditioned, the uniform power allocation performance is close to water-filling.

Note that for a pure LoS channel, the degrees-of-freedom is one and thus, there is only one independent sub-channel. Therefore, the multiplexing and beamforming both use $\mathbf{W} = \sqrt{P}\mathbf{V}_1$ as precoder and result same capacity. Aim of this chapter is to compare above techniques in the presence of molecular re-radiation. As we discussed in chapter 4, in mmWave and THz bands, molecules can absorb and re-radiate electromagnetic energy in specific frequencies. This phenomena act such as scattering and can convert a pure LoS channel to a Rician or Rayleigh channel. In section 4.3, we showed characterized channel scattering richness by Rician K-factor which is a function of distance and channel medium absorption coefficient. Therefore, not only the SNR and absorption coefficient effects on MIMO performance but also the distance can play an important role. In next section, we simulate multiplexing and beamforming techniques and compare the performance under various SNR and absorption conditions.

5.2 Simulation Results

The simulation parameters and methodology are same as chapter 4. Note that the simulation results in previous chapter in Figure 4.7 and 4.13 are for MIMO multiplexing technique with uniform power allocation and blind precoding. It means the transmitter does not need CSI which leads to signaling overhead and complexity in the transmitter. As discussed before, beamforming is proposed as a major solution to overcome high path loss in higher frequency such as mmWave, especially in short range communication where the channel is LoS and there is not enough spatial diversity to take advantage of multiplexing. In order to compare Optimal Beamforming (OBF) and Multiplexing (MP) performance in presence of molecular re-radiation, we simulate various realistic scenarios where the transmit power and distance are chosen base on practical applications. We calculate the MIMO capacity of optimal beamforming (BF-rx/tx CSI), multiplexing with water-filling power allocation (MP-rx/tx CSI) and multiplexing with uniform power allocation (MP-rx CSI) and blind precoding. All three techniques are simulated in two conditions: with or without re-radiation.

5.2.1 Beamforming and Multiplexing in mmWave Band

The results for mmWave band are shown in Figures 5.2 and 5.3. First, it can be observed in Figure 5.2(a) for a 5 m distance where the SNR is significantly high, the MP technique with or without CSI at transmitter results significantly higher capacity at frequencies with high molecular re-radiation in comparison with OBF. For example at 60 GHz, While the SISO capacity is around 8 bps/Hz, the capacity increases to about 60 bps/Hz and 87 bps/Hz for MP without and with CSI at the transmitter. For low absorption frequency windows, OBF and MP with CSI in transmitter bring higher capacity in compare with MP with CSI only at receiver. As discussed before if we ignore the re-radiation, the MIMO performance is flat over entire band and only higher spreading loss decreases it in higher frequencies. Figure 5.2(b), 5.3(a) and 5.3(b), the channel is simulated for longer distance. Equation (4.16) showed the longer distance leads more scattering because of more molecules in the channel,

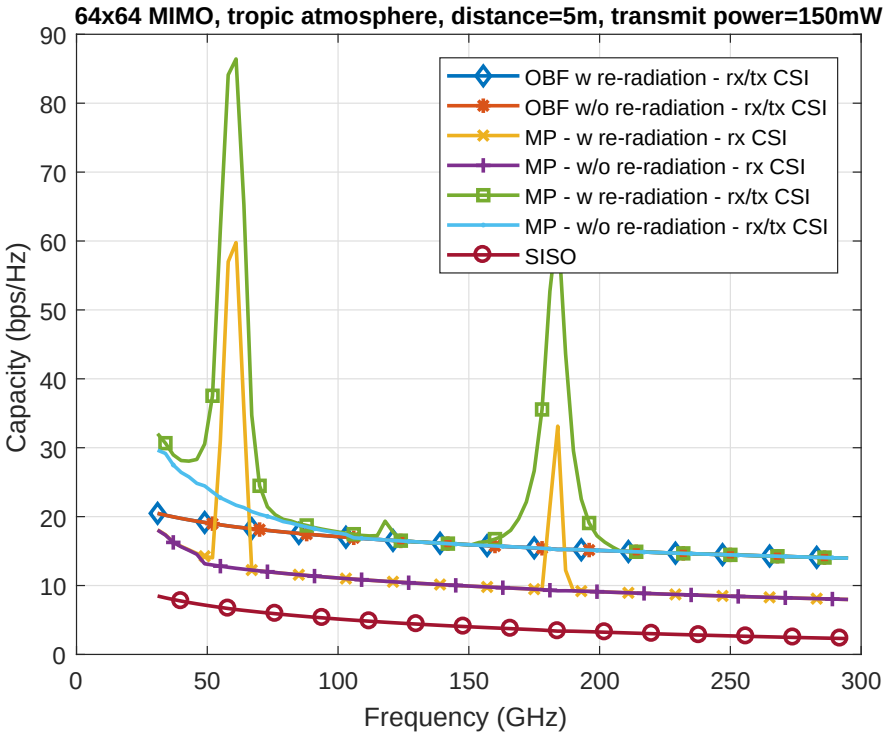

(a)

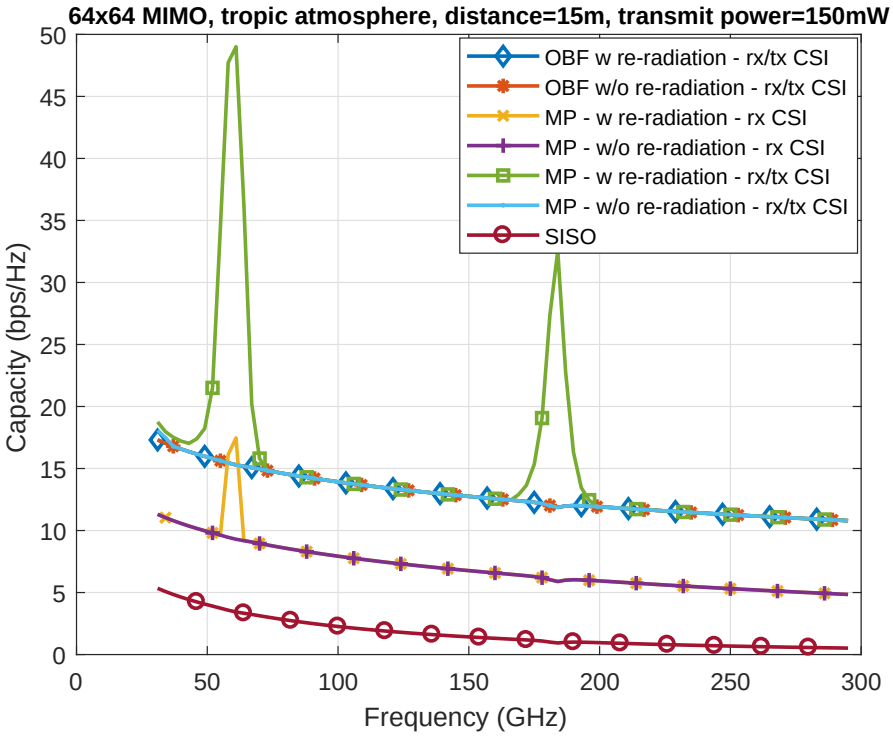

(b)

Figure 5.2: The 64X64 MIMO channel performance over mmWave band for distance 5 and 15 m.

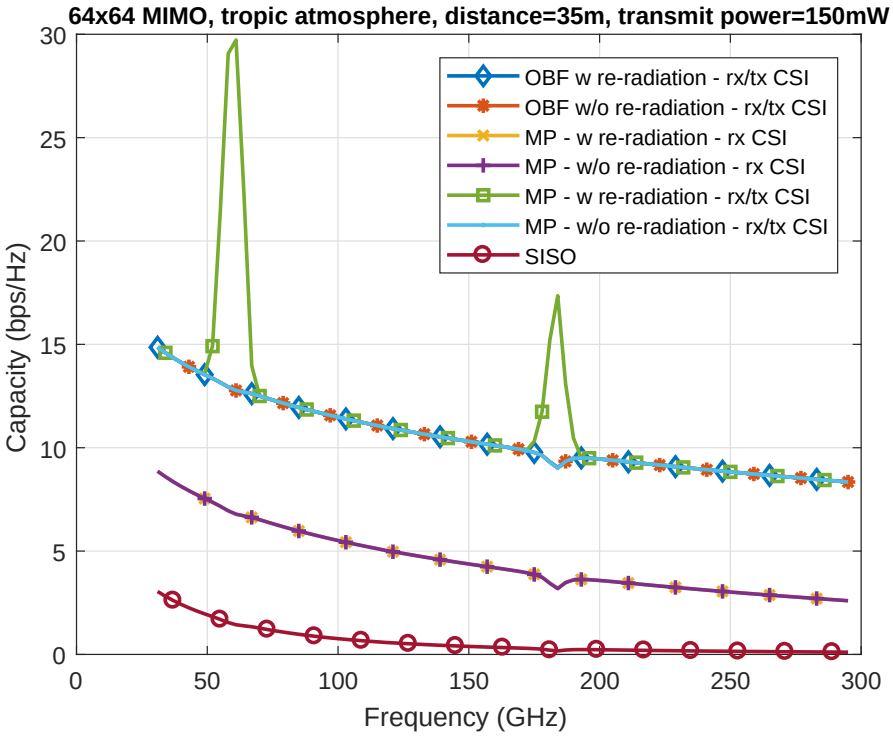

(a)

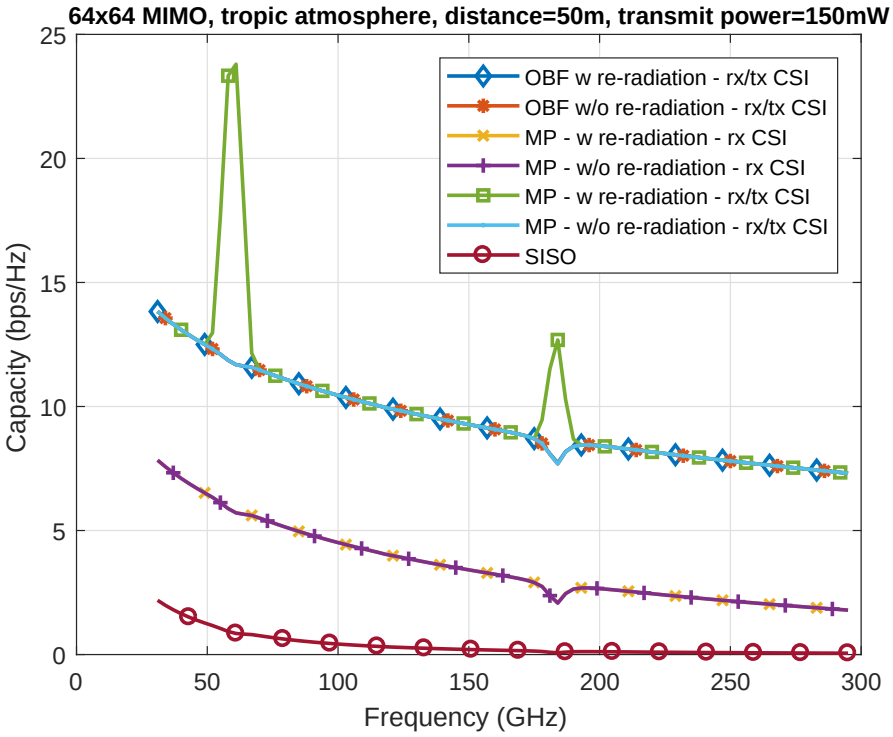

(b)

Figure 5.3: The 64X64 MIMO channel performance over mmWave band for distance 35 and 50m.

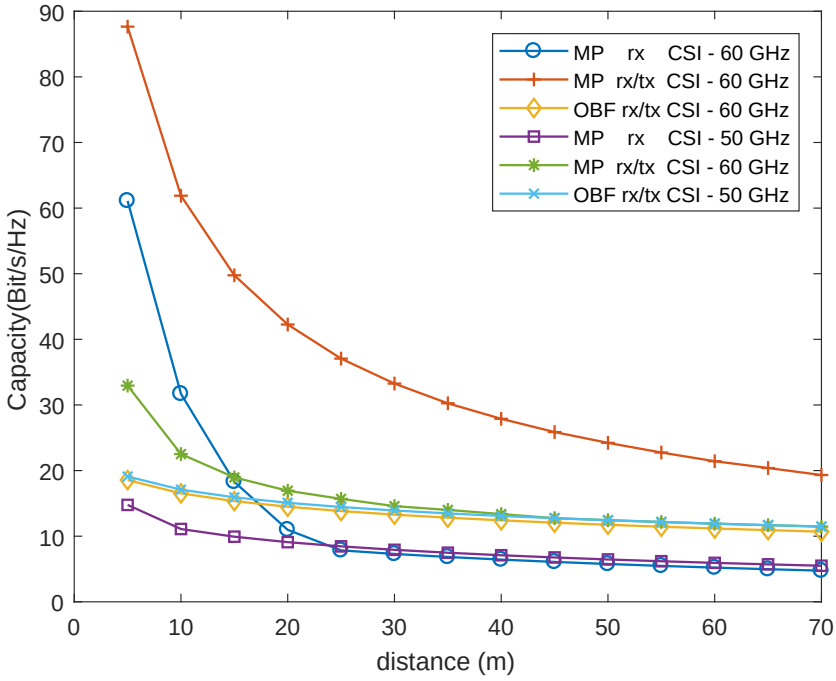

Figure 5.4: The MIMO capacity using different techniques over communication distance. Total transmit power is 150 mw.

but also the reception SNR will be much lower which reduces the MP gain. Thus, it can be seen in Figure 5.4 for distance further than 20 m, MP technique without CSI at the transmitter cannot take advantage of molecules re-radiation. However, the MP with rx/tx CSI is still providing higher capacity than OBF technique.

5.2.2 Beamforming and Multiplexing in THz Band

In this section, we extend our investigation to the THz band. The channel is simulated for two different transmit power and three distances. In THz band due to very high propagation loss, the applications are limited to short range communication. Furthermore, distances have been chosen to cover various application scenarios. For example, THz nanosensors are considered to communicate in a very short distance in the order of 0.1-10 cm or less, while THz communications are also nominated to provide terabit per second ultra high video communication link at around 0.1-1 m distance for home entrainment devices like TV or virtual reality (VR) devices. In addition, longer distances to a few meters characterize wireless personal or local

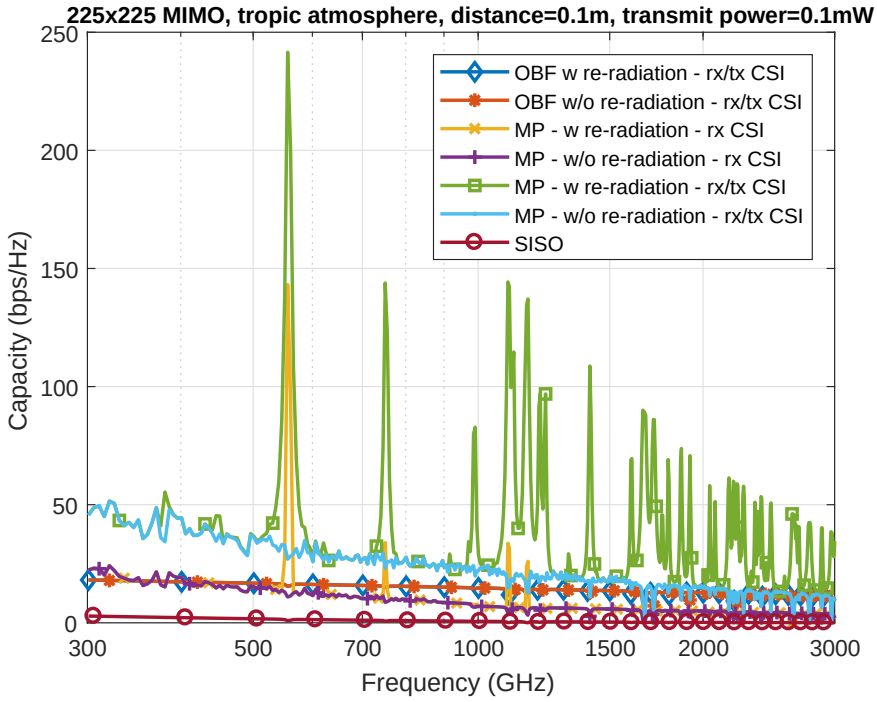

(a)

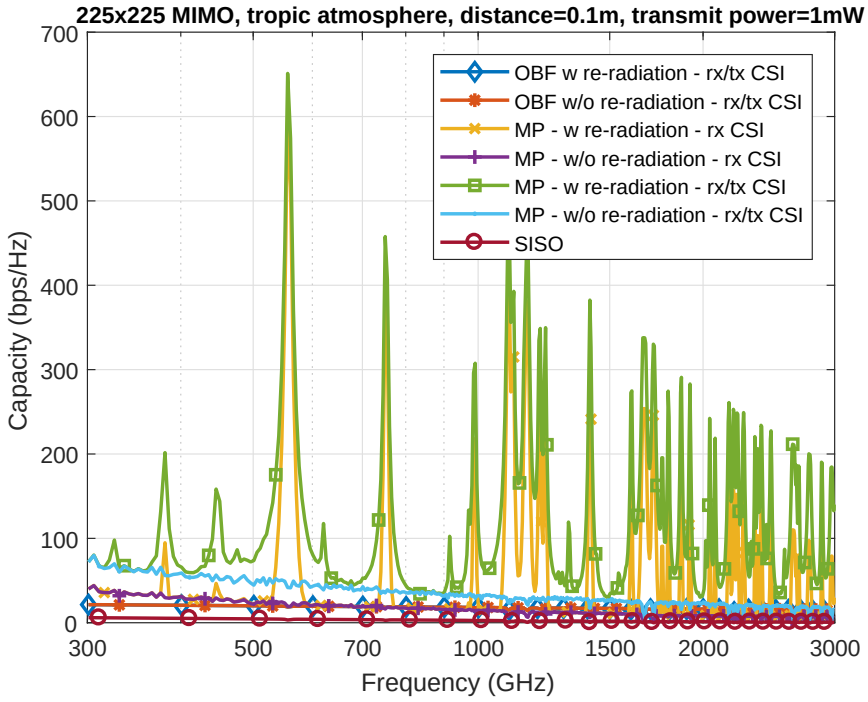

(b)

Figure 5.5: MIMO techniques performance for a very short range communication, 10 cm distance.

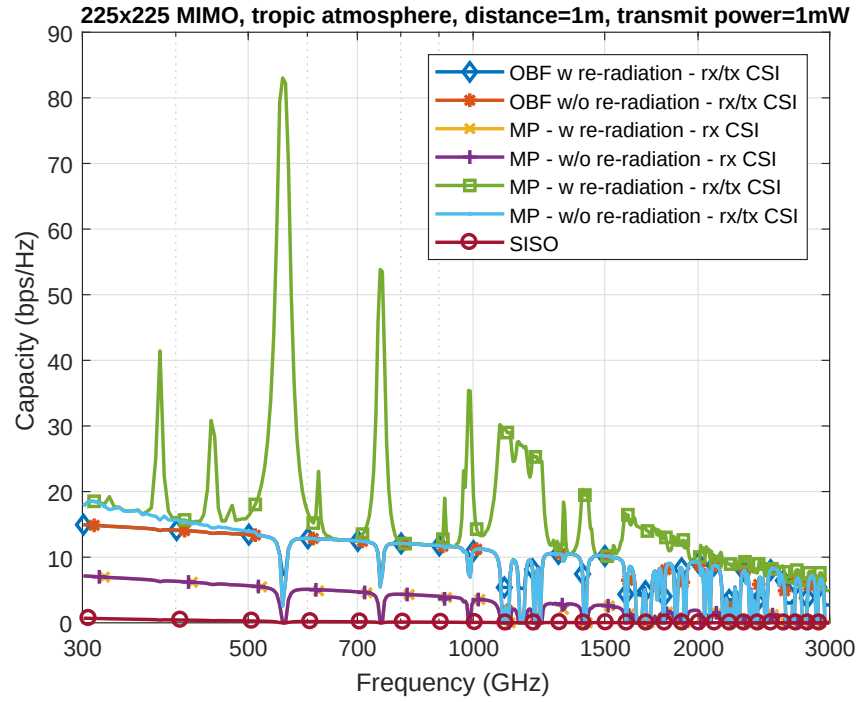

(a)

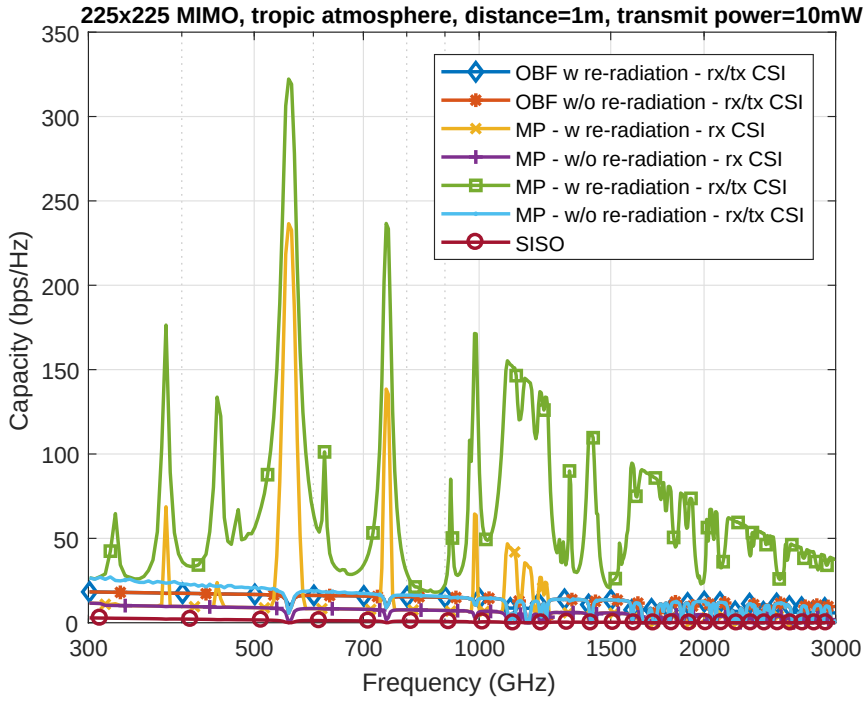

(b)

Figure 5.6: MIMO techniques performance for a short range communication, 1 m distance.

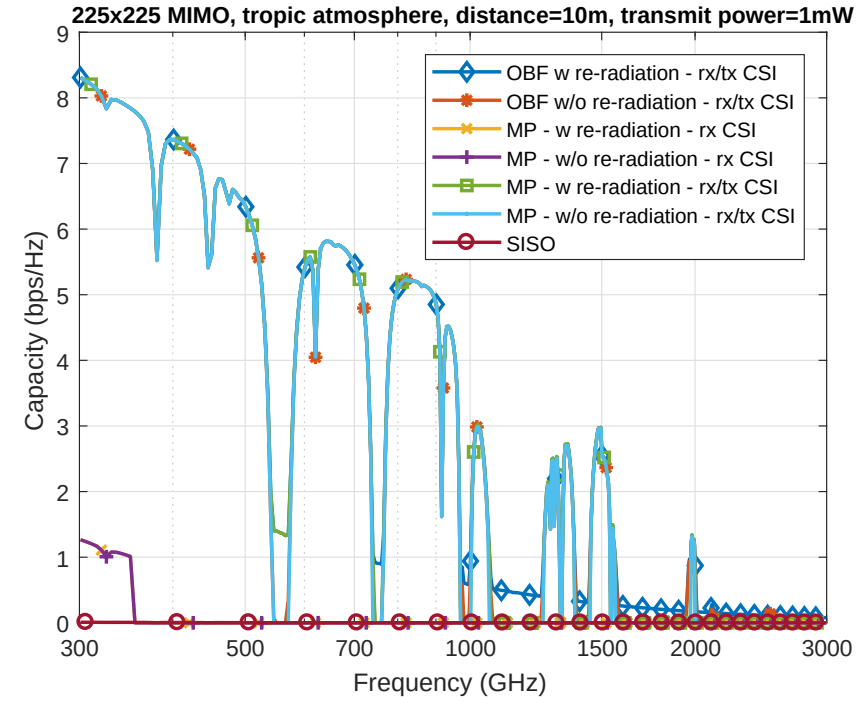

(a)

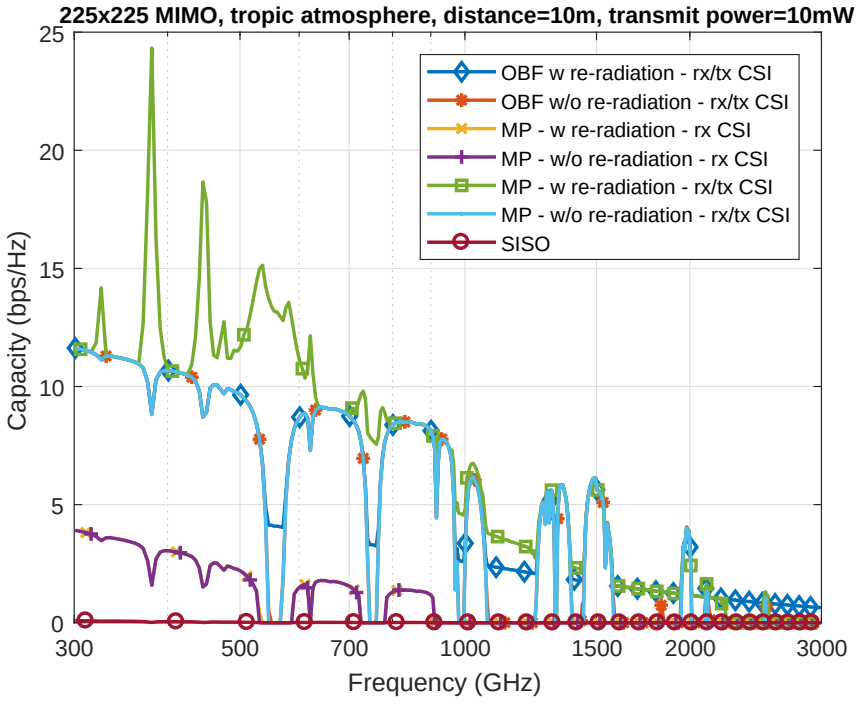

(b)

Figure 5.7: MIMO techniques performance for a medium range communication, 10 m distance.

networks.

Figure 5.5 illustrates the capacity of the investigated transmission techniques for a 10 cm distance. The transmit power is increased from 100 μW in Figure 5.5(a) to 1 mW in Figure 5.5(b). It can be seen that a huge performance difference exists between MP and OBF, thanks to the tremendous MP gain provided by the rich scattering environment due to molecule re-radiation. Furthermore, in very high absorption frequencies which existing studies consider as infeasible windows for THz communications, a significant capacity improvement can be observed. This is because more absorption leads to more re-radiation, which transforms a LoS dominant channel to Rayleigh channel. The details can be found in Section 4.3, where we have discussed how the re-radiation decreases the K-factor and creates a rich scattering environment. To sum up, the re-radiation improves the MP gain which is fundamentally supported by a better eigenvalue distribution and channel matrix rank in mathematical analysis. It is also observed that for ultra high absorption frequency such as 550 GHz, the MP technique with and without CSI at transmitter results same capacity. The reason is in very rich scattering in a Rayleigh channel, the uniform power allocation is close to optimum [75]. In other words, the water-filling scheme results in uniform power allocation.

In Figure 5.6, the distance is increased to 1 m. With a relatively large distance for THz communications, it can be seen the OBF gain is comparable with the MP gain. However, we can see the MP gain in high absorption windows, such as 540-580 GHz, is significantly higher than the rest of spectrum for a 10 mW transmit power. It is a different story for a 1 mW transmit power where the capacity of MP with uniform power allocation, drops to zero in high absorption windows. It is because of the equivalent SNR, $\left(\frac{P\lambda_i^2}{m\sigma^2}\right)$, of most parallel channels created by the MP technique is less than 0 dB and practically such parallel channels are not effective because the receiver cannot reliably detect the received signals and the bit error rate is very high. Such results are not surprising since it has been shown in several works on conventional communication band [105] that the blind MP performance drops dramatically in low SNR. However, considering the same implementation challenges of OBF and MP with transmitter CSI, the MP technique might still be a preferable

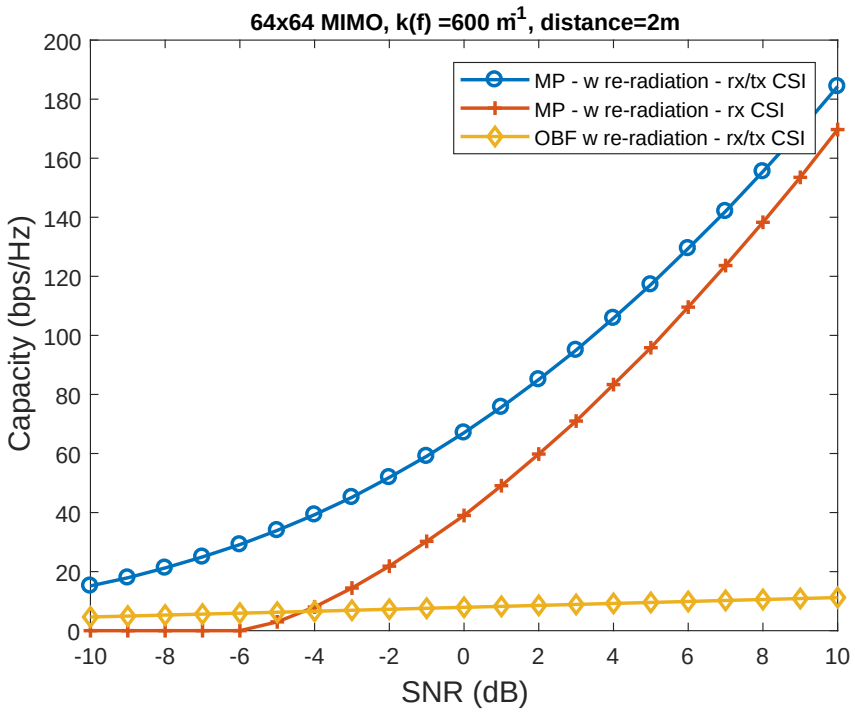

(a)

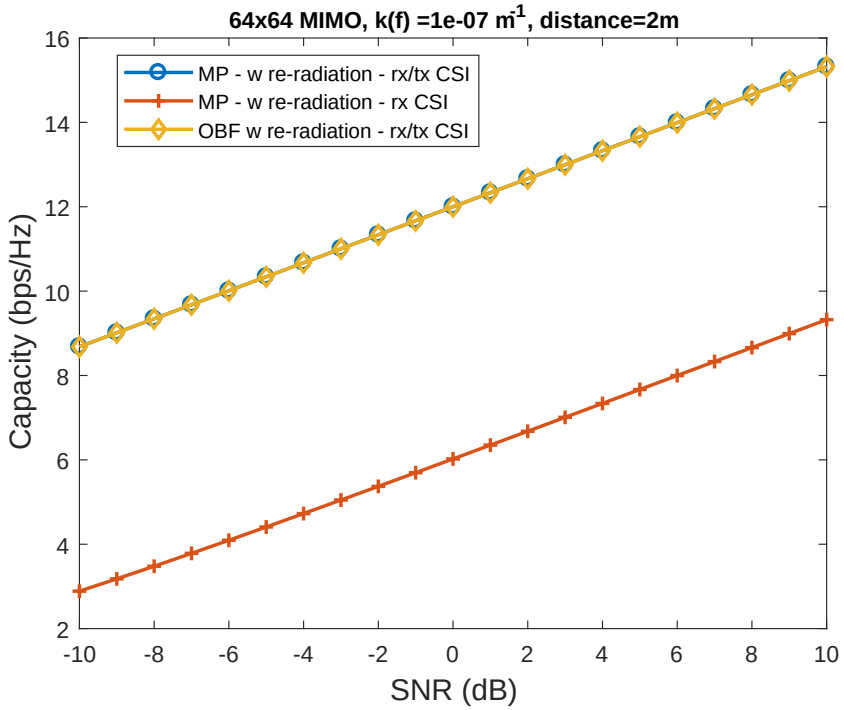

(b)

Figure 5.8: Capacity of MIMO vs. SNR for very low and very high absorption channel.

choice for frequency up to 1 THz. For example, it can be observed in Figure 5.6(a) at 0.9 THz, the capacity is 4 and 11.7 bps/Hz for the MP without and OBF/MP with transmitter CSI, respectively.

Finally, Figures 5.7 present the results for a 10 m distance case. For such a distance, path loss leads to a very low reception SNR and thus using CSI in the transmitter for both MP and OBF can increase the capacity significantly. The MP technique with uniform power allocation is almost impractical for very low SNR. It is well-known that OBF technique is not very effective where there are strong multipath rays [105]. Thus, it is observed that in very high absorption frequency windows, the OBF performance drops sharply. It is not only because of receiving strong NLoS rays caused by molecule re-radiation but also due to LoS signal attenuation. Note that the simple MP technique without CSI the transmitter can take advantage of same windows in high SNR as we discussed above for Figure 5.6(b).

To show the impact of SNR and absorption coefficient in capacity among the simulated techniques, the resulted capacity for extremely low and high absorption channel medium is shown in Figure 5.8 versus SNR which is the reception SNR of a single channel with same transmit power. The number of antennas is reduced to 64x64 to have a smaller gap and better resolution. Figure 5.8(a) presents a very high re-radiation channel where the power of NLoS re-radiated components is much stronger than LoS signal and the channel is Rayleigh. As can be seen for low SNR, blind precoding with uniform power allocation is almost unsuccessful to improve MIMO capacity. However, the impact of re-radiation becomes significant for SNR above -3 dB and we can see when SNR is high enough the blind MP capacity is close to MP with CSI at the transmitter. On the other hand, the capacity of a channel with a very low absorption coefficient is illustrated in Figure 5.8(b). The re-radiation is almost negligible and it is a pure LoS channel. For such channel, it can be observed the MP with rx/tx CSI results in the same capacity as beamforming which is because the channel rank is one an all the power is allocated to a single data stream on one information path. Hence, when there is not enough signal strength at receiver, the transmitter should have CSI to steering beam toward the receiver. Furthermore, the advantage of water-filling MP in comparison with OBF is that

MP can take advantage of both beam shaping and multiplexing over a few parallel path in the cost of more signaling overhead. To sum up, Once again, The results are shown in Figure 5.8 highlight our theoretical discovery that re-radiation can be a key player in mmWave/THz MIMO communication.

5.3 Summary

In this Chapter, we compared the beam forming and multiplexing techniques of MIMO in the mmWave/THz band. We showed the received signal has enough strength, high transmit power or lower distance, the multiplexing technique can provide a considerable capacity gain compared with beamforming thanks to molecular re-radiation. Our theoretical model also showed re-radiation of molecules in the THz band can be helpful for massive MIMO system to improve the channel performance using multiplexing technique. The re-radiation can provide significantly strong multi path components to achieve a full spatial multiplexing gain where the receiver is in enough SNR coverage. It means some very high absorption frequency windows which have been formerly pointed as not feasible for communication might be a preferable choice for MIMO in some certain applications. On the other hand, for beyond a few meters such as 10 meters, there should be channel state information at the transmitter to exploit channel spatial multiplexing, otherwise, the multiplexing capacity drops to zero where the beamforming technique can still provide effective spectrum efficiency. However, providing channel state information at transmitter results in complexity and protocol overhead for both beamforming and multiplexing techniques. In summary, we showed in the mmWave/THz band, both low absorption and high absorption frequency windows can be used for communication through MIMO where the beamforming and multiplexing can be the effective techniques respectively.

Chapter 6

Conclusion and Future Work

In this chapter, we summarize and highlight the key research outcomes of this study, and discuss possible future work in this area.

6.1 Key Outcomes and Concluding Remarks

This thesis investigated molecular absorption and re-radiation in the frequency range of 0.03-10 THz. We first used the common assumption that re-radiation is simply noise, and used real atmospheric data from selected Australian cities to demonstrate the variation of channel composition. Accordingly, it results spatio-temporal channel variation. In a different approach, we considered the correlation between the main signal and molecular re-radiation, and showed that this phenomenon can enhance communication capacity at higher frequencies. The key outcomes and conclusions of this thesis are presented below.

- We applied well-known molecular absorption models to 12 months of hourly air quality and weather data collected from the three largest Australian cities in 2015. We found that even when there is no rain, there can be significant diurnal variation in both attenuation and noise between two communicating devices separated by a fixed distance. The attenuation and noise generally drops in the middle of the day when the temperature rises and humidity falls, but remains high during the night. The diurnal variation was more significant

in summer than in winter. This observation was valid for all bands within the mmWave/Thz spectrum except for the 60 GHz band, which remained very stable through the day. This is due to the fact that 60 GHz is mainly affected by the amount of oxygen in the air, which remains relatively stable despite fluctuations in temperature and humidity.

- We collected data from 273 weather stations in various Sydney suburbs. We found that temperature and humidity varied significantly between coastal and inland suburbs. We analyzed the impact of spatial atmosphere variation on high-speed mobile users and showed that it led to temporal channel variation when users traveled across the urban area.

- We assumed molecular re-radiation to comprise multipath signal components, and thus the mmWave/THz channel was modeled as a Rician channel. A channel transfer function was calculated by superposition of the LoS channel with deterministic elements and an i.i.d random channel resulting from the re-radiation. We used the well-known Rician K-factor to quantify the portion of re-radiation in the received signal. In the other word, the K-factor quantified the scattering richness of the channel.

- Based on the MIMO theory, we showed that molecular absorption can reduce the Rician K-factor and transfer the channel from being a pure LoS channel (very low absorption) to a fully random Rayleigh channel. Our analytical study revealed that significant molecular re-radiation in the channel could increase the MIMO capacity of an apparently LoS channel by increasing the degrees-of-freedom and improving statistical conditions.

- Since molecular absorption is frequency selective, we found that the MIMO performance was also frequency selective in the mmWave and THz bands, which is against the common understanding of MIMO. While the capacity gain can only be achieved in narrow windows centered around 60 GHz and 180 GHz within the mmWave spectrum, the gains are achievable across a large part of the THz spectrum.

- In spite of the MIMO multiplexing gains dropping dramatically for low SNRs,

we showed that for some conditions, blind multiplexing can still result in notable MIMO capacity in comparison of beamforming, which adds complexity and signaling overhead to the channel.

- Our results revealed that for high SNR and high re-radiation conditions, the multiplexing technique with blind precoding achieves an enormous capacity gain, much larger than that of beamforming and comparable to multiplexing with optimum precoding. Note that the key advantage of blind multiplexing is its lower complexity and lack of signaling overhead.

- We showed that for very low SNRs, blind precoding is not practical. However, in the presence of sufficient re-radiation, multiplexing with CSI at the transmitter can still result in better capacity gains than beamforming.

6.2 Future Work

Our theoretical study was based on the well-known molecular absorption and re-radiation model which has been published in several important studies [7, 10–12, 35, 50, 54]. However, experimental measurements are required to validate simulation results. Hence, in the first step, we suggest measuring the K-Factor in a preferably open space environment and at one of the high absorption frequency bands such as 60 or 180 GHz. Secondly, a prototype MIMO system should be developed to measure MIMO performance with and without re-radiation, for example, in a vacuum chamber. The simple idea is to measure the K-factor or impulse response of channel in the vacuum chamber and compare with a chamber containing normal air.

Furthermore, a theoretical or experimental study should investigate the channel coherent time in the presence of molecular re-radiation. We believe that this has a very important impact on our theoretical findings, especially when MIMO is designed to use CSI at the transmitter for precoding purposes. The key point here is to discover how quickly the current CSI expires, and how soon the channel measurement feedback data should be updated. There is a new challenge here. The copied signal from molecules has a random phase which may change much faster than

communication signal period time. Therefore, the conventional coding/modulation techniques may not be practical to detect distorted signal and to remove the inter-symbol interference.

Moreover, the channel scatterers are molecules which are moving constantly. On the other hand, the thermal energy of molecules is also variable. Therefore, the same question as above is how dynamic the CSI could be. However, the huge number of molecules in the channel medium may cause a steady channel where the summation of a very large number of random received phase can have an i.i.d Gaussian distribution. To verify the CSI variation, authors suggest a Monte Carlo simulation of channel environment in the time domain to investigate the variation of received NLoS (re-radiated) signal components at the receiver such as done in [106].In this approach, a large number of wandering photons can be simulated which are propagated in all directions, hit molecules and is re-radiated in a random direction. The photon is traced through several collisions and by repeating this with a vast number of photons, the flow of photons at the receiver can be characterized.

Bibliography

[1] Gustavo A. Siles, Jose Manuel Riera, and Padro Garcia-del Pino. Atmospheric Attenuation in Wireless Communication Systems at Millimeter and THz Frequencies [Wireless Corner]. *IEEE Antennas and Propagation Magazine*, 57(1):48–61, 2015.

[2] Ian F. Akyildiz and Josep Miquel Jornet. Realizing ultra-massive mimo (1024x1024) communication in the (0.06-10) terahertz band. *Nano Communication Networks*, 8:46 – 54, 2016.

[3] Beating the heat in the world big cities. `http://earthobservatory.nasa.gov/Features/GreenRoof/`.

[4] L.S. Rothman, I.E. Gordon, Y. Babikov, A. Barbe, D. Chris Benner, P.F. Bernath, M. Birk, L. Bizzocchi, V. Boudon, L.R. Brown, A. Campargue, K. Chance, E.A. Cohen, L.H. Coudert, V.M. Devi, B.J. Drouin, A. Fayt, J.-M. Flaud, R.R. Gamache, J.J. Harrison, J.-M. Hartmann, C. Hill, J.T. Hodges, D. Jacquemart, A. Jolly, J. Lamouroux, R.J. Le Roy, G. Li, D.A. Long, O.M. Lyulin, C.J. Mackie, S.T. Massie, S. Mikhailenko, H.S.P. MÃijller, O.V. Naumenko, A.V. Nikitin, J. Orphal, V. Perevalov, A. Perrin, E.R. Polovtseva, C. Richard, M.A.H. Smith, E. Starikova, K. Sung, S. Tashkun, J. Tennyson, G.C. Toon, Vl.G. Tyuterev, and G. Wagner. The hitran2012 molecular spectroscopic database. *Journal of Quantitative Spectroscopy and Radiative Transfer*, 130:4 – 50, 2013.

[5] Cisco Visual Networking Index. Global mobile data traffic forecast update, 2016–2021 white paper. *link: https://goo.gl/KTqw1f*, 2016.

[6] Juha Karjalainen, Maziar Nekovee, Howard Benn, Wuk Kim, JeongHo Park, and Hwang Sungsoo. Challenges and opportunities of mm-wave communication in 5g networks. In *Cognitive Radio oriented Wireless networks and communications (CROWNCOM), 2014 9th International Conference on*, pages 372–376. IEEE, 2014.

[7] Ian F. Akyildiz, Josep Miquel Jornet, and Chong Han. Terahertz band: Next frontier for wireless communications. *Physical Communication*, 12:16 – 32, 2014.

[8] Theodore S Rappaport, Shu Sun, Rimma Mayzus, Hang Zhao, Yaniv Azar, Kevin Wang, George N Wong, Jocelyn K Schulz, Mathew Samimi, and Felix Gutierrez. Millimeter wave mobile communications for 5g cellular: It will work! *IEEE access*, 1:335–349, 2013.

[9] Konstantinos Ntontin and Christos Verikoukis. Towards the performance enhancement of microwave cellular networks through thz links. *IEEE Transactions on Vehicular Technology*, 2016.

[10] Josep Miquel Jornet Montana. *Fundamentals of electromagnetic nanonetworks in the terahertz band*. PhD thesis, Georgia Institute of Technology, 2013.

[11] Joonas Kokkoniemi, Janne Lehtomäki, and Markku Juntti. A discussion on molecular absorption noise in the terahertz band. *Nano Communication Networks*, 2015.

[12] Joonas, Kokkoniemi. *Nanoscale Sensor Networks: The Thz Band as a Communication Channel*. PhD thesis, UNIVERSITATIS OULUENSIS, 2017.

[13] Yong-Ping Zhang, Peng Wang, and A. Goldsmith. Rainfall effect on the performance of millimeter-wave mimo systems. *Wireless Communications, IEEE Transactions on*, 14(9):4857–4866, Sept 2015.

[14] Jayavardhana Gubbi, Rajkumar Buyya, Slaven Marusic, and Marimuthu Palaniswami. Internet of things (iot): A vision, architectural elements, and future directions. *Future Generation Computer Systems*, 29(7):1645 – 1660, 2013.

[15] Jean Sebanstien-Bedo Orange, Ana Garcia Armada, Barry Evans, Alex Galis, and Holger Karl. White paper for research beyond 5g. 2016.

[16] Christopher J Hansen. Wigig: Multi-gigabit wireless communications in the 60 ghz band. *Wireless Communications, IEEE*, 18(6):6–7, 2011.

[17] Richard J. Weiler, Michael Peter, Wilhelm Keusgen, and Mike Wisotzki. Measuring the busy urban 60 GHz outdoor access radio channel. *Proceedings - IEEE International Conference on Ultra-Wideband*, (November):166–170, 2014.

[18] Wilhelm Keusgen, Andreas Kortke, Michael Peter, and Richard Weiler. A Highly Flexible Digital Radio Testbed and 60 GHz Application Examples. *Microwave Conference (EuMC), European*, pages 740–743, 2013.

[19] Xiaoyi Zhu, Angela Doufexi, and Taskin Kocak. A performance evaluation of 60 GHz MIMO systems for IEEE 802.11ad WPANs. *IEEE International Symposium on Personal, Indoor and Mobile Radio Communications, PIMRC*, pages 950–954, 2011.

[20] Wilhelm Keusgen, Andreas Kortke, Leszek Koschel, Michael Peter, Richard Weiler, Herbert Zirath, Marcus Gavell, and Zhongxia He. An NLOS-capable 60 GHz MIMO demonstrator: System concept & performance. *2011 IEEE 9th International New Circuits and Systems Conference, NEWCAS 2011*, pages 265–268, 2011.

[21] Michael Peter, Wilhelm Keusgen, and Jian Luo. A survey on 60 Ghz broadband communication: capability, applications and system design. *2008 European Microwave Integrated Circuit Conference, EuMIC 2008*, (November):1–4, 2008.

[22] Lin Kai Chiu, Ming Chen Chiang, Pei Li Chiang, Yu Jen Chi, Sau Hsuan Wu, and Fu Chiarng Chen. Empirical MIMO capacity of a 2ÃŮ2 dual-polarized planar antenna array in indoor 60 GHz channels. *2013 8th International ICST Conference on Communications and Networking in China, CHINACOM 2013 - Proceedings*, pages 260–265, 2013.

[23] Michael Peter, Richard Weiler, BarÄśÅ§ Goktepe, Wilhelm Keusgen, and Kei Sakaguchi. Channel Measurement and Modeling for 5G Urban Microcellular Scenarios. *Sensors*, 16(8):1330, 2016.

[24] Ahmadreza Jafari, Theodoros Mavridis, Luca Petrillo, Julien Sarrazin, Michael Peter, Wilhelm Keusgen, Phillipe De Doncker, and Aziz Benlarbi-Delai. Uwb interferometry tdoa estimation for 60-ghz ofdm communication systems. *IEEE Antennas and Wireless Propagation Letters*, 15:1438–1441, 2016.

[25] Ieee standard for information technology–telecommunications and information exchange between systems–local and metropolitan area networks–specific requirements-part 11: Wireless lan medium access control (mac) and physical layer (phy) specifications amendment 3: Enhancements for very high throughput in the 60 ghz band. *IEEE Std 802.11ad-2012 (Amendment to IEEE Std 802.11-2012, as amended by IEEE Std 802.11ae-2012 and IEEE Std 802.11aa-2012)*, pages 1–628, Dec 2012.

[26] T.S. Rappaport, Shu Sun, R. Mayzus, Hang Zhao, Y. Azar, K. Wang, G.N. Wong, J.K. Schulz, M. Samimi, and F. Gutierrez. Millimeter wave mobile communications for 5g cellular: It will work! *Access, IEEE*, 1:335–349, 2013.

[27] Shu Sun and Theodore S Rappaport. Wideband mmwave channels: Implications for design and implementation of adaptive beam antennas. In *Microwave Symposium (IMS), 2014 IEEE MTT-S International*, pages 1–4. IEEE, 2014.

[28] Mustafa Riza Akdeniz, Yuanpeng Liu, Mathew K Samimi, Shu Sun, Sundeep Rangan, Theodore S Rappaport, and Elza Erkip. Millimeter wave channel modeling and cellular capacity evaluation. *IEEE journal on selected areas in communications*, 32(6):1164–1179, 2014.

[29] Mathew K Samimi and Theodore S Rappaport. Ultra-wideband statistical channel model for non line of sight millimeter-wave urban channels. In *Global Communications Conference (GLOBECOM), 2014 IEEE*, pages 3483–3489. IEEE, 2014.

[30] Mathew Samimi, Kevin Wang, Yaniv Azar, George N Wong, Rimma Mayzus, Hang Zhao, Jocelyn K Schulz, Shu Sun, Felix Gutierrez, and Theodore S Rappaport. 28 ghz angle of arrival and angle of departure analysis for outdoor cellular communications using steerable beam antennas in new york city. In *Vehicular Technology Conference (VTC Spring), 2013 IEEE 77th*, pages 1–6. IEEE, 2013.

[31] Felix Gutierrez, Shatam Agarwal, Kristen Parrish, and Theodore S Rappaport. On-chip integrated antenna structures in cmos for 60 ghz wpan systems. *IEEE Journal on Selected Areas in Communications*, 27(8), 2009.

[32] Josep Miquel Jornet and Ian F Akyildiz. Graphene-based Plasmonic Nano-transceiver for Terahertz Band Communication. In *8th European Conference on Antennas and Propagation (EuCAP)*, pages 2–6, The Hague, The Netherlands, 2014.

[33] Tadilo Endeshaw Bogale and Long Bao Le. Massive mimo and mmwave for 5g wireless hetnet: Potential benefits and challenges. *IEEE Vehicular Technology Magazine*, 11(1):64–75, 2016.

[34] Sylvain Collonge, Gheorghe Zaharia, and G EL Zein. Influence of the human activity on wide-band characteristics of the 60 ghz indoor radio channel. *IEEE Transactions on Wireless Communications*, 3(6):2396–2406, 2004.

[35] Josep Miquel Jornet and Ian F. Akyildiz. Femtosecond-Long Pulse-Based Modulation for Terahertz Band Communication in Nanonetworks. *IEEE Transactions on Communications*, 62(5):1742–1754, May 2014.

[36] Eisa Zarepour, Mahbub Hassan, Chun Tung Chou, and Adesoji Adesina. Open-loop power adaptation in nanosensor networks for chemical reactors. *IEEE Transactions on Molecular, Biological and Multi-Scale Communications*, 1(3):1–16, 2016.

[37] Ian Akyildiz, Josep Jornet, and Chong Han. Teranets: Ultra-broadband communication networks in the terahertz band. *IEEE Wireless Communications*, 21(4):130–135, 2014.

[38] Thomas Kürner. Towards Future THz Communications Systems. 5(1):11–17, 2012.

[39] K. Ishigaki, M. Shiraishi, S. Suzuki, M. Asada, N. Nishiyama, and S. Arai. Direct intensity modulation and wireless data transmission characteristics of terahertz-oscillating resonant tunnelling diodes. *Electronics Letters*, 48(10):582, 2012.

[40] Konstantinos Konstantinidis, Alexandros P Feresidis, and Michael J Lancaster. Micromachined periodic surfaces for planar terahertz antennas. In *Antennas and Propagation (EuCAP), 2014 8th European Conference on*, pages 215–219. IEEE, 2014.

[41] Pavel Penchev, Xiaobang Shang, S Dimov, and M Lancaster. Novel manufacturing route for scale up production of terahertz technology devices. *Journal of Micro and Nano-Manufacturing*, 4(2):021002, 2016.

[42] C. Han, A. O. Bicen, and I. F. Akyildiz. Multi-ray channel modeling and wideband characterization for wireless communications in the terahertz band. *IEEE Transactions on Wireless Communications*, 14(5):2402–2412, May 2015.

[43] P. Boronin, D. Moltchanov, and Y. Koucheryavy. A molecular noise model for thz channels. In *Communications (ICC), 2015 IEEE International Conference on*, pages 1286–1291, June 2015.

[44] Yu L Babikov, I E Gordon, and S N Mikhailenko. "HITRAN on the Web " , a new tool for HITRAN spectroscopic data manipulation. In *the proceeding of the ASA-HITRAN Conference*, Reims, France, Aug 29-31, 2012.

[45] U.S. Department of Commerce, National Institute of Standards and Technology, NIST Atomic Spectra Database, http://www.wareable.com/wearable-tech/a-brief-history-of-wearables.

[46] E. Zarepour, M. Hassan, C. T. Chou, and A. A. Adesina. Frequency Hopping Strategies for Improving Terahertz Sensor Network Performance over Composition Varying Channels. In *IEEE WoWMoM*, Sydney, Australia, June, 2014.

[47] J.S. Seybold. *Introduction to RF Propagation*. Wiley, 2005.

[48] G.R. Maccartney, T.S. Rappaport, M.K. Samimi, and S. Sun. Millimeter-wave omnidirectional path loss data for small cell 5g channel modeling. *Access, IEEE*, 3:1573–1580, 2015.

[49] Attenuation by atmospheric gases, international telecommunication union itu-r recommendation p.676-10. 2013.

[50] F. Box. Utilization of atmospheric transmission losses for interference-resistant communications. *Communications, IEEE Transactions on*, 34(10):1009–1015, Oct 1986.

[51] J. Sayers, S. R. Golwala, P. A. R. Ade, J. E. Aguirre, J. J. Bock, S. F. Edgington, J. Glenn, A. Goldin, D. Haig, A. E. Lange, G. T. Laurent, P. D. Mauskopf, H. T. Nguyen, P. Rossinot, and J. Schlaerth. Studies of millimeter-wave atmospheric noise above mauna kea. *The Astrophysical Journal*, 708(2):1674, 2010.

[52] JM Jornet and IF Akyildiz. Channel modeling and capacity analysis for electromagnetic wireless nanonetworks in the terahertz band. *IEEE Transactions on Wireless Communications*, 10(10):3211–3221, October 2011.

[53] Josep Jornet and Ian F. Akyildiz. Information capacity of pulse-based Wireless Nanosensor Networks. In *the proceeding of the 8th IEEE Communications Society Conference on Sensor, Mesh and Ad Hoc Communications and Networks*, pages 80–88, Salt Lake City, UT, June 27-30, 2011.

[54] Massimiliano Pierobon, Josep Miquel Jornet, Nadine Akkari, Suleiman Almasri, and Ian F. Akyildiz. A routing framework for energy harvesting wireless nanosensor networks in the Terahertz Band 1. *Wireless Networks (Springer)*, 20(5):1169–1183, November July 2014.

[55] TL Frey. The Effects of the Atmosphere and Weather on the Performance of a mm-Wave Communication Link. *Applied Microwave and Wireless*, 10:0–2, 1999.

[56] Hans J Liebe. An updated model for millimeter wave propagation in moise air. *Radio Science*, 20(5):1069–1089, 1985.

[57] Zhouyue Pi and F. Khan. An introduction to millimeter-wave mobile broadband systems. *Communications Magazine, IEEE*, 49(6):101–107, June 2011.

[58] State of australian cities 2014-2015.

[59] P. Kumari, N. Gonzalez-Prelcic, and R. W. Heath. Investigating the ieee 802.11ad standard for millimeter wave automotive radar. In *Vehicular Technology Conference (VTC Fall), 2015 IEEE 82nd*, pages 1–5, Sept 2015.

[60] Vutha Va, Takayuki Shimizu, Gaurav Bansal, Robert W Heath Jr, et al. Millimeter wave vehicular communications: A survey. *Foundations and Trends® in Networking*, 10(1):1–113, 2016.

[61] Shahid Mumtaz, Josep Miquel Jornet, Jocelyn Aulin, Wolfgang H Gerstacker, Xiaodai Dong, and Bo Ai. Terahertz communication for vehicular networks. *IEEE Transactions on Vehicular Technology*, 66(7):5617–5625, 2017.

[62] Ke Guan, Guangkai Li, Thomas Kuerner, Andreas F Molisch, Bile Peng, Ruisi He, Bing Hui, Junhyeong Kim, and Zhangdui Zhong. On millimeter wave and thz mobile radio channel for smart rail mobility. *IEEE Transactions on Vehicular Technology*, 2016.

[63] Jun Yao, Salil S Kanhere, and Mahbub Hassan. Improving qos in high-speed mobility using bandwidth maps. *IEEE Transactions on Mobile Computing*, 11(4):603–617, 2012.

[64] GE Athanasiadou, D Zarbouti, and GV Tsoulos. Automatic location of base-stations for optimum coverage and capacity planning of lte systems. In *Antennas and Propagation (EuCAP), 2014 8th European Conference on*, pages 2077–2081. IEEE, 2014.

[65] Justin Ormont, Jordan Walker, Suman Banerjee, Ashwin Sridharan, Mukund Seshadri, and Sridhar Machiraju. A city-wide vehicular infrastructure for

wide-area wireless experimentation. In *Proceedings of the third ACM international workshop on Wireless network testbeds, experimental evaluation and characterization*, pages 3–10. ACM, 2008.

[66] Jun Yao, Salil S Kanhere, and Mahbub Hassan. Quality improvement of mobile video using geo-intelligent rate adaptation. In *Wireless Communications and Networking Conference (WCNC), 2010 IEEE*, pages 1–6. IEEE, 2010.

[67] Ayub Bokani, Mahbub Hassan, Salil Kanhere, and Xiaoqing Zhu. Optimizing http-based adaptive streaming in vehicular environment using markov decision process. *IEEE Transactions on Multimedia*, 17(12):2297–2309, 2015.

[68] Bayan Taani and Roger Zimmermann. Spatio-temporal analysis of bandwidth maps for geo-predictive video streaming in mobile environments. In *Proceedings of the 2016 ACM on Multimedia Conference*, pages 888–897. ACM, 2016.

[69] David Tse and Pramod Viswanath. *Fundamentals of wireless communication*. Cambridge university press, 2005.

[70] Oussama Souihli and Tomoaki Ohtsuki. Benefits of rich scattering in mimo channels: a graph-theoretical perspective. *IEEE Communications Letters*, 17(1):23–26, 2013.

[71] Andrea Goldsmith, Syed Ali Jafar, Nihar Jindal, and Sriram Vishwanath. Capacity limits of mimo channels. *IEEE Journal on selected areas in Communications*, 21(5):684–702, 2003.

[72] Dhananjay A Gore and Arogyaswami J Paulraj. Mimo antenna subset selection with space-time coding. *IEEE Transactions on signal processing*, 50(10):2580–2588, 2002.

[73] Shaozhen Zhu, Tahereh S Ghazaany, Steven MR Jones, Raed A Abd-Alhameed, Jimes M Noras, Tyler Van Buren, Jonathan Wilson, Tim Suggett, and Simon Marker. Probability distribution of rician k-factor in urban, suburban and rural areas using real-world captured data. *IEEE Transactions on Antennas and Propagation*, 62(7):3835–3839, 2014.

[74] Ioannis Sarris and Andrew R Nix. Maximum mimo capacity in line-of-sight. In *Information, Communications and Signal Processing, 2005 Fifth International Conference on*, pages 1236–1240. IEEE, 2005.

[75] S. K. Jayaweera and H. V. Poor. On the capacity of multi-antenna systems in the presence of rician fading. In *Proceedings IEEE 56th Vehicular Technology Conference*, volume 4, pages 1963–1967 vol.4, 2002.

[76] Ming Kang and Mohamed-Slim Alouini. Capacity of mimo rician channels. *IEEE Transactions on Wireless Communications*, 5(1):112–122, 2006.

[77] Shu Sun, Theodore S Rappaport, Robert W Heath, Andrew Nix, and Sundeep Rangan. Mimo for millimeter-wave wireless communications: beamforming, spatial multiplexing, or both? *IEEE Communications Magazine*, 52(12):110–121, 2014.

[78] Wonil Roh, Ji-Yun Seol, Jeongho Park, Byunghwan Lee, Jaekon Lee, Yungsoo Kim, Jaeweon Cho, Kyungwhoon Cheun, and Farshid Aryanfar. Millimeter-wave beamforming as an enabling technology for 5g cellular communications: Theoretical feasibility and prototype results. *IEEE communications magazine*, 52(2):106–113, 2014.

[79] Taeyoung Kim, Jeongho Park, Ji-Yun Seol, Suryong Jeong, Jaeweon Cho, and Wonil Roh. Tens of gbps support with mmwave beamforming systems for next generation communications. In *Global Communications Conference (GLOBECOM), 2013 IEEE*, pages 3685–3690. IEEE, 2013.

[80] Josep Miquel Jornet and Ian F Akyildiz. Graphene-based plasmonic nano-antenna for terahertz band communication in nanonetworks. *IEEE Journal on selected areas in communications*, 31(12):685–694, 2013.

[81] Kumud Ranjan Jha and G. Singh. Terahertz planar antennas for future wireless communication: A technical review. *Infrared Physics & Technology*, 60:71 – 80, 2013.

[82] Ahmed Memon RIZWAN, Leung Y.C. DENNIS, and Chunho LIU. A review on the generation, determination and mitigation of urban heat island. *Journal of Environmental Sciences*, 20(1):120 – 128, 2008.

[83] Peter Brimblecombe. *Air composition and chemistry*. Cambridge University Press, 1996.

[84] EPA. Managing particles and improving air quality in nsw. 2013.

[85] Air quality data for nsw. `hhttp://www.environment.nsw.gov.au/aqms/`.

[86] RalphF. Keeling. Measuring correlations between atmospheric oxygen and carbon dioxide mole fractions: A preliminary study in urban air. *Journal of Atmospheric Chemistry*, 7(2):153–176, 1988.

[87] Michael Clugston and Rosalind Flemming. *Advanced chemistry*. Oxford University Press, 2000.

[88] Online historical weather. `http://weatherspark.com`.

[89] Online historical weather. `http://www.wunderground.com/history/`.

[90] David G Andrews. *An introduction to atmospheric physics*. Cambridge University Press, 2010.

[91] Afonso Eduardo, Ivo Sousa, and Antonio Rodrigues. Link adaptation strategies for cellular downlink with low-fixed-rate d2d underlay. 2014.

[92] Marco Giordani, Marco Mezzavilla, Aditya Dhananjay, Sundeep Rangan, and Michele Zorzi. Channel dynamics and snr tracking in millimeter wave cellular systems. In *European Wireless 2016; 22th European Wireless Conference; Proceedings of*, pages 1–8. VDE, 2016.

[93] Sang V Tran and Ahmed M Eltawil. Link adaptation for wireless systems. *Wireless Communications and Mobile Computing*, 14(16):1509–1521, 2014.

[94] Kin K. Leung, Peter F Driessen, Kapil Chawla, and Xiaoxin Qiu. Link adaptation and power control for streaming services in egprs wireless networks. *IEEE Journal on Selected Areas in Communications*, 19(10):2029–2039, 2001.

[95] S. Rangan, T. S. Rappaport, and E. Erkip. Millimeter-wave cellular wireless networks: Potentials and challenges. *Proceedings of the IEEE*, 102(3):366–385, Mar. 2014.

[96] Laurence D Barron. *Molecular light scattering and optical activity*. Cambridge University Press, 2004.

[97] M. Chiani, M. Z. Win, and A. Zanella. On the capacity of spatially correlated mimo rayleigh-fading channels. *IEEE Transactions on Information Theory*, 49(10):2363–2371, Oct 2003.

[98] David Tse and Pramod Viswanath. Chapter 07: MIMO I : spatial multiplexing and channel modeling. *Fundamentals of Wireless Communication*, pages 290–331, 2005.

[99] Farrokh R Farrokhi, Gerard J Foschini, A Lozano, and Reinaldo A Valenzuela. Link-optimal space-time processing with multiple transmit and receive antennas. *IEEE Communications Letters*, 5(3):85–87, 2001.

[100] Guillaume Lebrun, Mike Faulkner, Mansoor Shafi, and Peter J Smith. Mimo ricean channel capacity: an asymptotic analysis. *IEEE Transactions on Wireless Communications*, 5(6):1343–1350, 2006.

[101] S. A. Hosseini, E. Zarepour, M. Hassan, and C. T. Chou. Analyzing diurnal variations of millimeter wave channels. In *2016 IEEE Conference on Computer Communications Workshops (INFOCOM WKSHPS)*, pages 377–382, April 2016.

[102] Eisa Zarepour, Mahbub Hassan, Chun Tung Chou, and Adesoji A Adesina. Semon: Sensorless event monitoring in self-powered wireless nanosensor networks. *ACM Transactions on Sensor Networks (TOSN)*, 13(2):15, 2017.

[103] S-H Park, Heunchul Lee, and S-R Lee. A new beamforming structure based on transmit-mrc for closed-loop mimo systems. *IEEE Transactions on Communications*, 57(6):1847–1856, 2009.

[104] Shajahan Kutty and Debarati Sen. Beamforming for millimeter wave communications: An inclusive survey. *IEEE Communications Surveys & Tutorials*, 18(2):949–973, 2016.

[105] David Gesbert, Mansoor Shafi, Da-shan Shiu, Peter J Smith, and Ayman Naguib. From theory to practice: An overview of mimo space-time coded wireless systems. *IEEE Journal on selected areas in Communications*, 21(3):281–302, 2003.

[106] Joonas Kokkoniemi, Janne Lehtomäki, Kenta Umebayashi, and Markku Juntti. Frequency and time domain channel models for nanonetworks in terahertz band. *IEEE Transactions on Antennas and Propagation*, 63(2):678–691, 2015.

Appendix A

Acronyms

mmWave millimeter wave i

THz Terahertz i

MIMO Multiple-Input and Multiple-Output i

NLoS Non-Line-of-Sight i

LoS Line-of-Sight i

5G 5th Generation mobile networks 1

WLAN Wireless Local Area Network 1

SNR Signal-to-Noise-Ratio 3

IoT Internet of Things 7

PM Particulate Matter 24

CSI Channel State Information 5

SISO Single-Input and Single-Output 59

OBF Optimal Beamforming 75

MP Multiplexing 75

PSD Power Spectral Density 12

i.i.d independent and identically distributed 50

UNSW University of New South Wales iv

dB	Decibel
Gbps	Giga bit per second
GHz	Giga Hertz
ITU	International Telecommunication Union
CSIRO	Commonwealth Scientific and Industrial Research Organisation